



ITN-5VC

Integrated Telematics for Next Generation 5G Vehicular Communications

ITN-5VC D4.9

Year 3 Project Popular-Science Workshop

Version v1.0

Date: 2023/08/31

Document properties:

Grant Number:	955629
Document Number:	D4.9
Document Title:	Year 3 Project Popular-Science Workshop
Partners involved:	UPV
Authors:	Danaisy Prado, Jose F. Monserrat
Contractual Date of Delivery:	2023/08/31
Dissemination level:	PU ¹
Version:	1.0
File Name:	ITN-5VC D4.9_v1.0

¹ CO = Confidential, only members of the consortium (including the Commission Services)

PU = Public

Table of Contents

Executive summary	4
1 Introduction	5
2 Year 3 Project popular-science workshop.....	5
Brief overview	5
ESR participation	5
Presentation material	6

Executive summary

The dissemination of scientific results plays a vital role in societal development because it allows the public to understand scientific advances and how they may impact their lives. Additionally, it helps to build trust in science and researchers and encourages young people to pursue a career in science. One of the goals of this project is to help students acquire abilities that will enable them to become excellent communicators in addition to researchers. For that reason, the project hosts annual popular science workshops. This document provides details of the popular science workshop corresponding to the third year of the project.

Disclaimer: This work has been performed in the framework of the H2020 project ITN-5VC co-funded by the EU. This information reflects the consortium's view, but the consortium is not liable for any use that may be made of any of the information contained therein. This deliverable has been submitted to the EU commission, but it has not been reviewed and it has not been accepted by the EU commission yet.

1 Introduction

In the ITN-5VC project, it is expected to develop a series of dissemination and outreach activities which are scheduled in advance. The popular science workshops are an example; they aim to add exposure to the research carried out during the project. These activities allow for increased awareness about the obtained results and represent an opportunity for the ESRs to receive valuable feedback in a more relaxed venue than a conference or congress.

The training school jointly organized by the University of Twente and Volkswagen AG was a fantastic opportunity to hold the third Popular-Science Workshop. The audience comprised lecturers from the training and Volkswagen AG personnel involved in RF design and testing. Given the venue's characteristics and the project stage, the presentations focused on the latest research results of the ESRs. While some of these results had already been presented in conferences such as EUCAP and VTC or are scheduled to be presented in future events, this represented a unique opportunity to share the progress done without stringent time limitations and in a more open-to-debate manner. Discussions about the motivations for the work and short-term future research directions were also held.

The given presentations, as well as flyers with information about the project, were distributed among the audience. They were encouraged to share the received information with their colleagues to increase the activity's reach.

2 Year 3 Project popular-science workshop

Brief overview

- Host: Volkswagen AG
- Venue: Volkswagen Campus
- Time: September 2023

ESR participation

Name	Participation
ESR1 Reza Gheybi Zarnagh	YES
ESR2 Alejandro Antón Ruiz	YES
ESR3 Coen van de Ven	YES
ESR4 Aamir Ullah Khan	YES
ESR5 Sayed Najaf Haider Shah	YES
ESR6 Yanet Estrada González	YES
ESR7 Nandan Dutta Chaudhury	YES
ESR8 Vishakha Shukla	YES
ESR9 Rubén Darío Riaño Álvarez	YES
ESR10 Yang Fu	YES
ESR11 Carlos Ravelo Pérez	YES

Presentation material

Impact of Excitation and Weighting Errors on Performance of Compact OTA Testing Systems

Alejandro Antón Ruiz and Andrés Alayón Glazunov



**UNIVERSITY
OF TWENTE.**
RS | **RADIO** 
SYSTEMS

- Introduction
- OTA setup and test zone FoM
- Study of chamber array excitation errors
- Study of DUT weighting errors
- Conclusions

- ITN-5VC

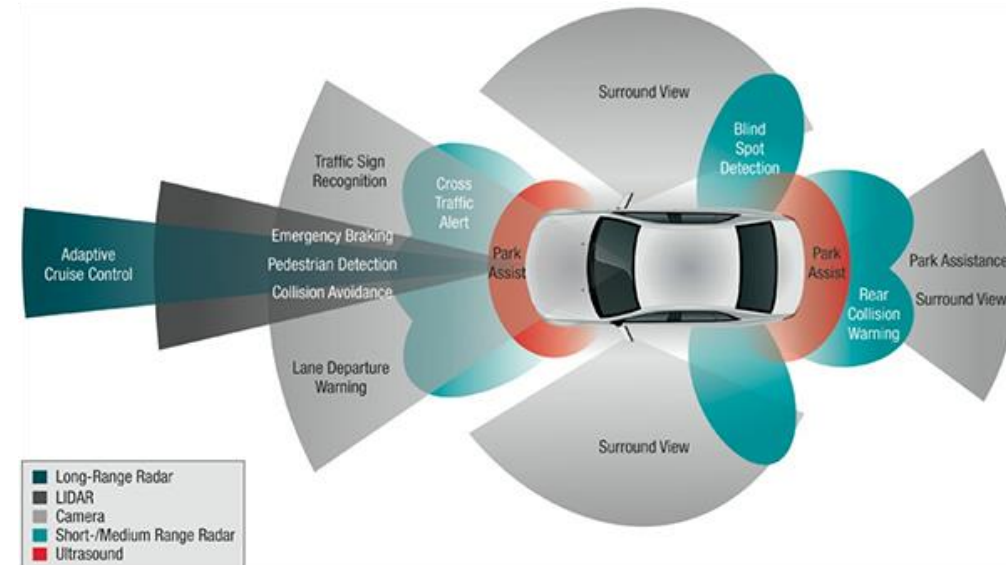
- Develop OTA measurements for vehicles

- Radar and telecom phased arrays
 - Joint communications and sensing (mmWave)
 - MIMO

- OTA testing for vehicles at FR2

- Most likely scenario: LOS

- Random-LOS
 - Multiple antennas: whole car within test zone
 - MIMO
 - Lack of suitable solutions

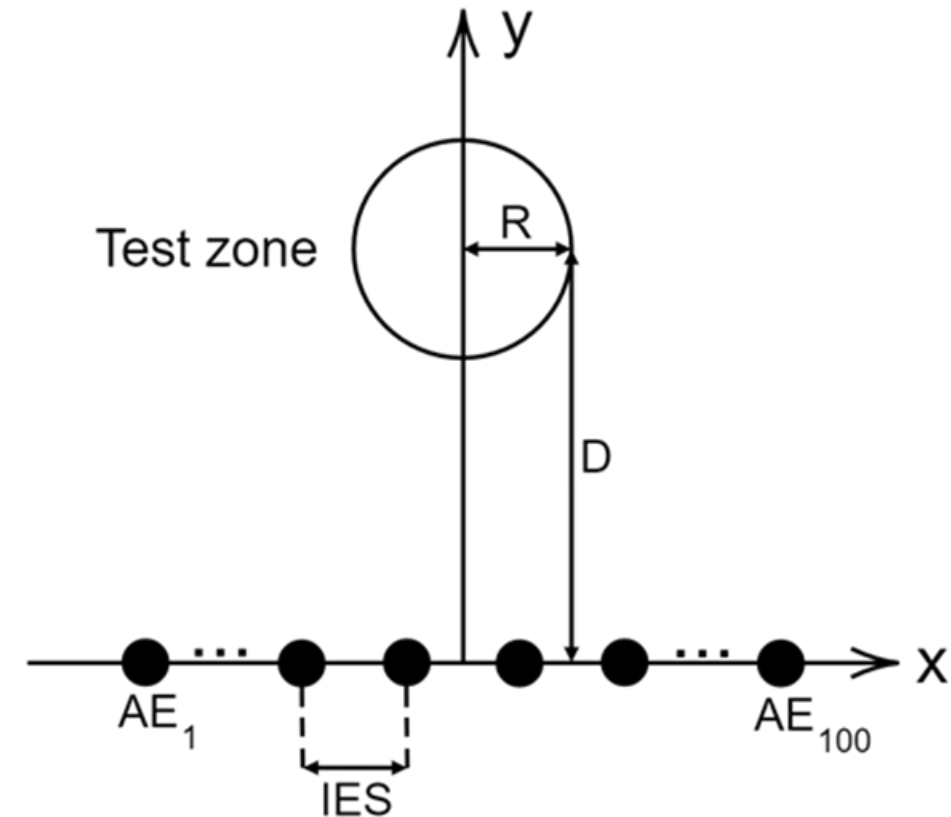


Source: Michigan Technological University

- This paper
 - n257 central frequency (28 GHz, narrowband)
 - Random-LOS approach
 - ULA to generate a plane wave
 - Compact chamber dimensions
 - 2D test zone
 - Impact of different sources of error
 - Chamber array excitation
 - DUT weights errors

OTA setup

- ULA with 100 ideal, vertically polarized (z-axis) isotropic AEs @28 GHz
- 0 dB to -6 dB linear taper to 25 AEs per side
- Variable IES: 0.5λ to 1.5λ , 0.05λ step
 - $L = 99IES$
 - L varies between 53.04 cm to 159.11 cm
- $R = \frac{99\lambda}{8} = 13.26$ cm (26.52 cm diameter)
- Variable D : 40λ to 2450λ , λ step
 - Max. D : half of the shortest Fraunhofer distance



- Objective: plane wave in the TZ
- Samples: constant density $\lambda/8$ mesh
- Electric field computed by superposition principle:

$$E_z = \sum_{i=1}^{N_C} t_{c_i} E_0 \frac{e^{-jkr_i}}{4\pi r_i} = \sum_{i=1}^{N_C} t_{c_i} \frac{e^{-jkr_i}}{4\pi r_i}$$

- Magnitude range

$$R_{mag} = \max\left(20\log_{10}(|E_z|)\right) - \min\left(20\log_{10}(|E_z|)\right).$$

- E_z contains all the electric field values within the TZ
- Ideal value: $R_{mag} = 0 \text{ dB}$
- Acceptable value: $R_{mag} \leq 1 \text{ dB}$

- Magnitude standard deviation

$$\sigma_{mag} = \sqrt{\frac{\sum_{s=1}^{N_s} (X_s - \bar{x})^2}{N - 1}}$$

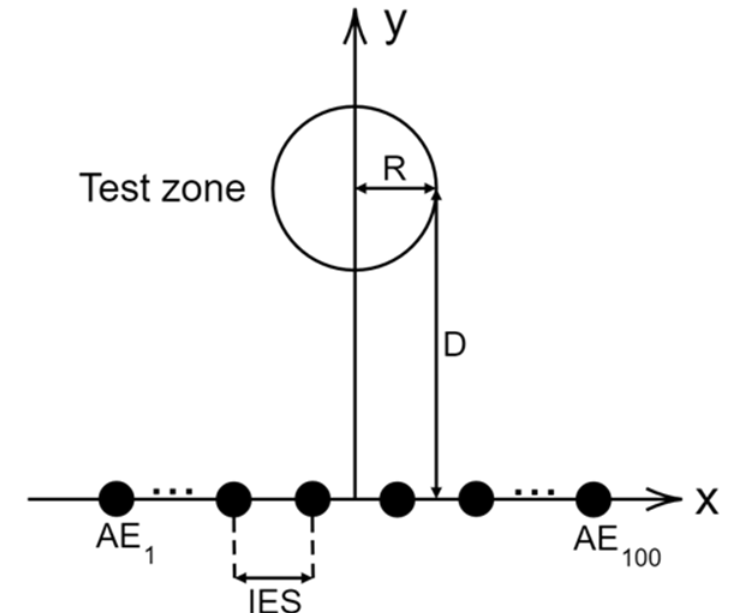
- X_s is the magnitude and \bar{x} is the average (all in log. units)
- Ideal value: $\sigma_{mag} = 0 \text{ dB}$
- Acceptable value: $\sigma_{mag} \leq 0.25 \text{ dB}$

- Phase range

$$R_{phs_{rows_n}} = \max(\angle \mathbf{E}_{z_n}) - \min(\angle \mathbf{E}_{z_n}),$$

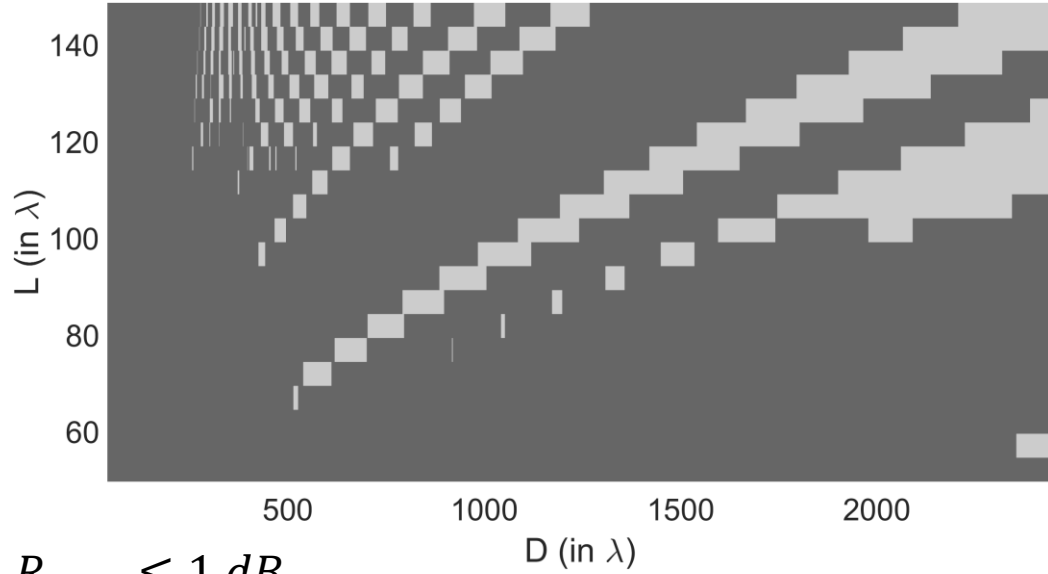
$$R_{phs} = \max(\mathbf{R}_{phs_{rows}}).$$

- \mathbf{E}_{z_n} is the electric field of the n-th row parallel to the chamber array
- $R_{phs_{rows_n}}$ is the phase range of the n-th row
- $\mathbf{R}_{phs_{rows}}$ contains the phase ranges of all rows
- Ideal value: $R_{phs} = 0^\circ$
- Acceptable value: $R_{phs} \leq 10^\circ$



- L (dependent on IES): defines chamber width
- D : defines chamber length
- Objective: find L and D combinations that fulfil the FoM limits
- For error study: use of stricter FoM limits
 - $R_{mag} \leq 1 \text{ dB}$, $\sigma_{mag} \leq 0.25 \text{ dB}$, $R_{phs} \leq 10^\circ$
 - $R_{mag} \leq 0.9 \text{ dB}$, $\sigma_{mag} \leq 0.225 \text{ dB}$, $R_{phs} \leq 9^\circ$
 - $R_{mag} \leq 0.8 \text{ dB}$, $\sigma_{mag} \leq 0.2 \text{ dB}$, $R_{phs} \leq 8^\circ$

Suitable L and D



$$R_{mag} \leq 1 \text{ dB},$$

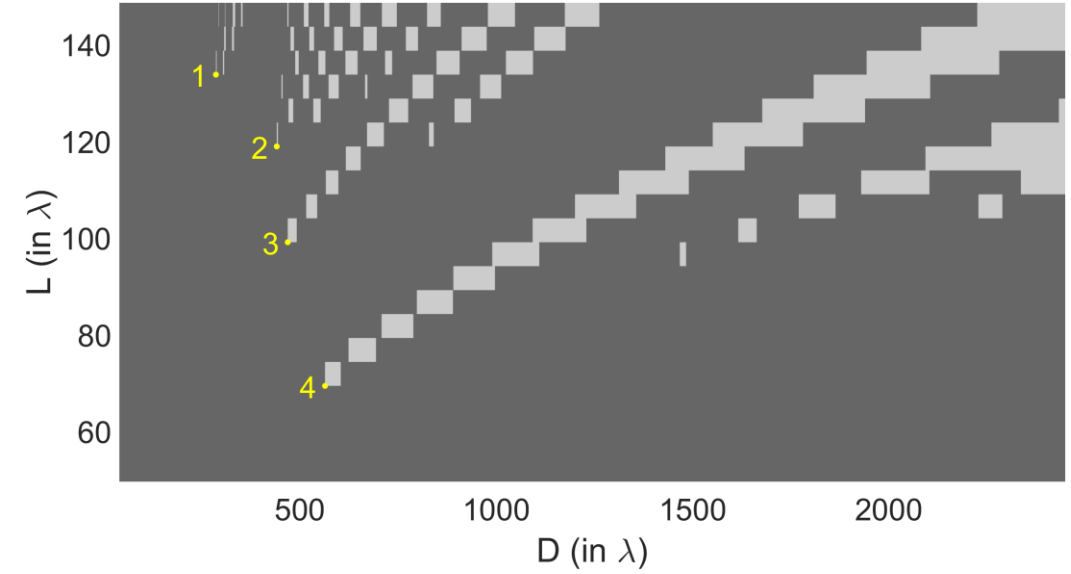
$$\sigma_{mag} \leq 0.25 \text{ dB},$$

$$R_{phs} \leq 10^\circ$$

$$R_{mag} \leq 0.8 \text{ dB},$$

$$\sigma_{mag} \leq 0.2 \text{ dB},$$

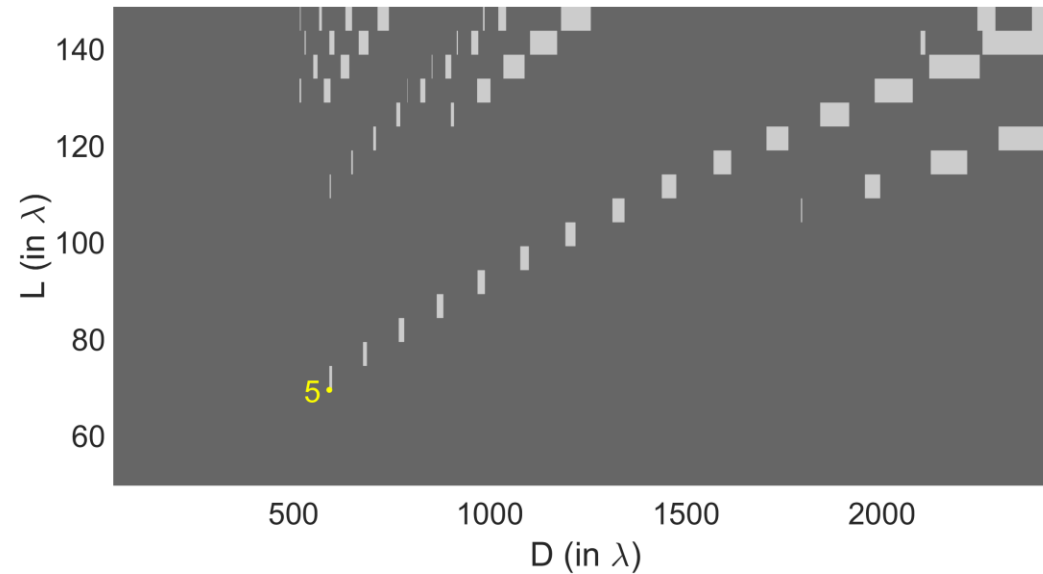
$$R_{phs} \leq 8^\circ$$



$$R_{mag} \leq 0.9 \text{ dB},$$

$$\sigma_{mag} \leq 0.225 \text{ dB},$$

$$R_{phs} \leq 9^\circ$$



- Objective: tolerance to excitation error
 - FoM compliance
 - Evaluated at 5 compact L and D points
- Error model

$$\epsilon_{ch_i} = \mathcal{N}(0, \sigma_{ch}) + j\mathcal{N}(0, \sigma_{ch}),$$

$$\sigma_{ch} = 10^{\sigma_{ch_{dB}}/20} - 1,$$

$$E_z = \sum_{i=1}^{N_C} (1 + \epsilon_{ch_i}) t_{c_i} \frac{e^{-jkr_i}}{4\pi r_i}.$$

Study of chamber array excitation errors

- Monte-Carlo simulations, $\sigma_{ch_{dB}}$ from 0.01 dB to failure, 0.01 dB step

L	IES	D	$\sigma_{ch_{dB}}$	FoM failed
1.43 m / 133.65λ	1.35λ	3.06 m / 286λ	0.05 dB	R_{mag}
1.27 m / 118.8λ	1.2λ	4.73 m / 441λ	0.12 dB	R_{mag}
1.06 m / 99λ	λ	5.03 m / 469λ	0.11 dB	R_{mag}
0.74 m / 69.3λ	0.7λ	6.04 m / 564λ	0.24 dB	R_{phs}
0.74 m / 69.3λ	0.7λ	6.33 m / 591λ	0.5 dB	R_{phs}

Study of chamber array excitation errors

L	IES	D	$\sigma_{ch_{dB}}$	FoM failed
1.43 m / 133.65λ	1.35λ	3.06 m / 286λ	0.05 dB	R_{mag}
1.27 m / 118.8λ	1.2λ	4.73 m / 441λ	0.12 dB	R_{mag}
1.06 m / 99λ	λ	5.03 m / 469λ	0.11 dB	R_{mag}
0.74 m / 69.3λ	0.7λ	6.04 m / 564λ	0.24 dB	R_{phs}
0.74 m / 69.3λ	0.7λ	6.33 m / 591λ	0.5 dB	R_{phs}

$$R_{mag} \leq 0.9 \text{ dB},$$

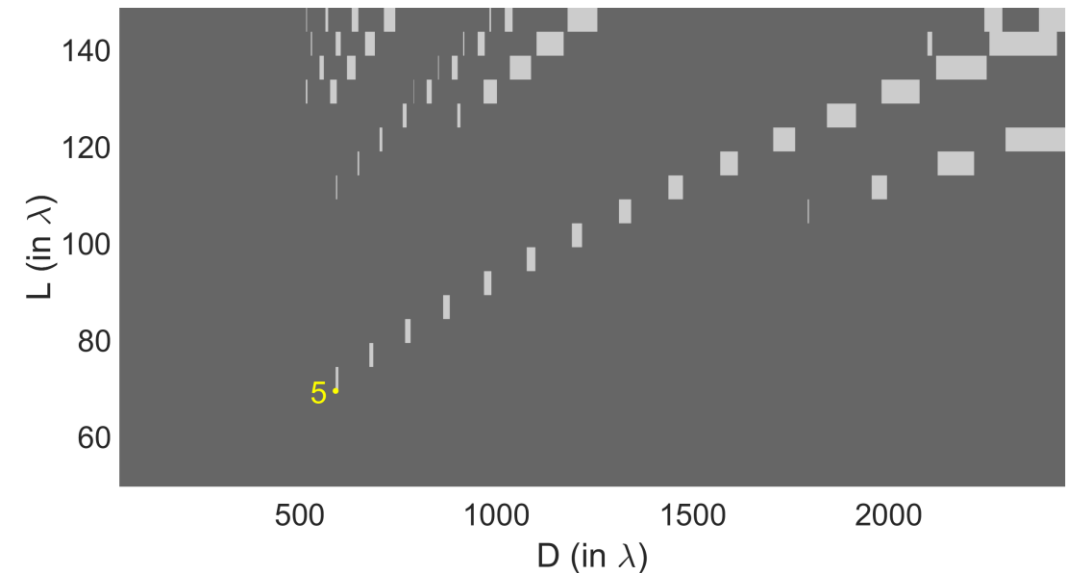
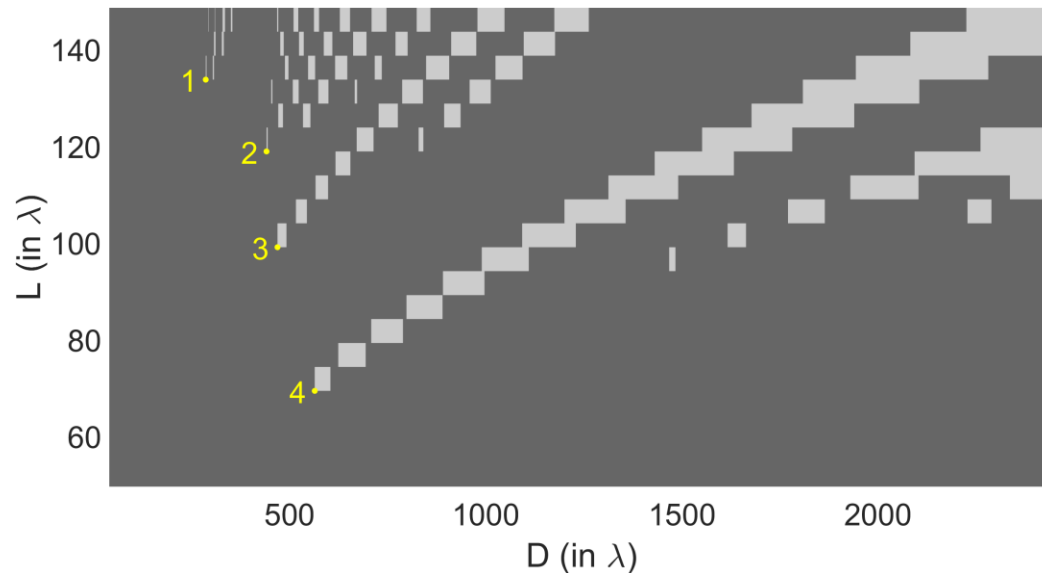
$$\sigma_{mag} \leq 0.225 \text{ dB},$$

$$R_{phs} \leq 9^\circ$$

$$R_{mag} \leq 0.8 \text{ dB},$$

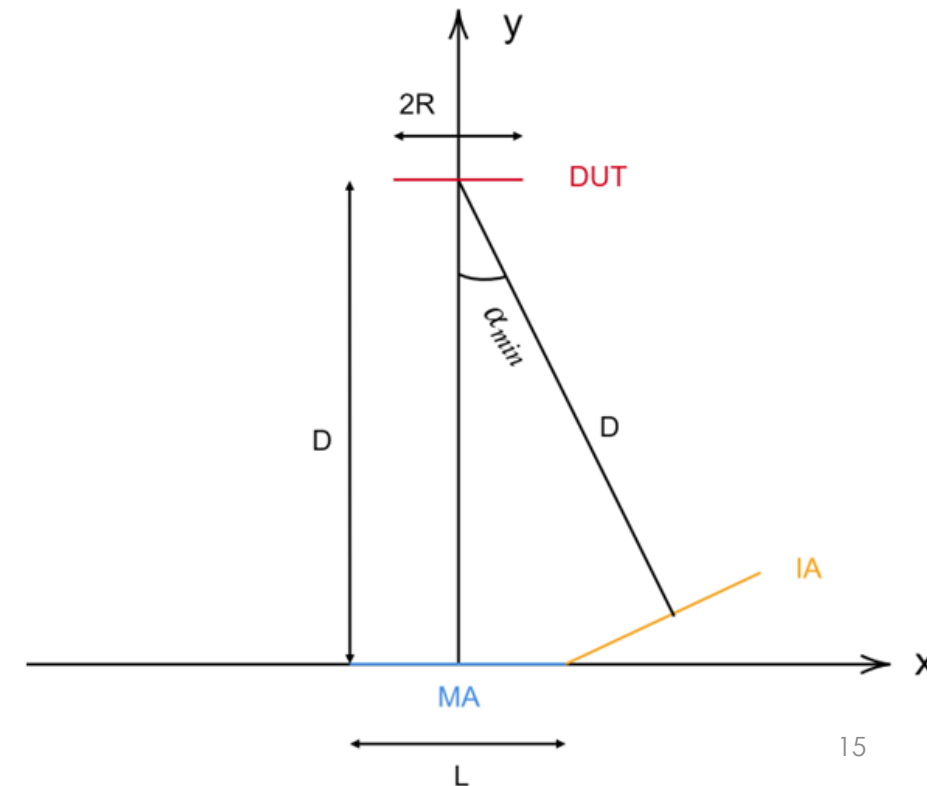
$$\sigma_{mag} \leq 0.2 \text{ dB},$$

$$R_{phs} \leq 8^\circ$$



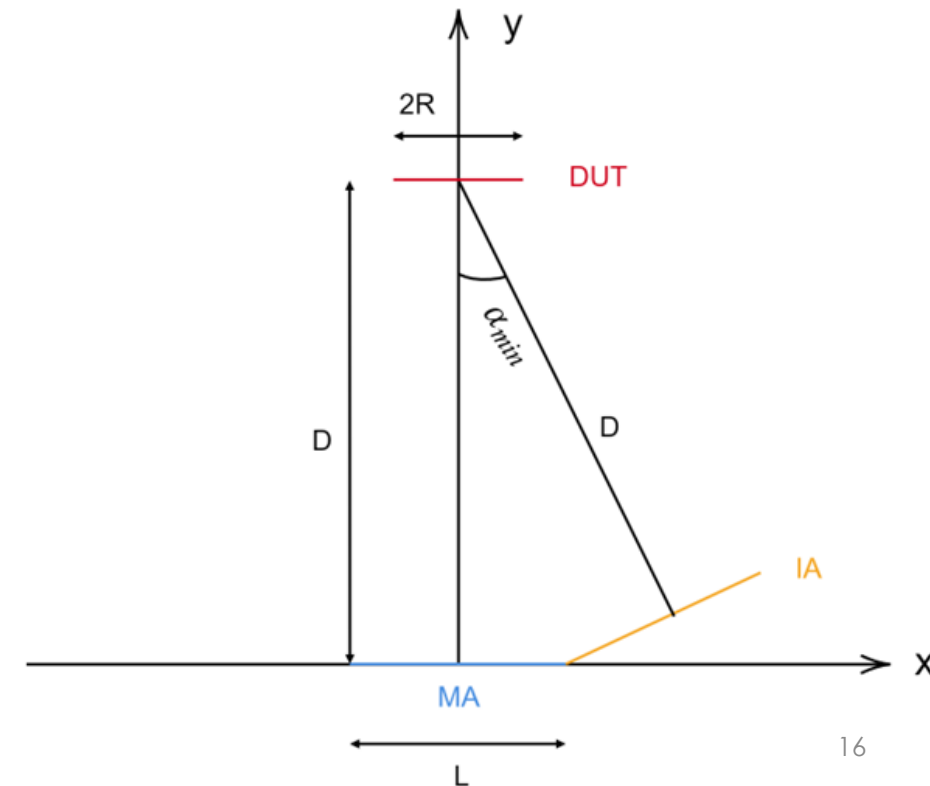
Study of DUT weighting errors

- Objective: evaluate the impact of weighting errors in sum rate
 - Evaluated at 5 compact L and D points and 2 angles α_{min} and $\alpha_{min} + 15^\circ$
 - Same error model, but $\sigma_{DUT_{dB}}$: 0 to 2 dB, 0.1 dB step
 - SNR of -10, 0, 10 and 20 dB
 - ZF and MF
- DUT: 49 AEs @ 0.5λ IES
- Main Array (MA): chamber array
- Interfering Array (IA): identical to MA

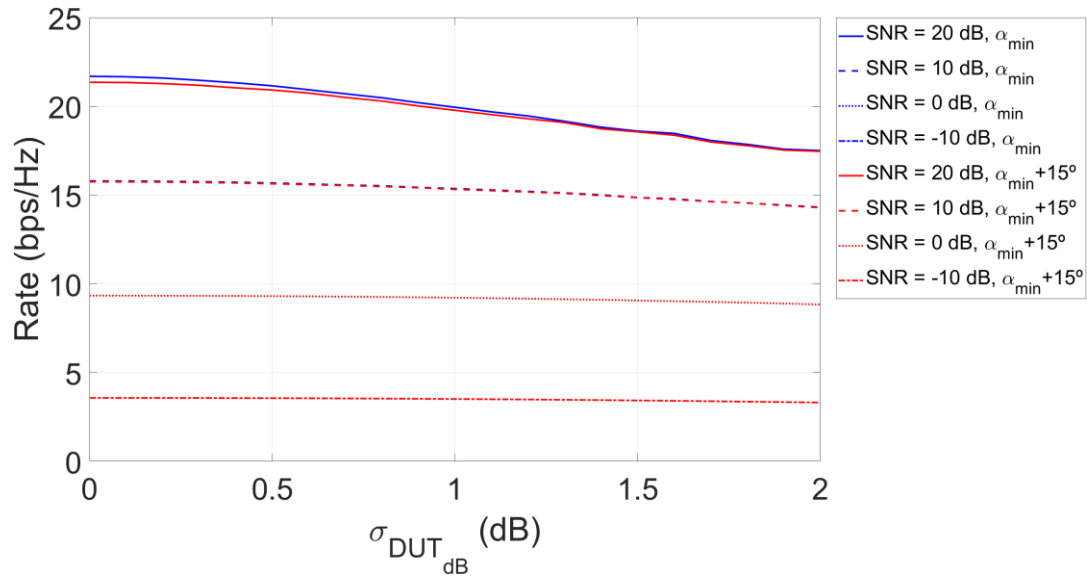


Study of DUT weighting errors

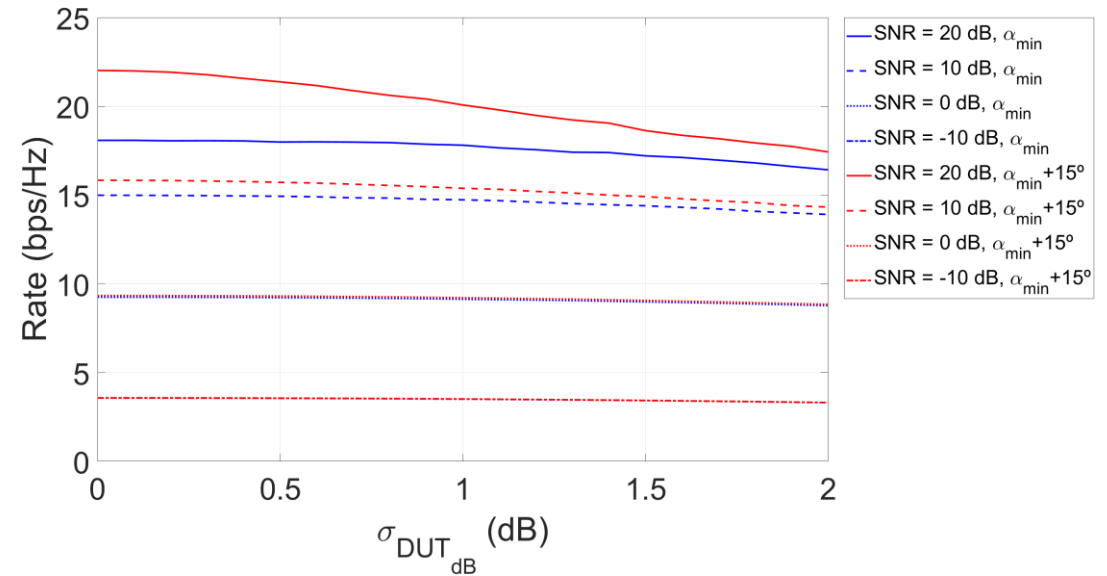
- MA and IA are UEs, DUT is BS. Monte-Carlo simulation
- H is computed with superposition principle
- Weights are computed
 - $\mathbf{W}_{ZF} = \mathbf{H}^\dagger (\mathbf{H}\mathbf{H}^\dagger)^{-1}$
 - $\mathbf{W}_{MF} = \mathbf{H}^\dagger$
- Weight error is applied
- Sum rate is computed (MA and IA to DUT)
 - $SR = \sum_{u=1}^2 \log_2(1 + SINR_u)$



Study of DUT weighting errors

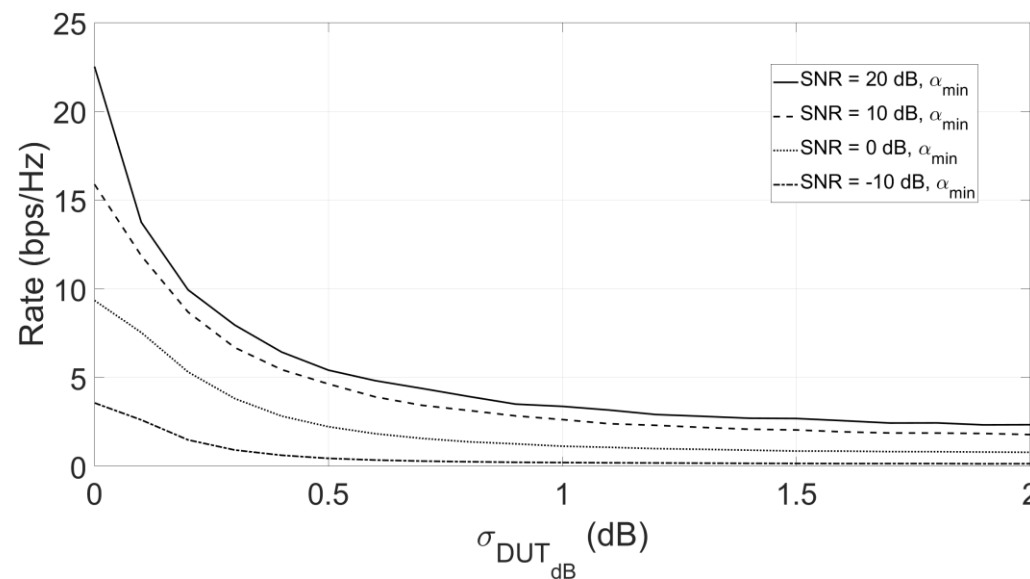


MF, $L = 133.65\lambda$, $D = 286\lambda$



MF, $L = 69.3\lambda$, $D = 591\lambda$

ZF, $L = 133.65\lambda$, $D = 286\lambda$



- A relatively compact OTA system is possible
 - Lots of improvement headroom
- Relevance of errors when designing a compact OTA system
 - Performance must be assured under real error levels
- First step towards mmWave MIMO OTA system for vehicles
 - 3D test zone
 - Wideband
 - Use of other type of chamber array
 - Optimization
 - Consideration of other sources of error (e.g. AEs misplacement)

Impact of Excitation and Weighting Errors on Performance of Compact OTA Testing Systems

Alejandro Antón Ruiz and Andrés Alayón Glazunov



**UNIVERSITY
OF TWENTE.**
RS | **RADIO** 
SYSTEMS

Sensing Resources Reduction for Vehicle Detection with Integrated Sensing and Communications

Carlos Ravelo Pérez, David Martín-Sacristán, Syed Najaf Haider Shah, Carsten Smeenk, Giovanni Del Galdo, Jose F. Monserrat

ITN-5VC

carlos.ravelo@fivecomm.eu



Overview

Introduction

System Model

ISAC processing for OFDM

Sensing resources reduction

Simulation Results

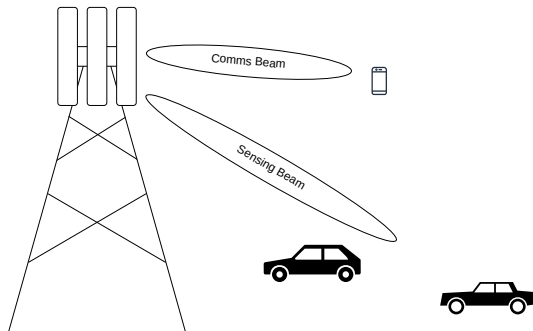
Conclusions

Introduction

- More efficient usage of spectrum
- Integration gains through cooperation (sensing-assisted communications, communications-assisted sensing)
- Next-generation mobile networks are expected to be designed with sensing as a core component
- Current networks could be modified to implement communication-centric ISAC

Application Considered

- Base Station serves communication users and simultaneously senses the street
- We will focus on the target detection of vehicles



- Majority of prior work considers full OFDM frame usage for sensing
 - Less resources for communications
 - More difficult to multiplex scanning beams
- In terms of beam planning, either consider fixed angle or 3dB beamwidth rotations

System Model

System Model

- Base Station capable of In-Band Full-Duplex
- Transmits one stream of data for communications and another for sensing

$$\mathbf{s}_t = \sqrt{\frac{P_t}{N_t}} (\sqrt{(1-\rho)} \mathbf{w}_c \mathbf{x}_c + \sqrt{\rho} \mathbf{w}_s \mathbf{x}_s), \quad (1)$$

- Sensing part of the transmitted signal:

$$\mathbf{s} = \sqrt{\rho \frac{P_t}{N_t}} \mathbf{w}_s \mathbf{x}_s. \quad (2)$$

System Model

- Signal at the sensing receiver

$$\mathbf{r}[t] = \sum_{l=0}^{L-1} h_l \mathbf{w}_s^* \mathbf{v}_l \mathbf{v}_l^* \mathbf{s}[t - \tau_l] e^{j2\pi f_{D,l} t} + \mathbf{z}[t], \quad (3)$$

- Path attenuation is given by (point-scatter model)

$$h_l = \sqrt{\frac{c_0^2 \sigma_{\text{RCS},l}}{(4\pi)^3 d_l^4 f_c^2}}, \quad (4)$$

- Transmit/receive array response given by

$$\mathbf{v}_l = [e^{j\frac{2\pi}{\lambda} (\mathbf{y} \sin \theta_l \cos \varphi_l + \mathbf{z} \sin \varphi_l)}], \quad (5)$$

- The received power from the echoes can be expressed in terms of the transmitted power, path attenuation, beamformer and array response

$$G_l = \frac{\mathbf{w}_s^* \mathbf{v}_l \mathbf{v}_l^* \mathbf{w}_s}{\mathbf{w}_s^* \mathbf{w}_s}. \quad (6)$$

$$P_{r_l} = \rho P_t G_l^2 h_l^2. \quad (7)$$

ISAC processing for OFDM

ISAC processing for OFDM

- Symbol domain processing for OFDM
- The received echoes can be put in terms of the resource elements of the OFDM grid

$$\mathbf{F}_{R_x(i,k)} = \sum_{l=0}^{L-1} h_l \mathbf{F}_{T_x(i,k)} e^{j2\pi T_0 f_{D,l} k} e^{-j2\pi \tau_l (i\Delta f + f_0)} e^{j\varphi_l} + \mathbf{Z}_{(i,k)}, \quad (8)$$

- Influence of the transmitted data can be removed through element-wise division

$$\mathbf{F} = \frac{\mathbf{F}_{R_x}}{\mathbf{F}_{T_x}}. \quad (9)$$

- For target detection and parameter estimation the processing is done over a 2D Periodogram

$$P_{\mathbf{F}}(n, m) = \frac{1}{NM} \left| \sum_{i=0}^{N_p-1} \left(\sum_{k=0}^{M_p-1} \mathbf{F} e^{-j2\pi \frac{km}{M_p}} \right) e^{j2\pi \frac{in}{N_p}} \right|^2, \quad (10)$$

- Given a target present at (n_0, m_0) , the periodogram will take value given by

$$P_{\mathbf{F}}(n_0, m_0) \leq NMP_{r_0}, \quad (11)$$

Target detection

- Target is distinguishable from noise
 - Given a CFAR detector and a predefined probability of false alarm p_{FA}

$$\eta_P = -\sigma_n^2 \ln(1 - (1 - p_{FA})^{\frac{1}{N_p M_p}}). \quad (12)$$

- The echo having a higher level than the noise can be put as

$$NMP_{r_l} > \eta_P. \quad (13)$$

- Target is distinguishable from other targets (resolution)

$$\min_i |d_{T_x-l} - d_{T_x-i}| \geq \Delta R, \quad (14)$$

$$\min_i |f_{D,l} - f_{D,i}| \geq \Delta f_D, \quad (15)$$

Sensing resources reduction

- OFDM characteristics limit the maximum sensing range and Doppler frequency

Table 1: Maximum sensing distance and velocity

System Configuration		Sensing Limits	
SCS (kHz)	f_c (GHz)	d_{\max} (m)	v_{\max} (km/h)
15	3.5	704	231
30	5	344	324
120	24	88	270

Grid Subsampling

- Based on the numerology, we can obtain the maximum separation between sensing subcarriers

$$\Delta f_{s_{\max}} = \frac{c_0}{2d_{\max}\Delta f}, \quad (16)$$

- Considering $0.1\Delta f$ as maximum Doppler shift the maximum separation between sensing symbols is $\Delta T_s = 5$
- The reduction on resources affects the probability of detection, we need to ensure

$$N_s M_s \rho P_t G^2 \frac{c_0^2 \sigma_{\text{RCS},\min}}{(4\pi)^3 d_{\max}^4 f_c^2} > \eta P. \quad (17)$$

Beam Planning

- Given a sensing scenario, create a grid with positions where array gain is almost equal
- Determine the minimum required array gain at each position

$$\mathbf{G}_{\min}(x, y) = \eta_P \frac{(4\pi)^3 d_{xy}^4 f_c^2}{N_s M_s \rho P_t c_0^2 \sigma_{\text{RCS}, \min}}. \quad (18)$$

- Obtain the $N_g \times N_t$ matrix with beamforming vectors to all positions of the grid \mathbf{W}
- Obtain the array gain matrix $\hat{\mathbf{W}}$ via

$$\hat{\mathbf{W}} = \frac{1}{N_t} (\mathbf{W}^* \mathbf{W}) \odot (\mathbf{W}^* \mathbf{W}), \quad (19)$$

- $\hat{\mathbf{W}}(i, j)$ represents the gain of beamforming vector j on location i

- By element-wise comparison between \mathbf{G}_{\min} and columns of $\hat{\mathbf{W}}(i, j)$ we can obtain the matrix $\tilde{\mathbf{W}} = [\tilde{\mathbf{w}}_0, \dots, \tilde{\mathbf{w}}_{N_g-1}]$
- There is one $\tilde{\mathbf{w}}_k$ for each beamforming vector and each of its elements is either zero if the beamformer doesn't offer enough gain for that position or one if it does
- Reduction of the number of beams as an optimization problem

$$\begin{aligned} & \min_{\mathbf{x}} \|\mathbf{x}\|_1, \\ \text{s.t.} \quad & x_0 \tilde{\mathbf{w}}_0 + \dots + x_{N_g-1} \tilde{\mathbf{w}}_{N_g-1} \succeq \mathbf{1} \end{aligned} \quad (20)$$

- With $\mathbf{x} \in \{0, 1\}^{N_g}$

Beam Planning

A solution to (20) can be found through the following algorithm

Data: $\tilde{\mathbf{W}} \in \{0, 1\}^{N_g \times N_g}$, $\mathbf{W} = [\mathbf{w}_0, \dots, \mathbf{w}_{N_g-1}]$

Result: $\mathbf{b}_n, \tilde{\mathbf{W}}_n$

$i \leftarrow 0$ $k \leftarrow 0$ **while** $\tilde{\mathbf{W}}_{0:i+1,k} == [\mathbf{1}]$ **do**

| $i \leftarrow i + 1$ $k \leftarrow k + 1$

end

$\mathbf{b}_n \leftarrow \mathbf{w}_i$ **while** $\tilde{\mathbf{W}}_{i+1,k} == 1$ **do**

| $i \leftarrow i + 1$

end

$\tilde{\mathbf{W}}_n = \tilde{\mathbf{W}}_{i+j:N_g, k+1:N_g}$

Algorithm 1: Beam searching algorithm

Simulation Results

Table 2: Parameters for simulated scenarios

Parameter	5 GHz
SCS (kHz)	30
Bandwidth (MHz)	50
N_{T_x}	16
N_{R_x}	16
d_{\max} (m)	300
v_{\max} (km/h)	150
σ_{\min} (dBsm)	5
Scenario length (m)	300
Scenario width (m)	14

Simulation results

- With the simulation parameters we selected $\Delta f_s = 12$, $\Delta T_s = 7$
- The capacity of the communication channel with sensing subsampling follows closely the case of no sensing

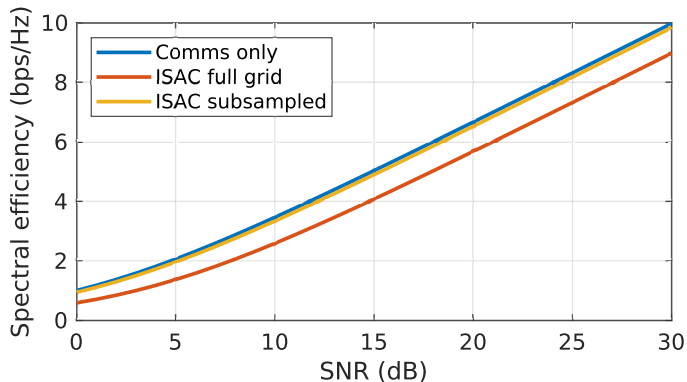


Figure 1: Spectral efficiency comparison

Simulation Results

The beam planning algorithm found two beams to cover the entire scenario

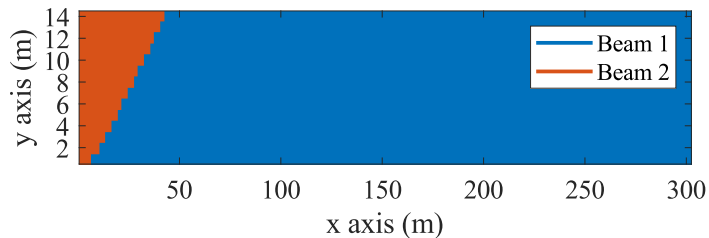


Figure 2: Coverage of beams for the 5 GHz scenario

Simulation Results

- From the SUMO simulation an analysis of the detectability in terms of the resolution was done
- With maximum resource usage, only 151 from 2200 vehicles were at some point undetectable, for a maximum of 15% of their time in the scenario

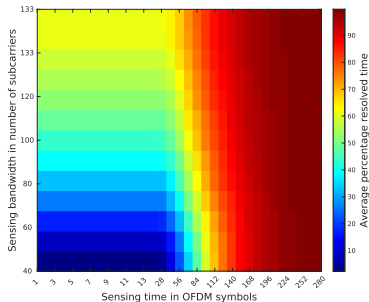


Figure 3: Average percentage resolved time

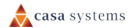
Conclusions

Conclusions and Next Steps

- The applicability of ISAC for vehicle detection was showcased
- The beam planning algorithm showed the possibility of reducing spatial resources for sensing
- Next steps include:
 - Consideration of the influence of sensing stream in communication users and vice versa
 - Strategies to optimize resource allocation for target tracking and finer parameter estimation



THANK YOU



An aerial photograph of a city skyline at sunset. The sky is a mix of blue and orange, with soft clouds. In the foreground, a multi-lane highway with cars is visible, curving through the city. The city buildings are silhouetted against the bright sky. The overall scene is hazy and atmospheric.

APWAVES

Automotive RADAR Planar Antenna
Optimization Based on Conformal
Transformation Optics

Workshop Volkswagen 06-09-2023, Coen van de Ven

Agenda

01. Introduction
02. Conformal transformation optics
03. Optical path rescaling
04. 2D simulation study
05. Results

06. Application view

07. Conclusion





Introduction



Automotive radar - Radome

- ITN-5VC - increase safety on the road
 - ICAS system
 - ESR topic: increase RADAR antenna performance
- Radome is a 'must'
 - How can we use the radome to improve performance

APWAVES

UNIVERSITY
OF TWENTE.





Conformal Transformation Optics



Conformal Transformation Optics

For a given coordinate transformation

- $Z = F(W)$ with Jacobian J

$$\epsilon_z = \frac{J\epsilon_w J^T}{\det(J)}, \mu_z = \frac{J\mu_w J^T}{\det(J)}$$

- $Z = x + iy, W = u, iv$

Using a strictly conformal coordinate transformation

$$\frac{JJ^T}{\det(J)} = \begin{bmatrix} 1 & 0 & 0 \\ 0 & 1 & 0 \\ 0 & 0 & \left(\frac{\partial u}{\partial x}\right)^2 + \left(\frac{\partial u}{\partial y}\right)^2 \end{bmatrix}$$

Transverse magnetic propagation

Transformation only acts on magnetic field

- Relative permeability implements transformation

Plastic implementation can only change relative permittivity

- Conversion is needed via refractive index

$$n(x, y) = \sqrt{\epsilon_r(x, y)_{\mu_r=1}} = \sqrt{\mu_r(x, y)_{\epsilon_r=1}}$$

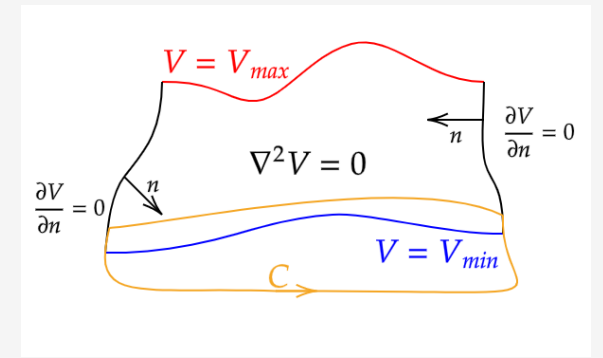
- Conversion is equivalent when $n(x, y)$ changes 'slowly' with respect to the wavelength

- On automotive RADAR antenna scale this does not hold

- An 'conversion error' is introduced



Equivalence with TEM-mode



Conformal transformation

Orthogonal divergence $\frac{\partial u}{\partial x} = \frac{\partial v}{\partial y}$
 $\frac{\partial u}{\partial y} = -\frac{\partial v}{\partial x}$

u, v -components obey Laplace's equation

Dielectric constants $\Rightarrow |\nabla u| = |\nabla v|$
 &
 Conformal modulus



TEM mode

Orthogonal electric and magnetic field

electric scalar potential } obey Laplace's equation
 magnetic scalar potential }

Electric field magnitude $|\nabla V|$
 &
 Characteristic impedance



Optical path rescaling



Optical path rescaling

Physical implementation

- Achievable $\epsilon_r > 1$

Simplification of the original method

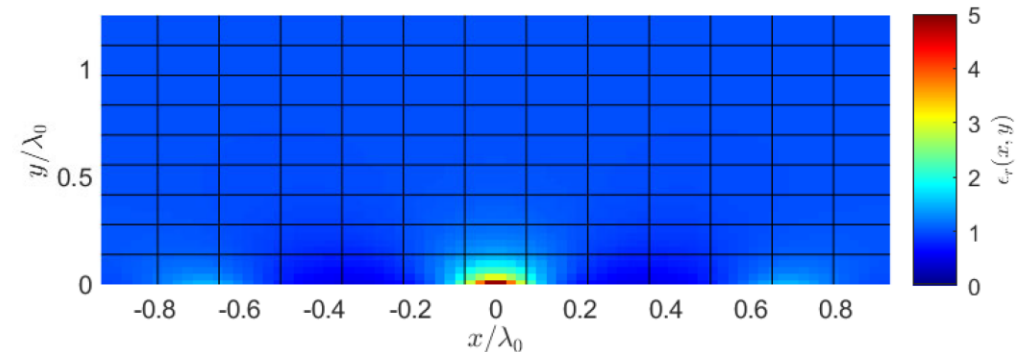
- Absolute path length is non-crucial
- More flexible rescaling

Rescaling function

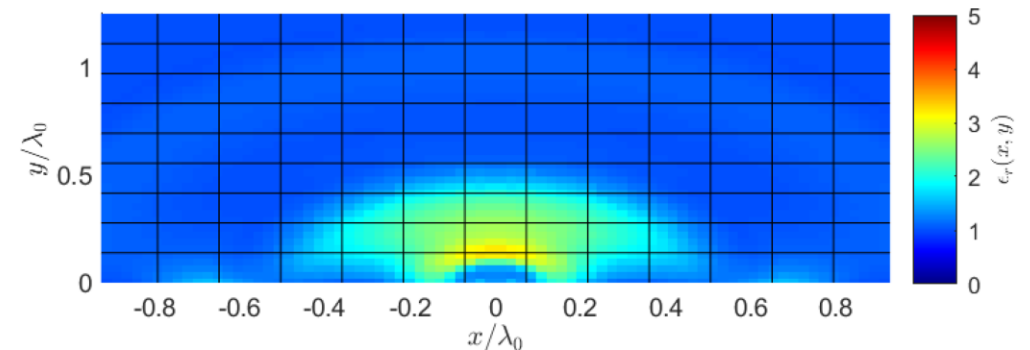
- $\epsilon_{res}(x, y) = \frac{\mu_r(x, y)}{\min\{\mu_r(\Phi(x, y))\}}$
- $\Phi(x, y)$ is the phase-front, orthogonal to the optical path

Figure of merit:

$$FOM_\epsilon = \frac{\max\{\mu_r\}}{\min\{\mu_r\}} \geq \max\{\epsilon_{res}\}$$



(a) ϵ_r implementation w/o rescaling



(b) ϵ_r implementation w/ rescaling





2D simulation study



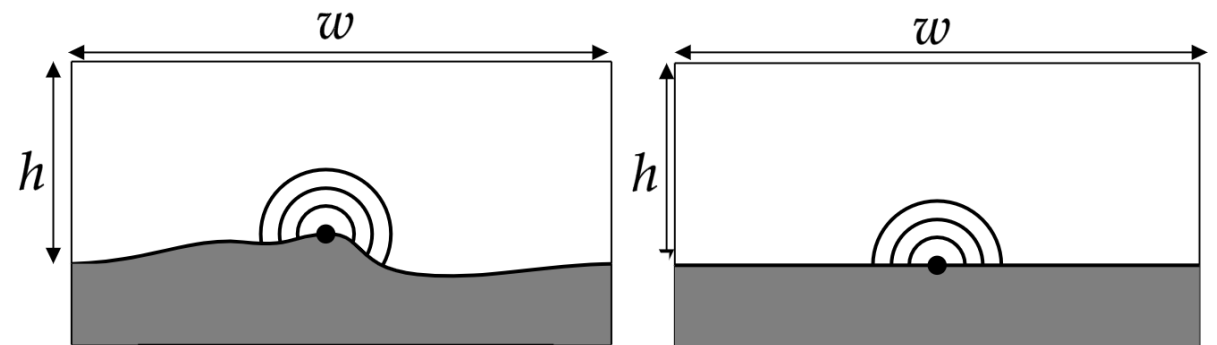
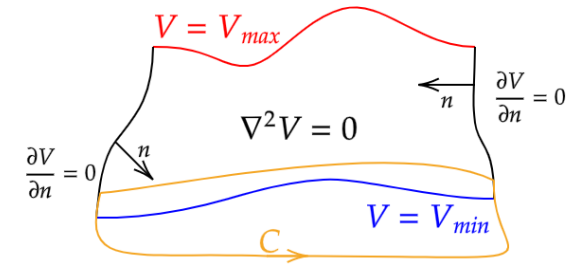
2D simulation

- Joint optimization problem – CST Studio Suite

1. Characteristic impedance
2. Minimized ripple on farfield pattern

- Groundplane to be optimized

- Polynomial
- (spline-) Interpolation curve
- ...



(a) Reference space

(b) Physical space

2D simulation

- Joint optimization problem – CST Studio Suite

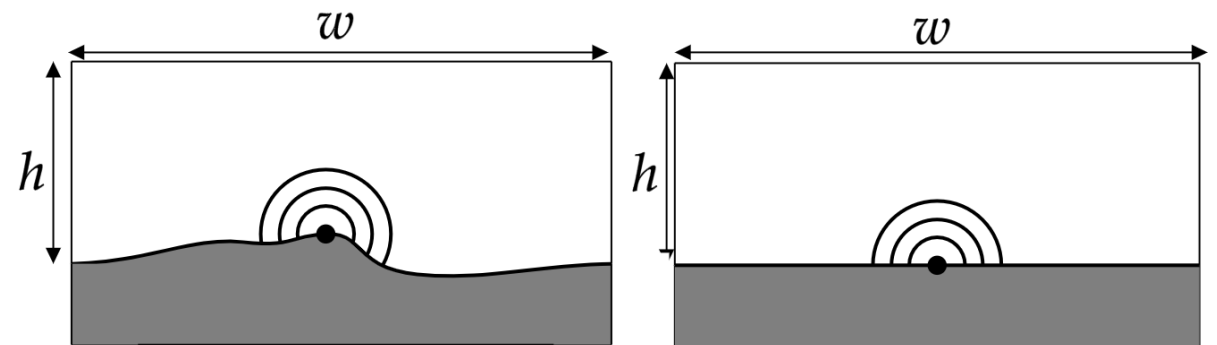
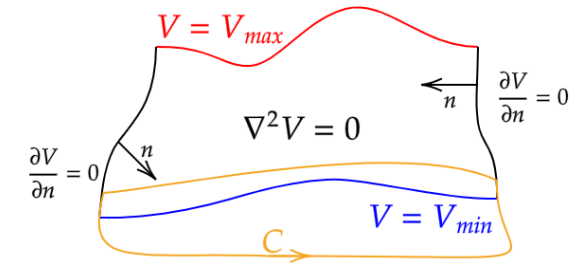
1. Characteristic impedance
2. Minimized ripple on farfield pattern

- Groundplane to be optimized

- Polynomial
- (spline-) Interpolation curve
- ...

Convergence issues

- Sum of cosines



(a) Reference space

(b) Physical space



Results

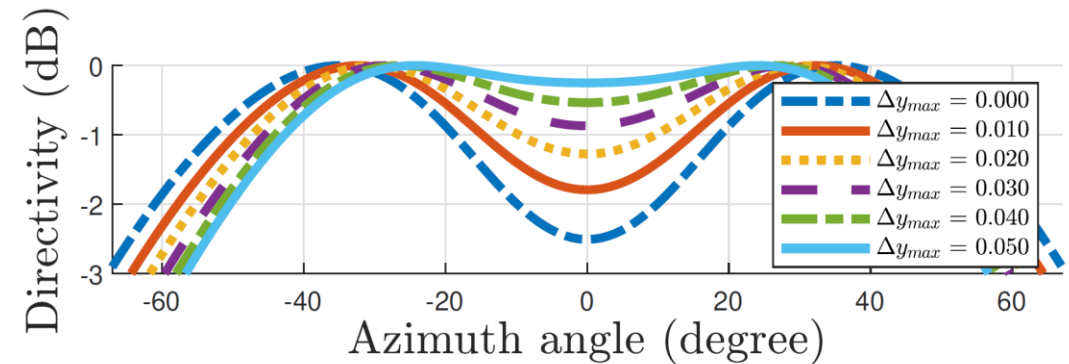
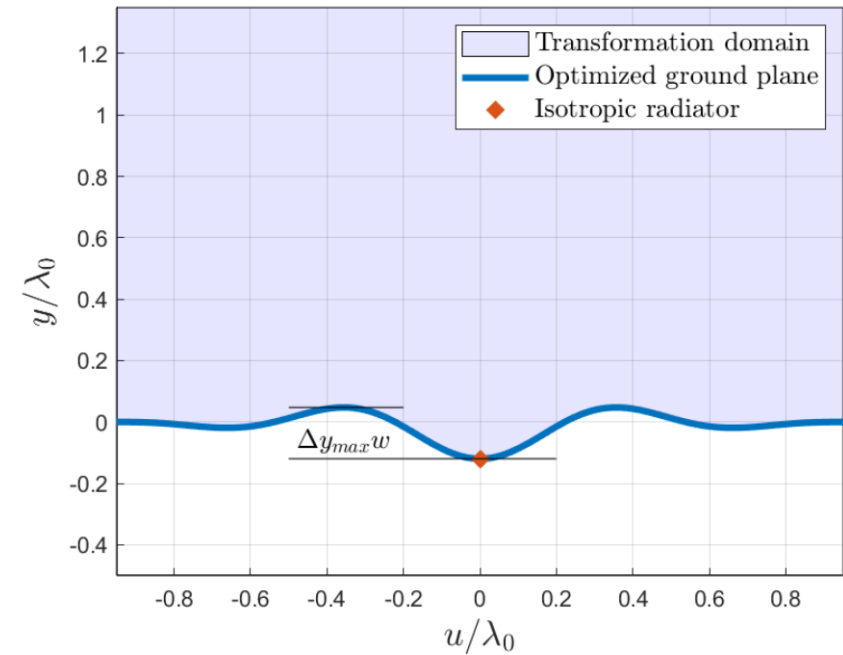


2D simulation

7 Simplified optimization curve

- Characteristic impedance converges
- Ripple can be minimized

Optimization result



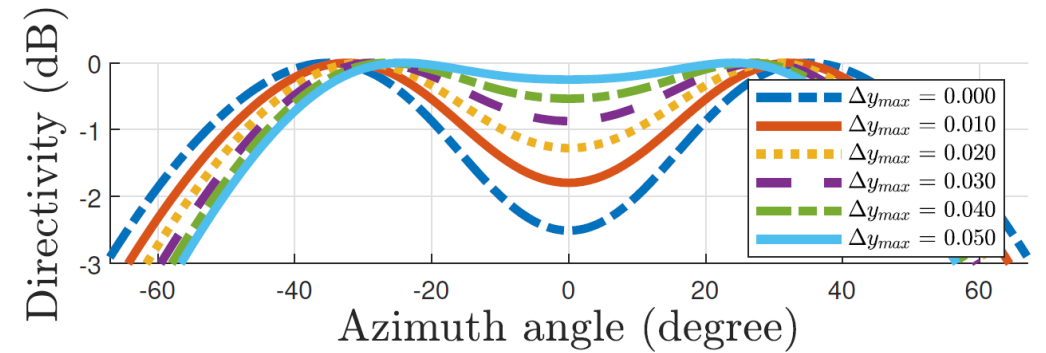
Optical path rescaling

Conversion error deteriorates performance

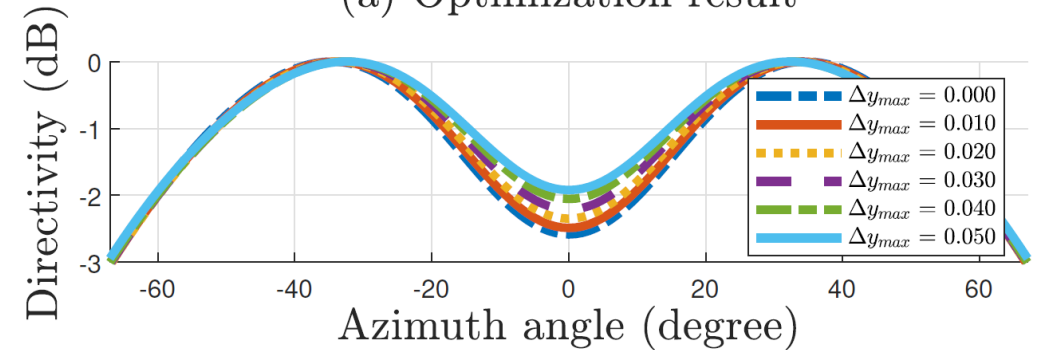
- Result (b)

Updated rescaling function minimizes this effect

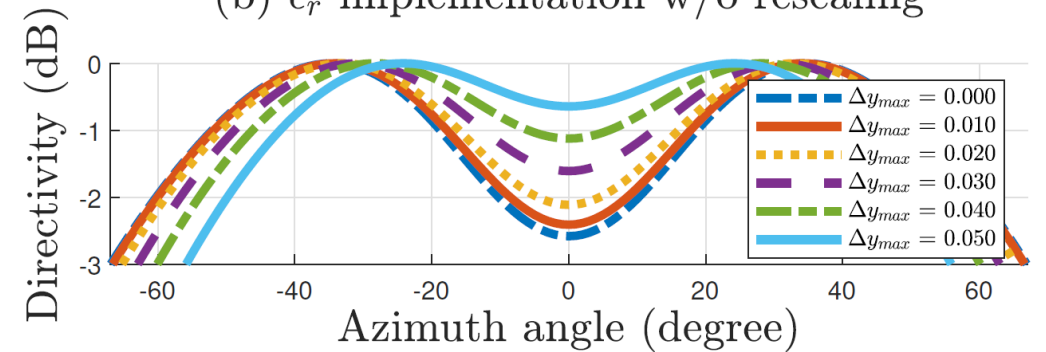
- Result (c)



(a) Optimization result



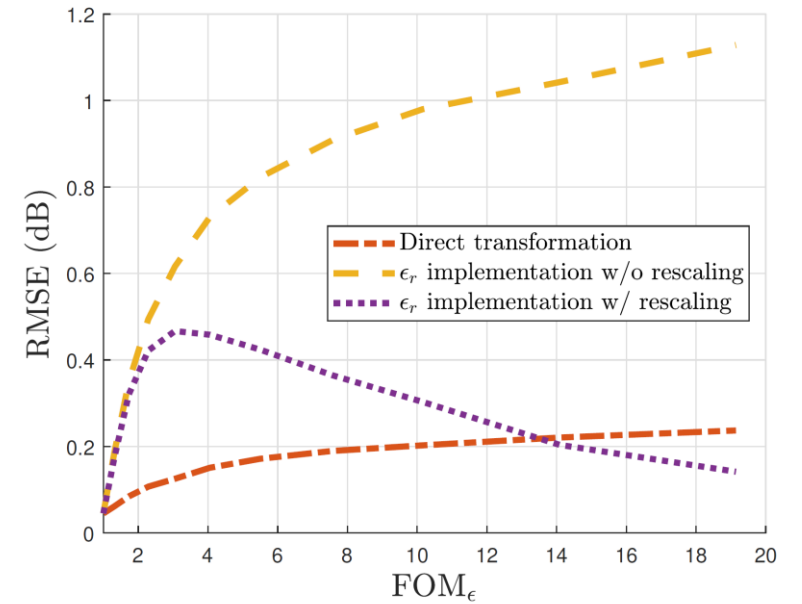
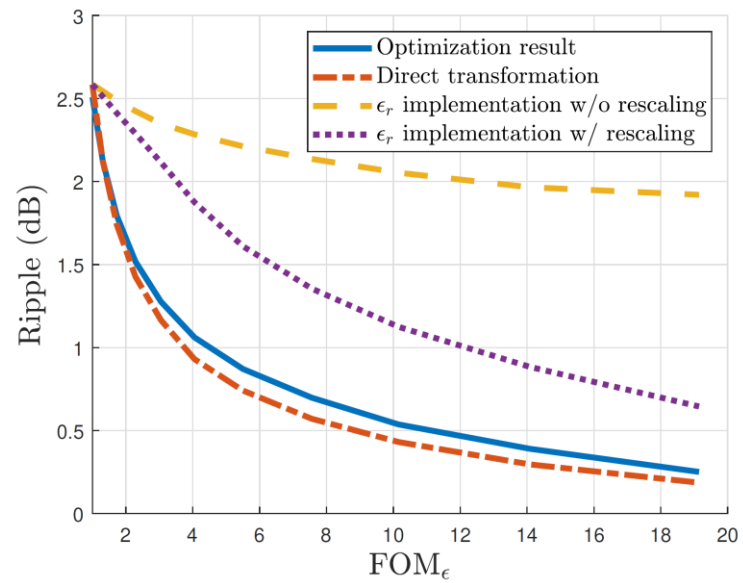
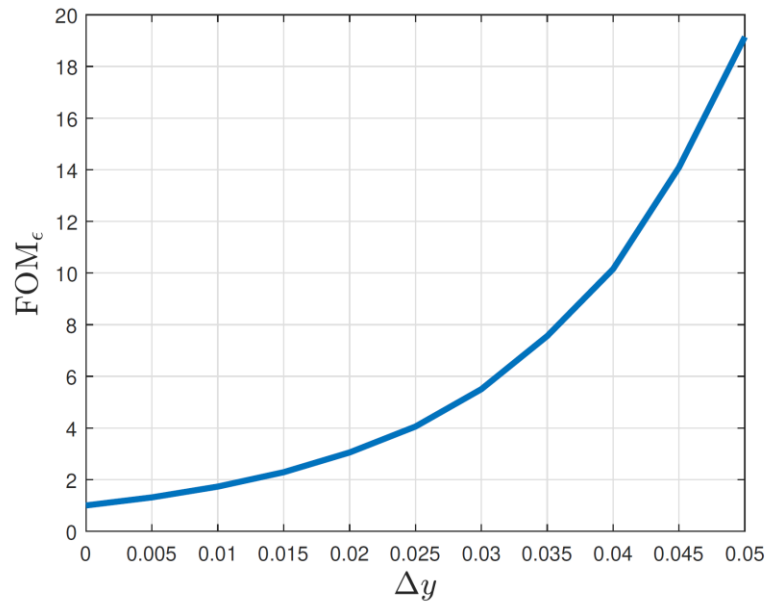
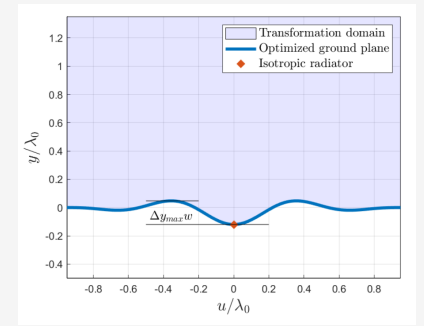
(b) ϵ_r implementation w/o rescaling



(c) ϵ_r implementation w/ rescaling



Figure of merit

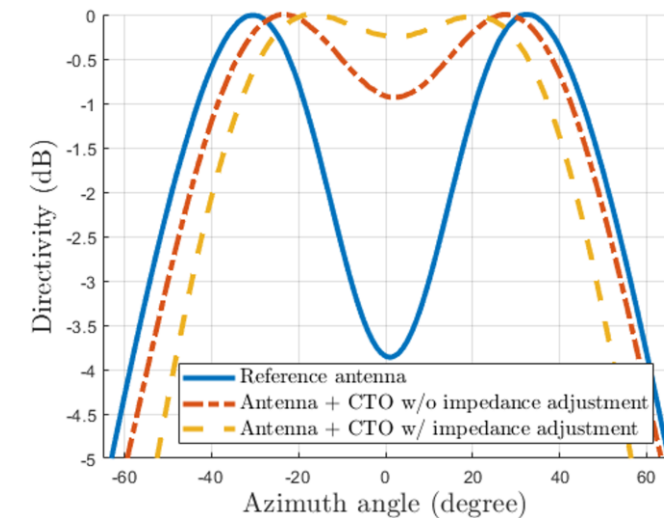
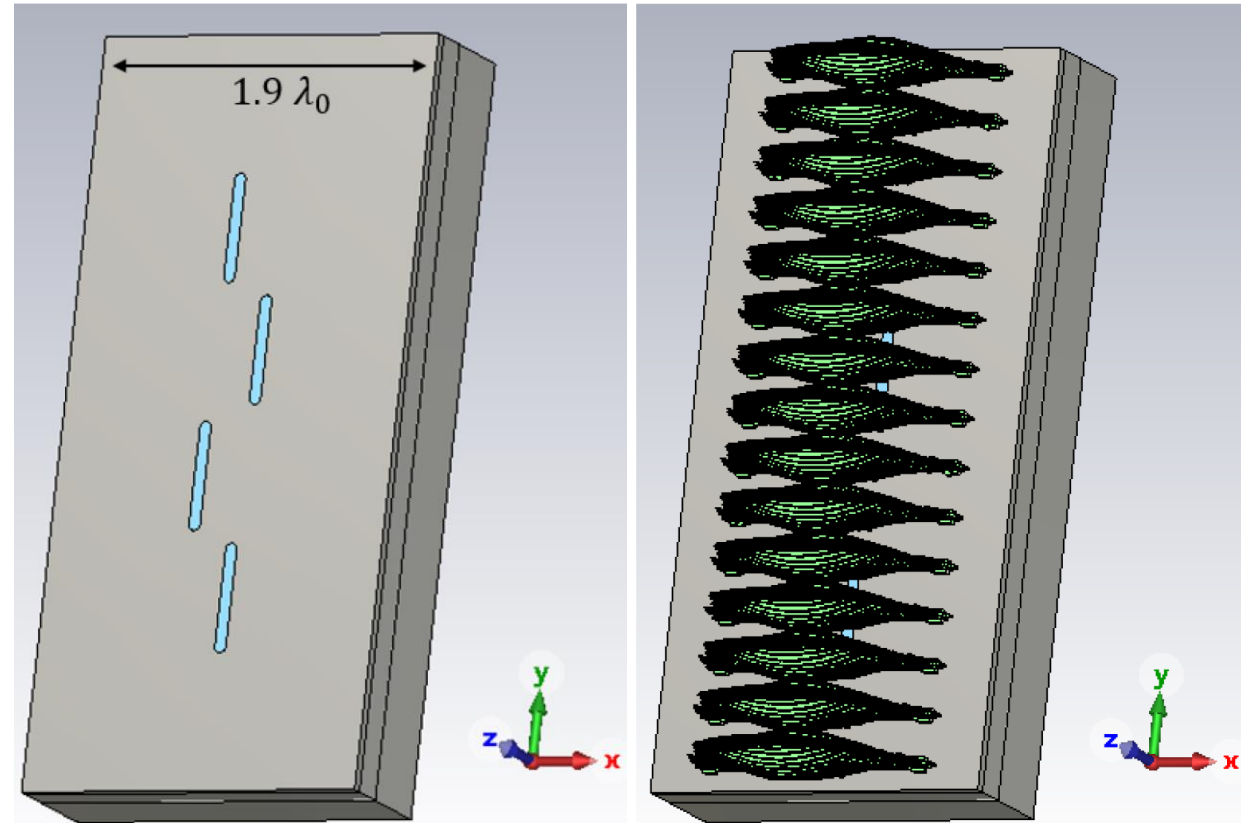


Application view



2D transformation on slotted Gapwaveguide

- Transformation assumes pure TM propagation
 - Additional error is introduced
- Dielectric CTO-lens loads antenna
 - Impedance adjustment by adjusting length of the slot
- Ongoing work into 3D application



Conclusion



Conclusions

1. Conformal Transformation Optics can be applied to improved radiation performance
 - Ongoing work pushing towards 3D applications
2. The TEM equivalence gives insight in the behaviour of CTO
 - This also allows joint optimization of the conformal modulus
3. The updated optical rescaling function can be used to minimize the conversion error for TM propagation



Radar-Enabled Resource Allocation in 5G-V2X Sidelink Communication

Syed Najaf Haider Shah
TU Ilmenau, Germany
syed-najaf-haider.shah@tu-ilmenau.de
Sept 8, 2023



Contents

- Motivation
- ISAC-capable 5G-V2X Sidelink System
 - System Model
 - Signal Model
- Proposed Approach
- Simulation Framework
- Simulation Results
- Outlook

Motivation

- Cellular Vehicle-to-Everything (C-V2X) networks are envisioned as a key enabler for future ITS supported by next-generation-cellular systems (5G-Advanced, 6G, etc.)
- In addition to communication capability, future C-V2X networks are also anticipated to have highly reliable and accurate radar sensing functionality to support environment-aware services.
- Integrated Sensing and Communication (ISAC) - a promising solution.
- Challenges in sharing the same spectral and hardware resources.

Our Focus:

- Integration of radar sensing into 5G-V2X Sidelink Communication (Mode 2/out-of-network coverage)
- ISAC-capable 5G-V2X Sidelink - exploiting sidelink signals for radar sensing



ISAC-capable 5G-V2X Sidelink System

System Model

Road Configuration:

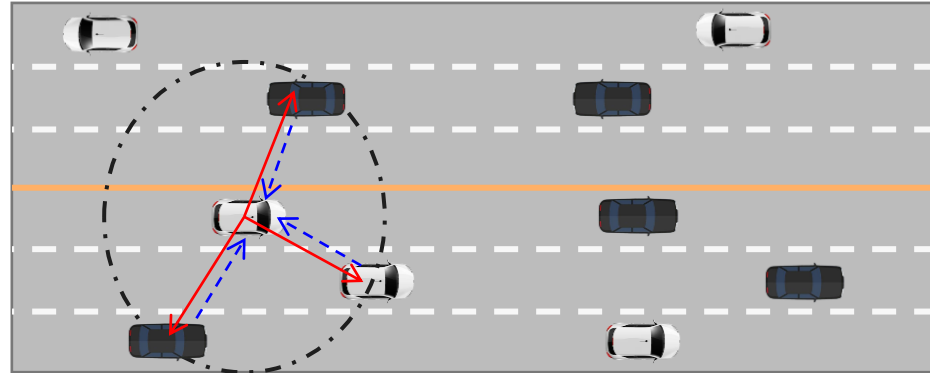
- Highway road model (3GPP TR 37.885¹)
- 2-way road with 3 lanes in each direction

All vehicles are equipped with in-band full-duplex (FD) transceivers for:

- simultaneous transmission and reception of data packets
- sensing the back-scattered sidelink signals (mono-static sensing)

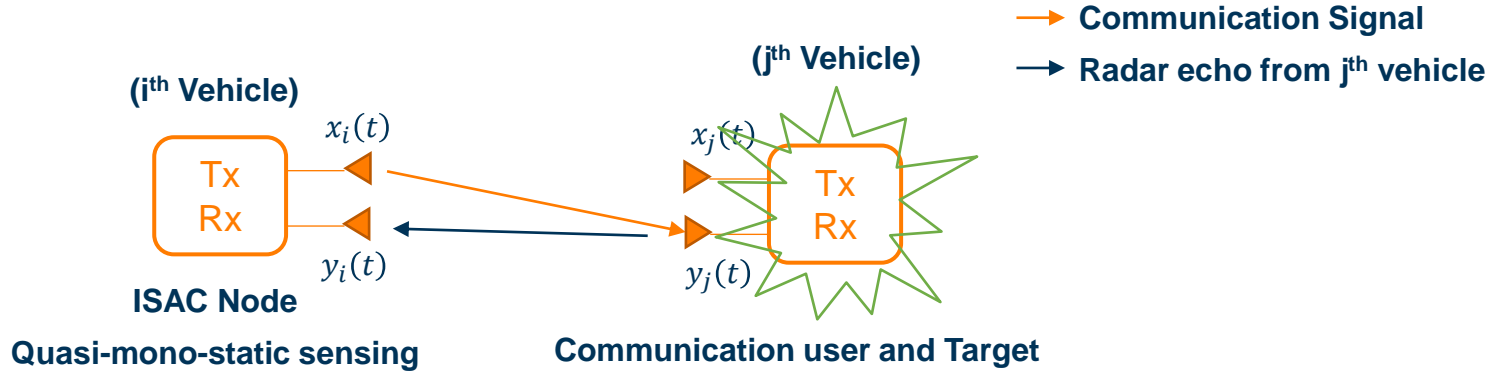
Communication with neighbor vehicles present in the communication range (dashed circle) through sidelink.

Detecting the range and relative velocity of neighbor vehicles through back-scattered signals under LoS conditions.



ISAC-capable 5G-V2X Sidelink System

Signal Model



Transmitted 5G-OFDM baseband signal from the i^{th} vehicle-UE:

$$x_i(t) = \underbrace{\sum_{m=0}^{M_c-1} \left(\sum_{n=0}^{N_c-1} s_{n,m}^{(c)} e^{j2\pi \frac{n}{T} t} \right) \text{rect}_T(t - mT_s)}_{\text{Communication resources}} + \underbrace{\sum_{m=0}^{M_r-1} \left(\sum_{n=0}^{N_r-1} s_{n,m}^{(r)} e^{j2\pi \frac{n}{T} t} \right) \text{rect}_T(t - mT_s)}_{\text{Radar resources}}$$

ISAC-capable 5G-V2X Sidelink System

Signal Model

Radar signal received back at the i^{th} vehicle-UE:

$$y_i(t) = x_i(t) * h_r(t) + z(t)$$
$$y_i(t) = \sum_{p=1}^P \gamma_p x_i(t - \tau_p) e^{j2\pi\alpha_p t} + z(t)$$

Communication signal received at the j^{th} vehicle-UE:

$$y_j(t) = x_i(t) * h_c(t) + \tilde{z}(t)$$
$$y_2(t) = \gamma x_1(t - \tau) e^{j2\pi\alpha t} + \tilde{z}(t)$$

Proposed Approach

Radar-Enabled Resource Allocation in NR Sidelink

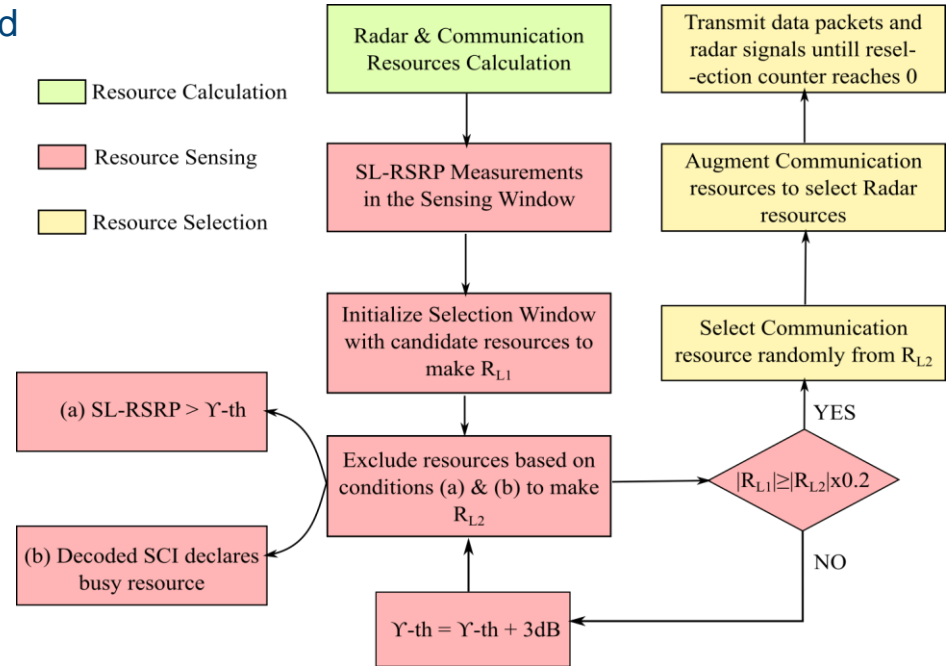
The proposed approach is based on sensing-based semi-persistent scheduling (SB-SPS).

In SB-SPS, the resource allocation is based on sensing the radio channel before selecting the resources for communication.

Our approach enables resource allocation for both communication and radar sensing tasks.

The approach consists of 3 steps:

- Resource Calculation
- Resource Sensing
- Resource Selection



Proposed Approach

Radar-Enabled Resource Allocation in NR Sidelink

Step 1: Resource Calculation

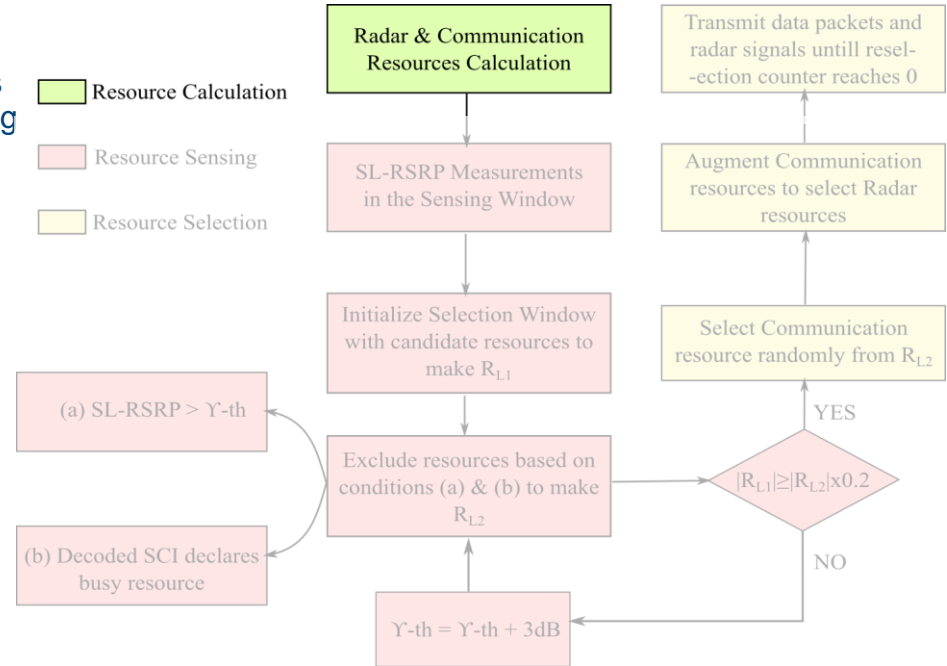
Given a 5G-OFDM resource pool, the number of resources (i.e., time slots and PRBs) needed to fulfill the radar sensing and communication requirements are first calculated.

• Radar Resources

$$\bullet \Delta r = \frac{c}{2N\Delta f} \Rightarrow N = \frac{c}{2\Delta r\Delta f}$$
$$\bullet \Delta v = \frac{c}{2f_c M T_s} \Rightarrow M = \frac{c}{2f_c \Delta v T_s}$$

• Communication Resources

- Time Resources \Rightarrow End-2-End Packet Latency
- Frequency Resources \Rightarrow Data rate and Reliability



Proposed Approach

Radar-Enabled Resource Allocation in NR Sidelink

Step 2: Resource Sensing

Sensing Window – SL-RSRP measurements

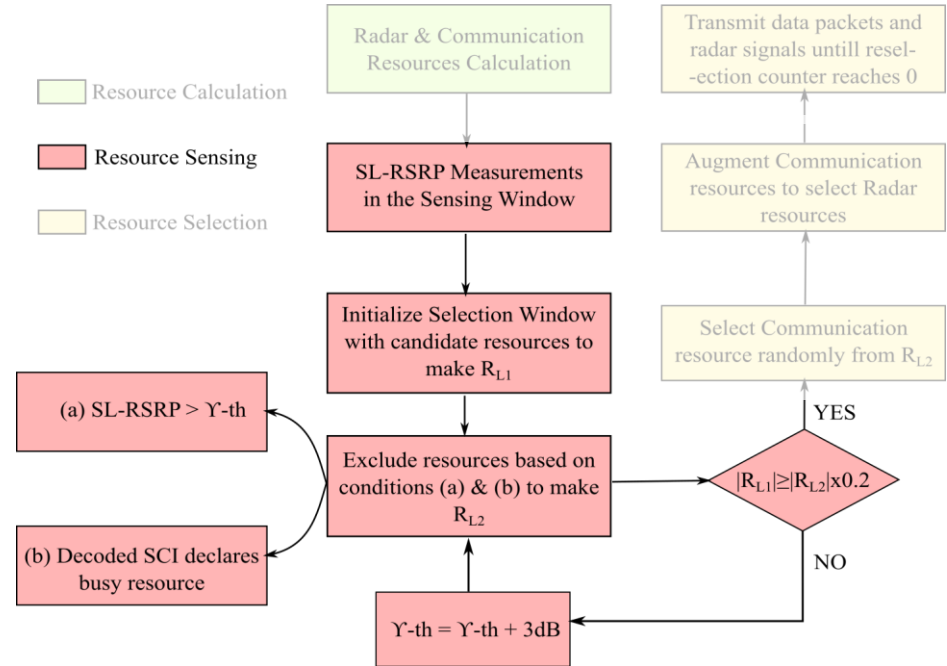
Selection Window – Set of candidate resources

Exclusion of resources from the selection window:

- The decoded SCI declares that the resource is occupied.
- The $SL\text{-RSRP} \geq \text{predefined threshold}$.

Check available resources:

- Are the available resources $\geq 20\%$ of candidate resources?



Proposed Approach

Radar-Enabled Resource Allocation in NR Sidelink

Step 3: Resource Selection

The number of resources calculated in Step 1 will be selected for both communication and radar sensing tasks.

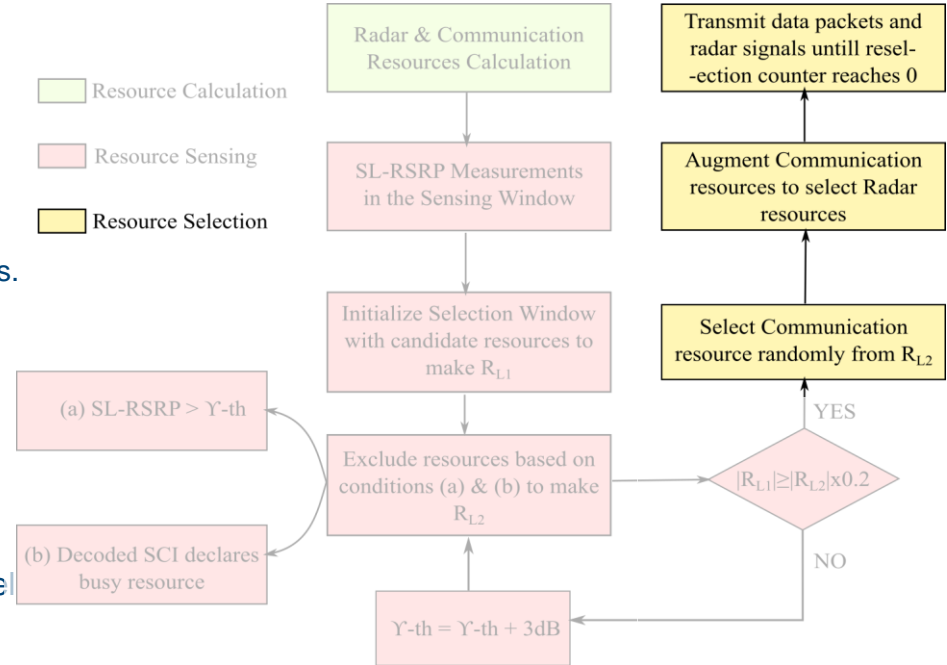
• Communication Resource Selection

- Random resource selection from the available resources.
- Resource reservation for the next n_{rc} transmissions

• Radar Resource Selection

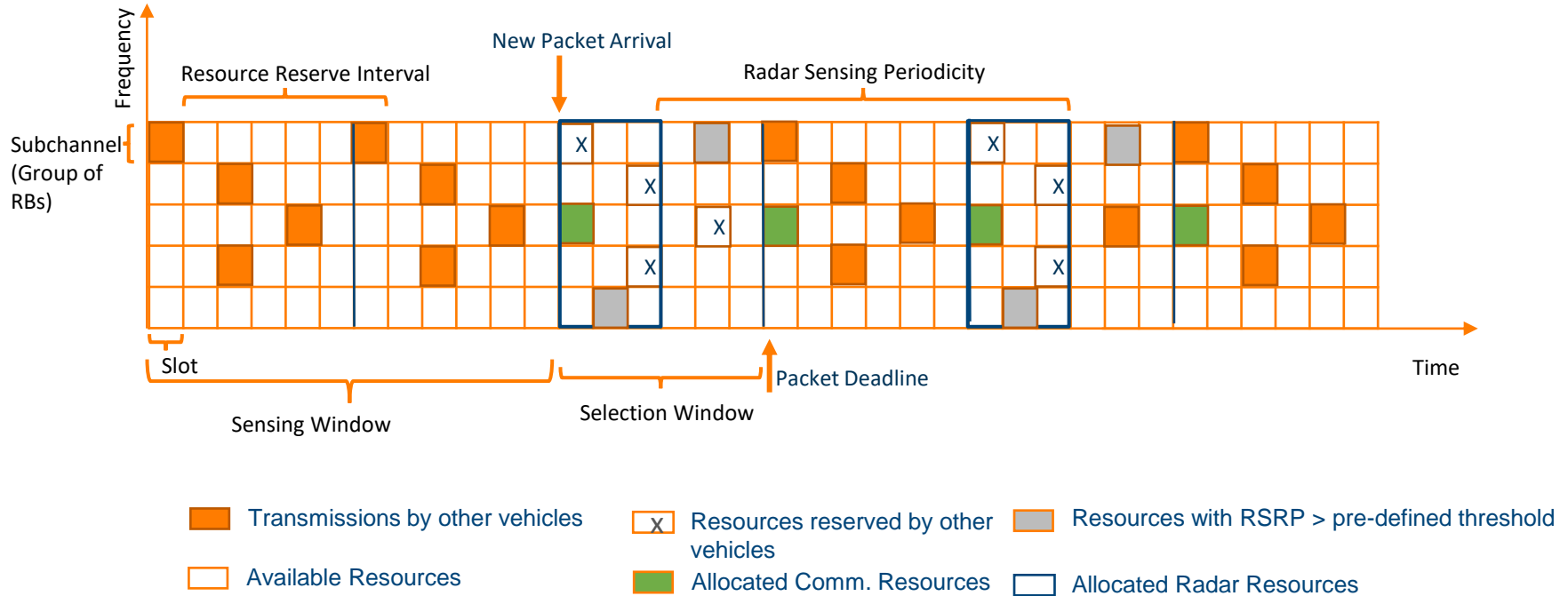
- Augmentation of communication resources (both time and frequency domain resources) to select radar resources.
- No reservation of radar resources to reduce channel occupancy

Transmission of ISAC resources until $n_{rc} = 0$.

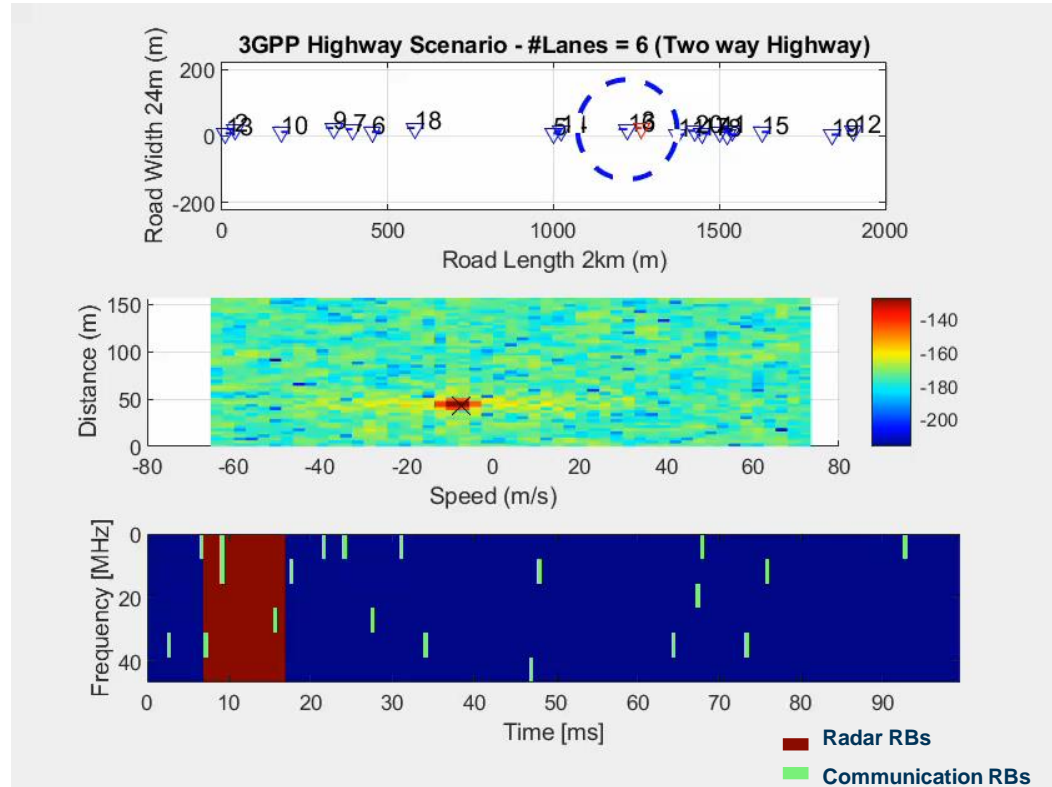
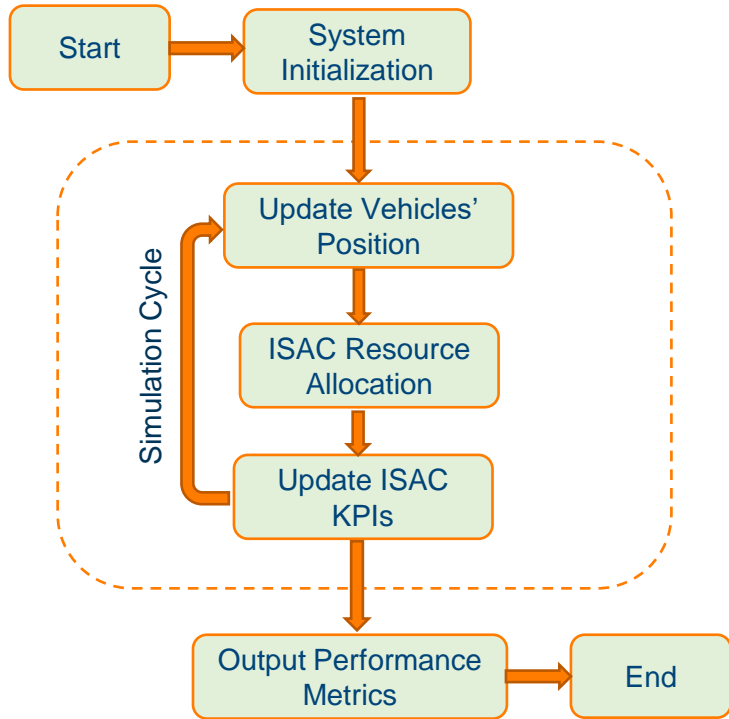


Proposed Approach - Overview

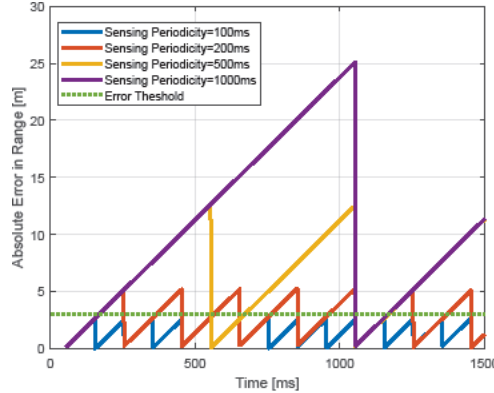
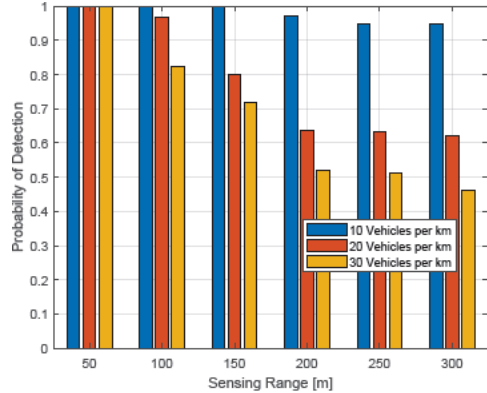
Radar-Enabled Resource Allocation in NR Sidelink



Simulation Framework



Simulation Results

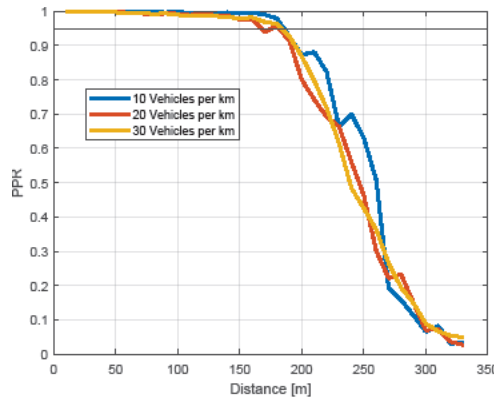
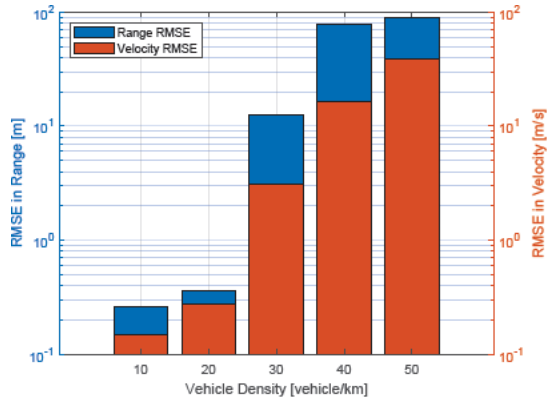


Top Left: Detection Probability as a function of Sensing Range under vehicle densities of 10, 20, and 30 vehicles per km.

$$PoD = \frac{\# \text{ Vehicles Detected}}{\# \text{ Total vehicles Present}}$$

Top Right: Absolute Error in Range Estimations under Sensing Periodicities of 100, 200, 500, and 1000 ms.

$$E_r = |r_{est} - r_{true}|$$



Bottom Left: RMSE in Range and Velocity estimations as a function of vehicle density

$$RMSE = \sqrt{\frac{\|k_{est} - k_{true}\|^2}{K}}$$

Bottom Right: Packet Reception Ratio as a function of the distance between TX and RX vehicles for vehicle densities of 10, 20, and 30 vehicles per km.

$$\text{Mean PRR} = \frac{1}{N} \sum_{n=1}^N \frac{P_{r,n}}{P_t}$$

Outlook

- **Realistic Environment and Propagation Model**
 - Different types of scatterers (Static clutter, diffused scattering, etc.)
 - Strong Multipath components
- **Power Allocation between Communication and Radar sensing tasks**
- **Sparse Resource Allocation**
 - Minimizing ISAC Resources
 - Efficient Spectrum Usage

Thank you for your attention





On Vehicular Model Reduction for Antenna Simulation Using Spherical Wave Expansion

N. D. Chaudhury⁽¹⁾⁽²⁾, L. Berkelmann⁽¹⁾, B. Jannsen⁽¹⁾, J. Robert⁽²⁾

(1) Volkswagen AG, Wolfsburg, Germany

(2) Technische Universität Ilmenau, Ilmenau, Germany

Agenda

- **Motivation**
- **Previous Methods of Model Reduction**
- **Simulation Model Reduction using Spherical Wave Expansion Theory**
- **Demonstration of the proposed Model Reduction Technique**
- **Conclusion**



Motivation

- **Free-space simulation of automotive antennas does not reveal the “true” picture of its performance.**
 - Antennas are electromagnetically coupled with metallic car body.
- **A car is electrically large.**
 - Lots of mesh cells
 - Demanding computer resources
 - Long simulation time
 - Delay in overall antenna development time.
- **Solution: Reduction of automotive CAD model.**
 - The car-antenna coupling limited within the immediate antenna neighborhood.
- **The idea is to find those electromagnetically significant regions of the car.**



Previous methods

1. Based on guess work.

- Depends on experience of simulation engineer.
- Not always correct.

2. Based on examining surface Electric currents/ Electric fields.

- Difficult to pinpoint properly the electromagnetically significant parts.
 - Depends on experience of simulation engineer.
- **Our proposed method performs model reduction, directly using the 3D far-field radiation.**



Simulation Model reduction using Spherical Wave Expansion

Short introduction to Spherical Wave Expansion (SWE)

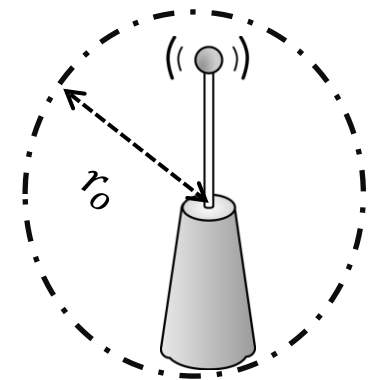
- Using SWE, the far-field can be expressed as a summation of spherical wave function.

$$\vec{E}(r, \theta, \varphi) = \frac{k}{\sqrt{\eta}} \sum_{s=1}^2 \sum_{n=1}^N \sum_{m=-n}^n Q_{smn} \cdot \vec{F}_{smn}(r, \theta, \varphi)$$

Outward propagating electric field
Expansion coeff.
Spherical wave function

- Theoretically, $N \rightarrow \infty$. But for all practical purposes, N can be taken as $N \cong [k \cdot r_o]$.
- Cumulative Modal Power (CMP) \rightarrow Total power of all modes of $n=1 \dots N$.

$$CMP = \frac{1}{2} \sum_{s=1}^2 \sum_{n=1}^N \sum_{m=-n}^n |Q_{smn}|^2$$



Simulation Model reduction using Spherical Wave Expansion

Application of SWE in model reduction

$$\vec{E}(r, \theta, \varphi) = \frac{k}{\sqrt{\eta}} \sum_{s=1}^2 \sum_{n=1}^N \sum_{m=-n}^n Q_{smn} \cdot \vec{F}_{smn}(r, \theta, \varphi)$$

- **Finding the cut off value of N , i.e., $N_{cut-off}$**
 - Enough to represent the far-field with "good accuracy"
 - Criteria: CMP (for $n=1$ to $N_{cut-off}$) \approx TRP of full-scale car simulation
 - Corresponding minimum sphere:

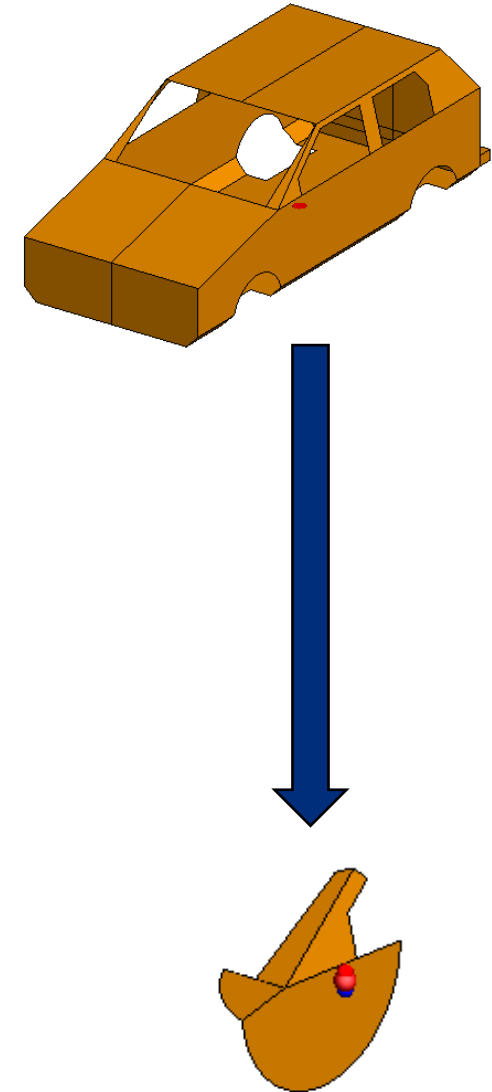
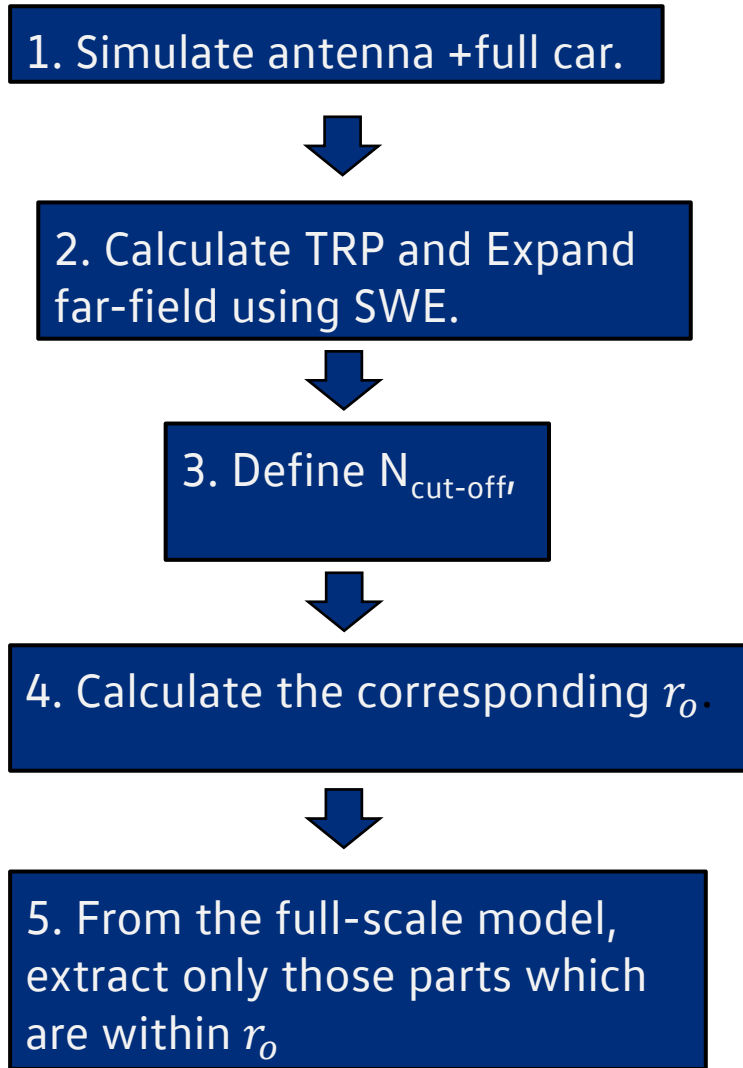
$$r_o \cong \frac{N_{cut-off}}{k}$$

- **Parts within minimum sphere are electromagnetically significant**



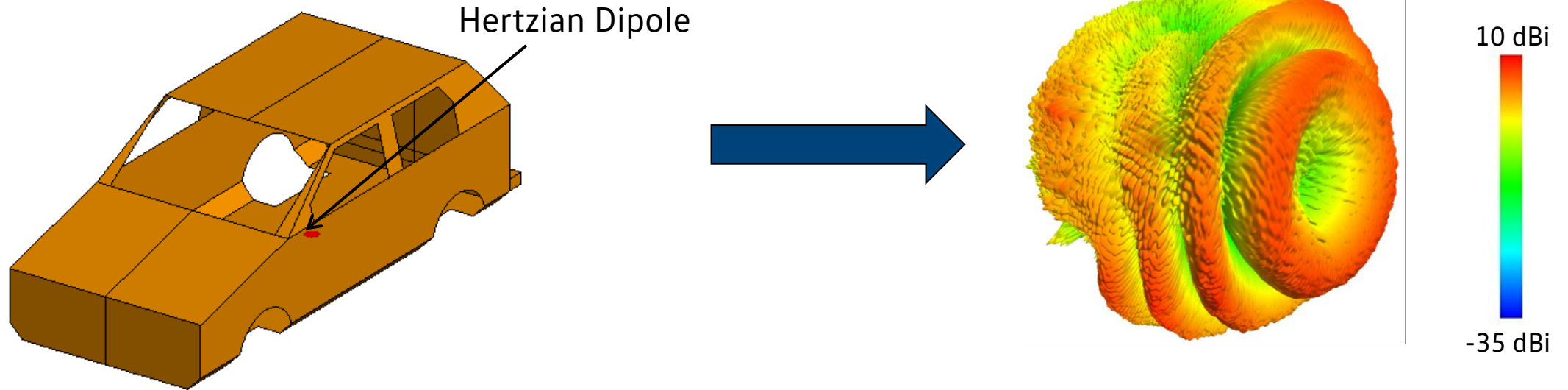
Simulation Model reduction using Spherical Wave Expansion

Application of SWE in model reduction



Demonstration of model reduction technique

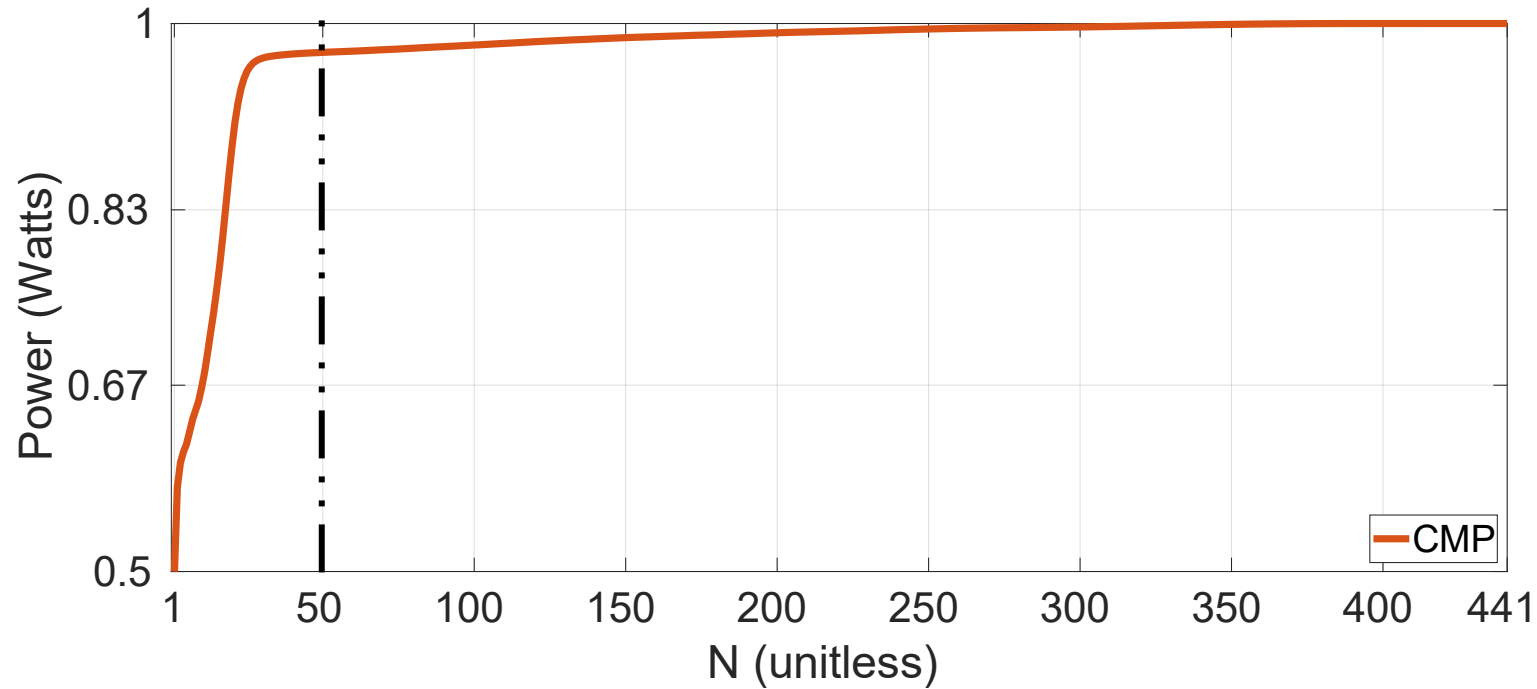
Simple car model simulation



- Antenna-chassis spacing: 2λ
- Frequency: 5.9 GHz
- Solver: Altair FEKO's MLFMM
- The TRP is set to 1 Watt

Demonstration of model reduction technique

SWE and CMP calculation

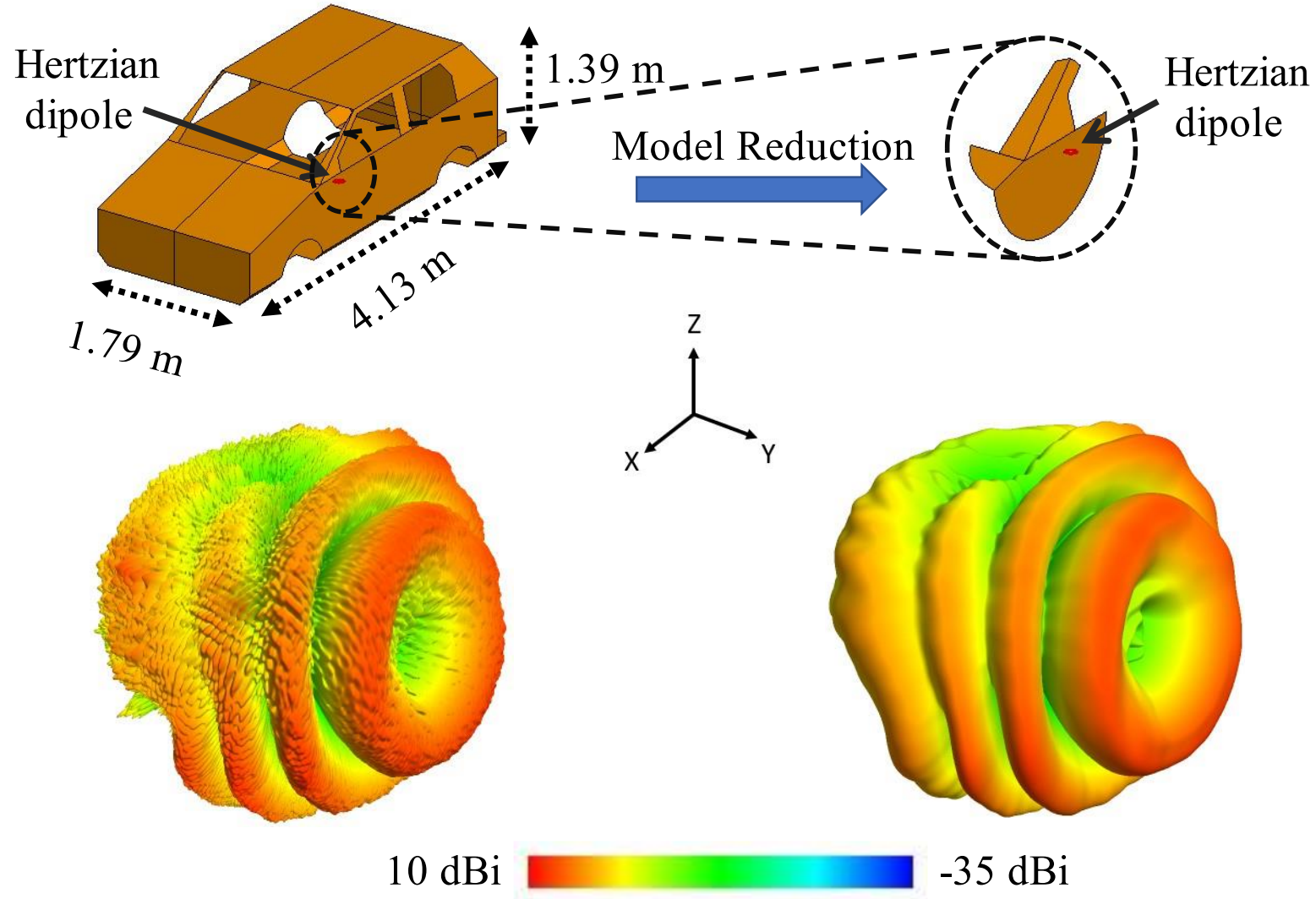


- **At $N = 50$**
 - CMP=0.97 Watts \rightarrow so $N_{cut-off} = 50$
 - $r_o = 0.41 m$



Demonstration of model reduction technique

Comparison



Demonstration of model reduction technique

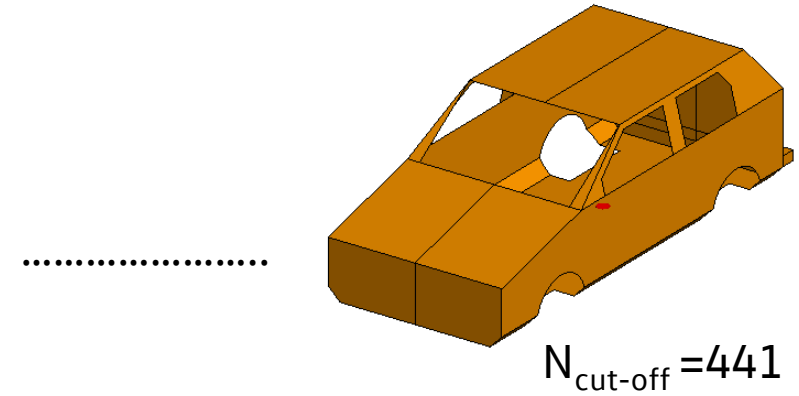
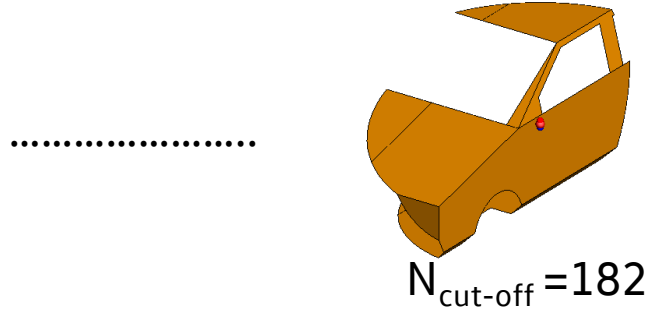
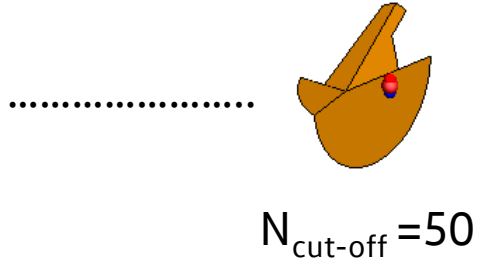
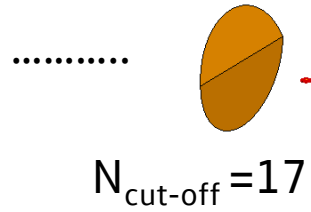
Comparison

Parameters	Full-scale structure	Reduced structure
Mesh cells	27,74,670	49,162 (-98%) 
Simulation time	1044.94 sec	36.5 sec (-96%) 
Memory requirement	16.1 GB	307.8 MB (-98%) 
Cosine Similarity ¹	-	0.97 

1. J. Singh, A. Asgharzadeh, R. Stephan and M. A. Hein, "Influence of Car Body Modeling on the Gain Patterns of Automotive Antennas," *2017 IEEE 85th Vehicular Technology Conference (VTC Spring)*, Sydney, NSW, Australia, 2017, pp. 1-5

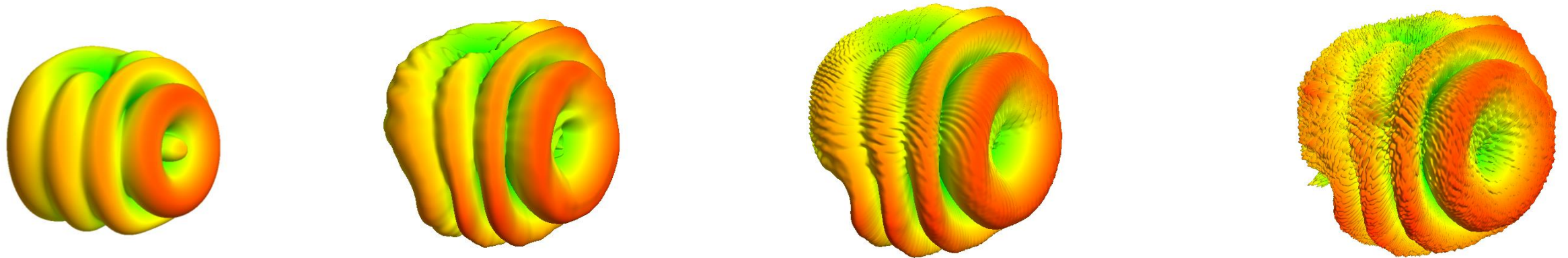
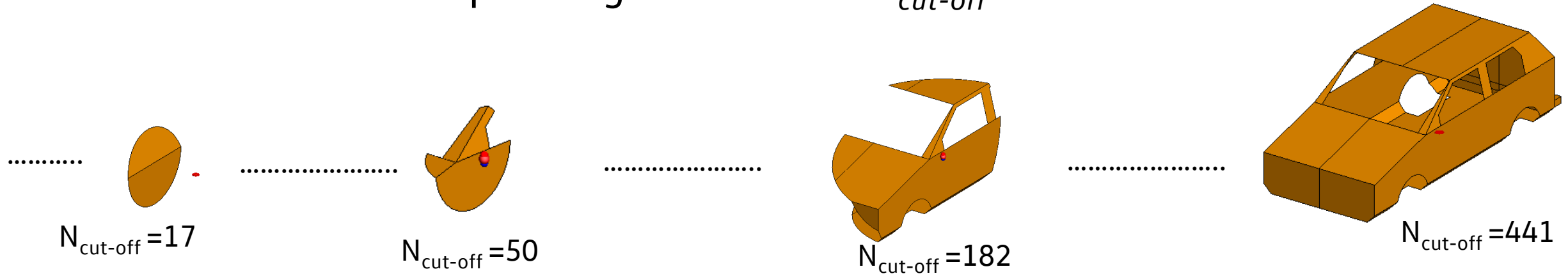
Demonstration of model reduction technique

Reduced models corresponding to different $N_{cut-off}$



Demonstration of model reduction technique

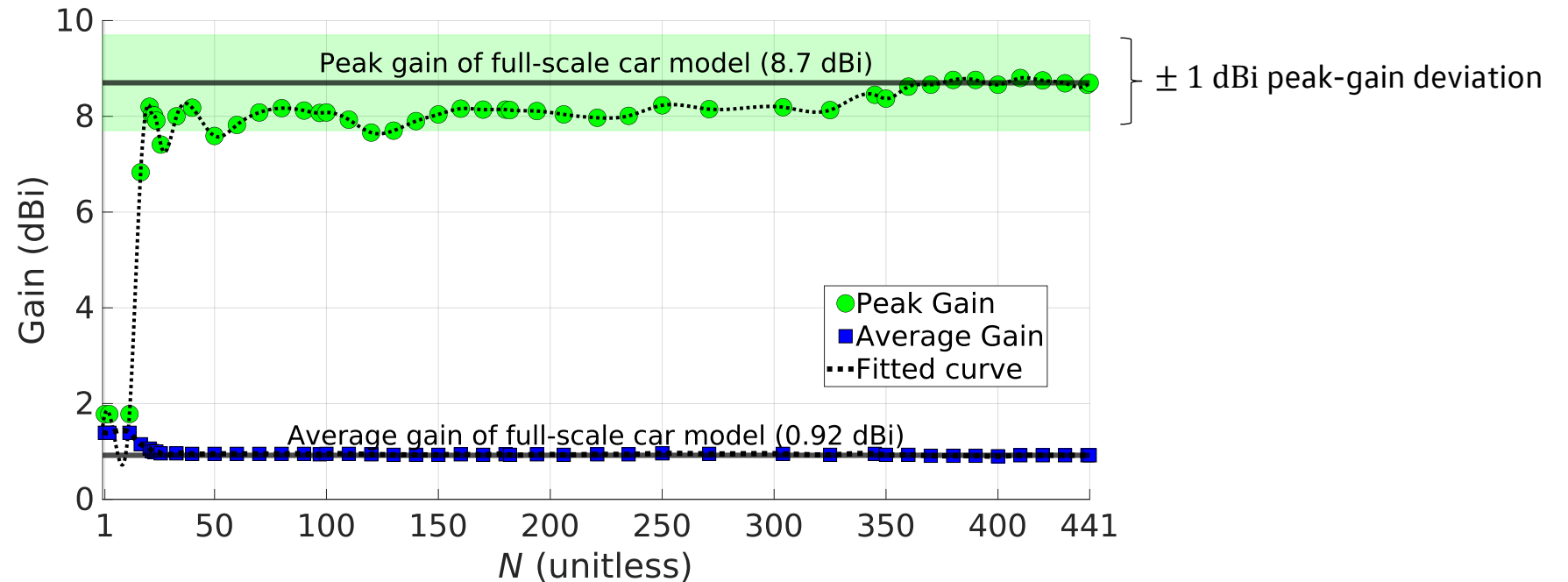
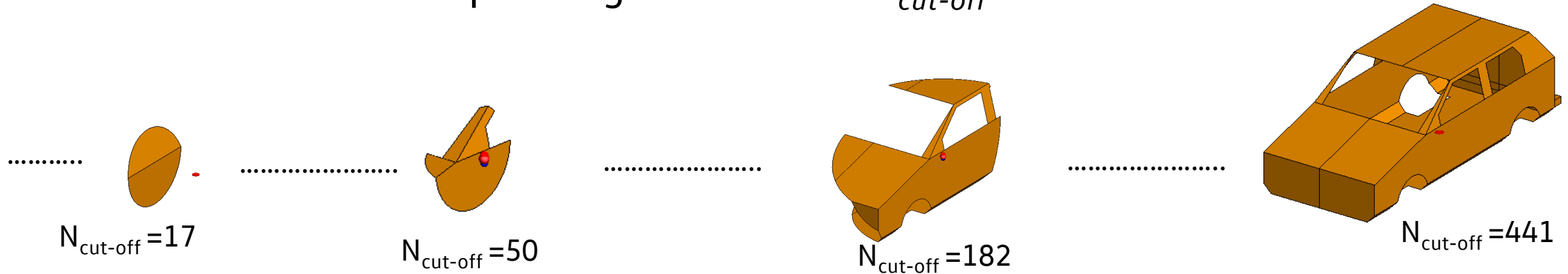
Reduced models corresponding to different $N_{cut-off}$



Accuracy increases along with simulation time!

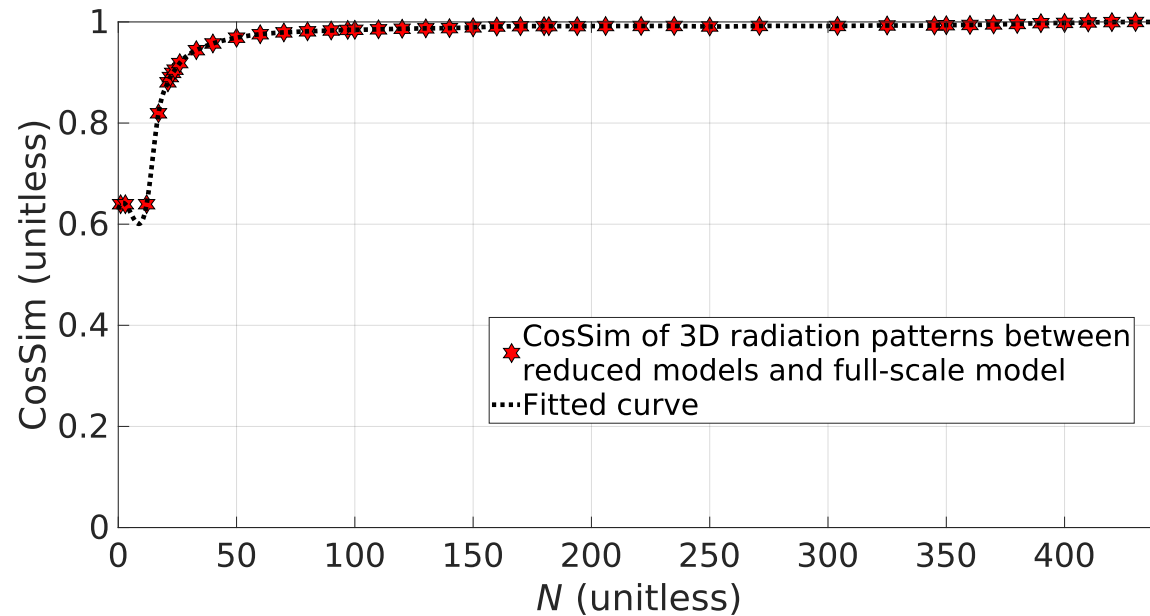
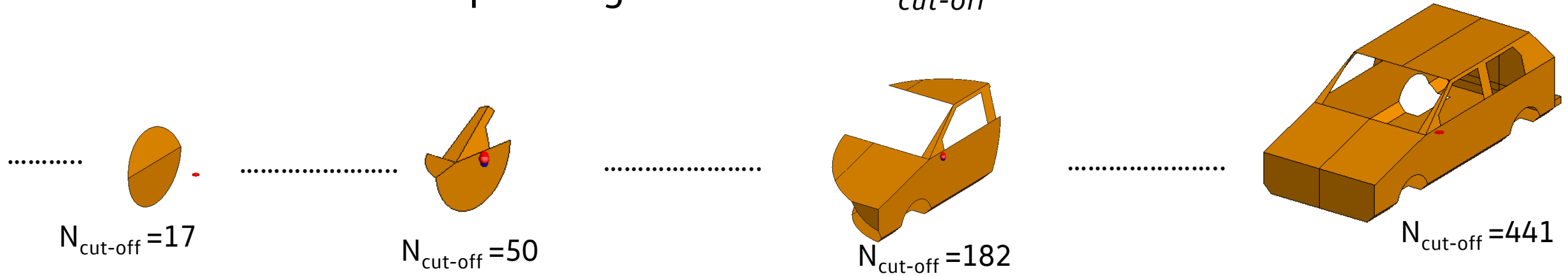
Demonstration of model reduction technique

Reduced models corresponding to different $N_{cut-off}$



Demonstration of model reduction technique

Reduced models corresponding to different $N_{cut-off}$



Demonstration of model reduction technique

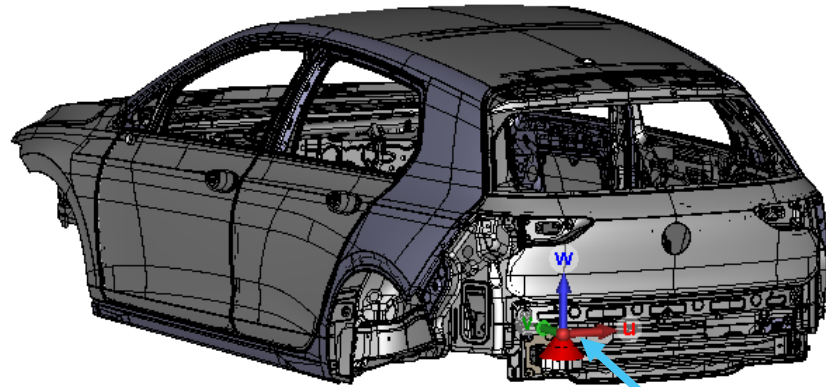
Further comments

- **One apparent problem with this technique:**
 - Need to simulate the antenna + full car in the step-1.
- **Solution:**
 - Extract reduced model using simple antennas (for e.g., Hertzian dipole, Monopole).
 - Use the reduced model to simulate more complex real-life antenna.
 - Details will be submitted in the extended version of this work.



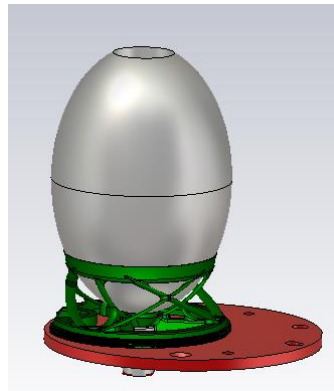
Demonstration of model reduction technique

Short demonstration using real car model

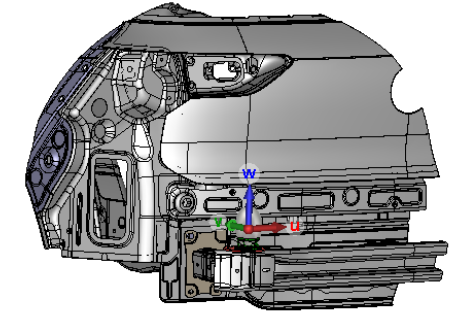


Location of $\lambda /4$ antenna

- Frequency: 2.3 GHz



Reference antenna for testing

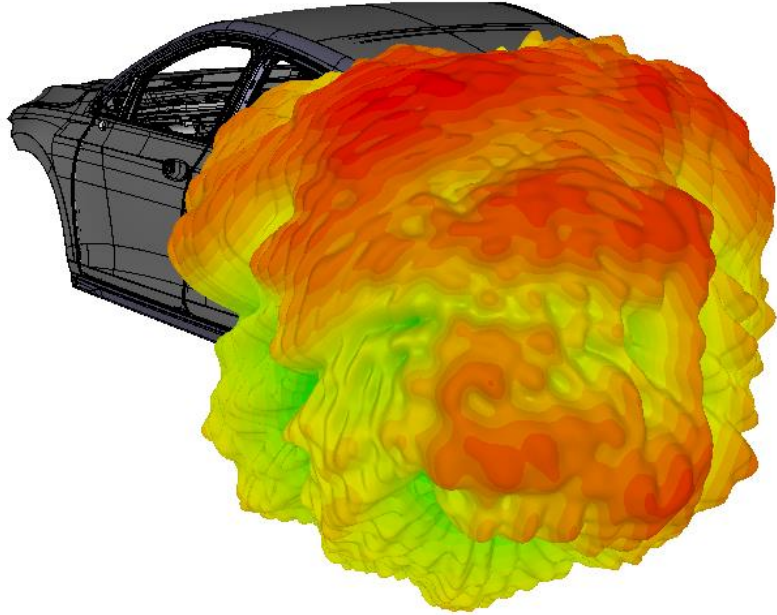


Reduced structure:

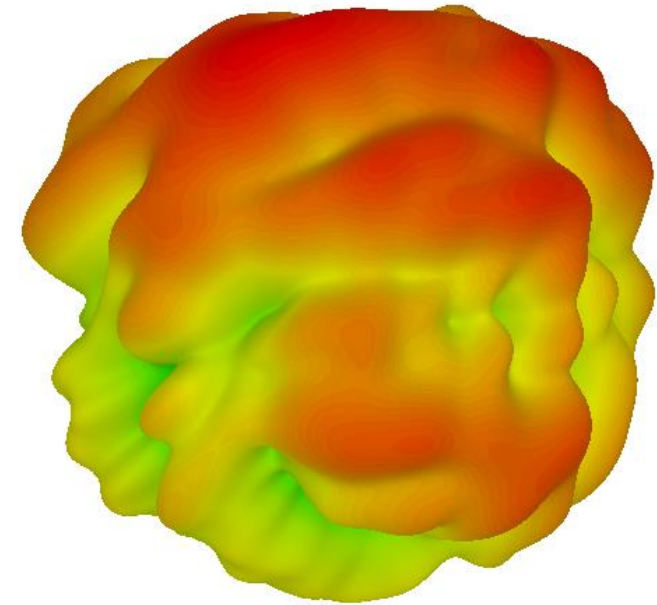
- $r_o = 0.56$ m (CMP=0.97 Watt)

Demonstration of model reduction technique

Short demonstration using real car model



Full-scale car model



Reduced car model

Cosine similarity: 0.98

Conclusion

- A novel model reduction technique has been developed using SWE.
- In this presentation, a demonstration of technique was shown using a simple car model and Hertzian dipole antenna.
- In the demonstration, we were able to achieve a significant reduction in Mesh cells, simulation time and memory requirement without compromising the far field results.
- Additionally, the choice of $N_{cut-off}$ depends on parameter of interest (Average gain or Peak gain).





Thank you for your attention!

Email: nandan.dutta.chaudhury@volkswagen.de

 : <https://de.linkedin.com/in/ndchaudhury>



UNIVERSITAT
POLITÈCNICA
DE VALÈNCIA



BOSCH

UNIVERSITY
OF TWENTE.



TECHNISCHE
UNIVERSITÄT
ILMENAU

4P WAVES



Fivecomm



casa systems



BLUETEST.se



DAIMLER



RanLOS



Fraunhofer
IIS

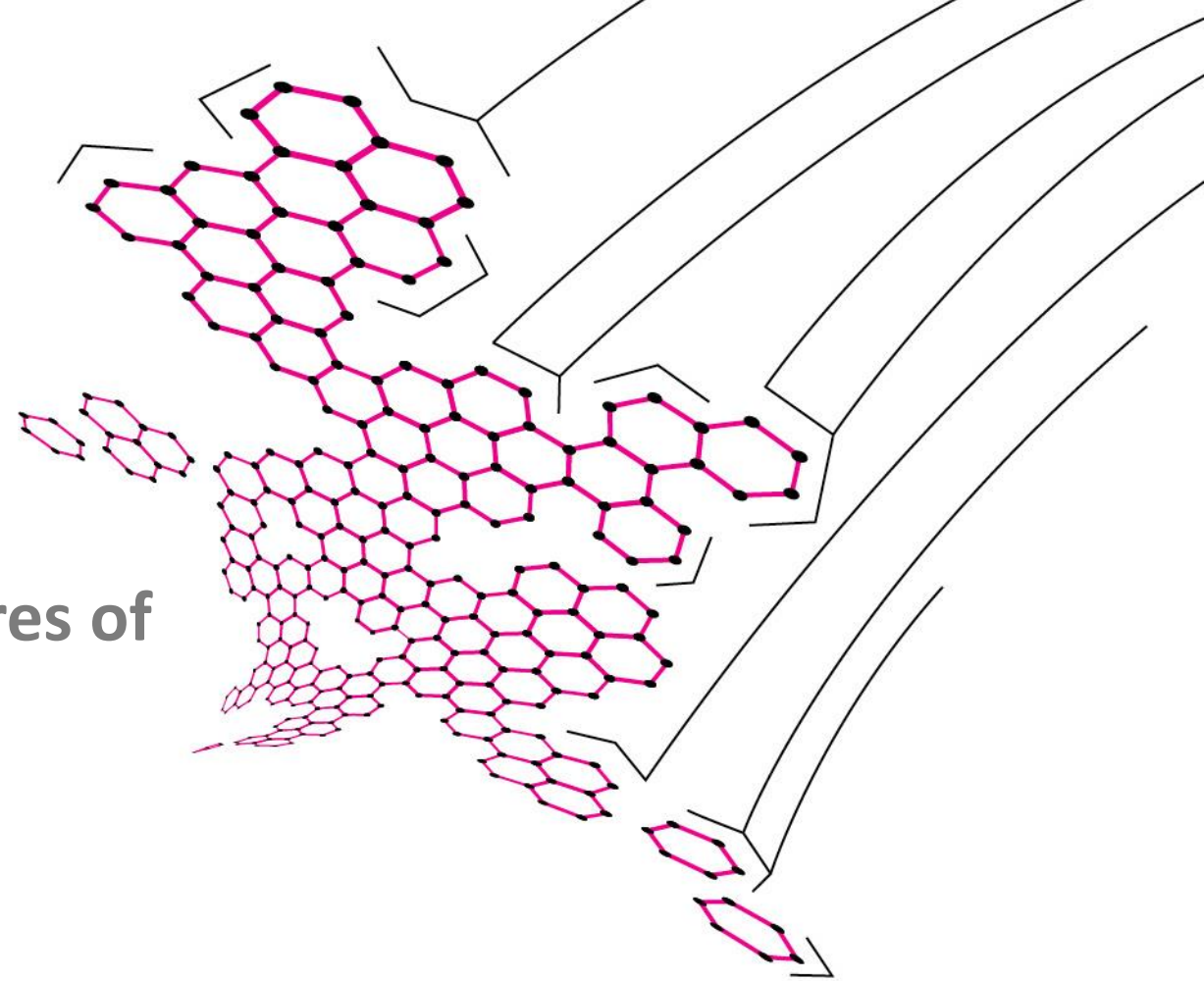
Correlation and Non-Orthogonality Figures of Merit of Beamforming Fields

Reza Gheybi Zarnagh, Andrés Alayón Glazunov

September 19, 2023

ITN-5VC

r.gheybizarnagh@utwente.nl



Outline



- Introduction
- Beam Correlation
- Beam Non-Orthogonality
- Franklin Array Antennas
- Results
- Conclusions

Introduction

- For multipath environments, the correlation coefficient between the antennas is often evaluated.
- The **envelope correlation coefficient (ECC)** is a measure of the signal correlation in a rich isotropic multipath (RIMP) environment:

$$\rho_{ECC} = \frac{|\oint F_1 \cdot F_2^* d\Omega|^2}{\oint |F_1|^2 d\Omega \oint |F_2|^2 d\Omega}$$

Where F_1 and F_2 are the embedded radiation patterns of the considered antennas and the symbol * denotes the complex conjugate operation.

Introduction

- In a pure line-of-sight (LOS) or equivalently in a Random LOS (RLOS or RanLOS), instead of the correlation the **polarization non-orthogonality** (or co-linearity) is evaluated:

$$\rho_{NOR} = \frac{|F_1 \cdot F_2^*|}{|F_1| |F_2|}$$

Where F_1 and F_2 are the embedded radiation patterns of the considered antennas.

- If the antennas are orthogonally polarized, it follows that $\rho_{ECC} = \rho_{NOR} = 0$.
- If the radiation patterns are the same, then $\rho_{ECC} = \rho_{NOR} = 1$.
- For all other conditions, partial correlation or partial non-orthogonality $0 < \rho_{ECC}, \rho_{NOR} < 1$.

Introduction

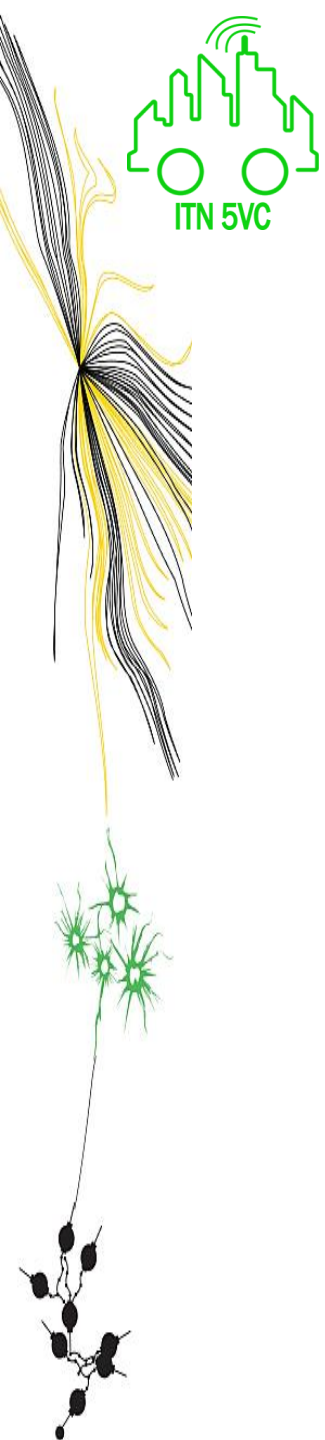
- In the case of **multiple-beam antennas** or **scanned-beam antennas**:



- The radiation pattern will change depending on the direction of observation.
- Depending on the scanning capability, the correlation and the non-orthogonality change.



We introduce a generalization of the envelope correlation coefficient and the polarization non-orthogonality to the case of multi-beam or scanning beam antennas.



Beam Correlation



- We introduce the beam correlation (BC) of an array antenna:

$$\rho_{11,BC}(\alpha, \beta) = \frac{\left| \oint F_1(\alpha) \cdot F_1^*(\beta) d\Omega \right|^2}{\oint |F_1(\alpha)|^2 d\Omega \oint |F_1(\beta)|^2 d\Omega}$$

Where $F_1(\alpha)$ and $F_1(\beta)$ are the beamforming fields of an array antenna at scanning (beamforming) angles of α and β , respectively.

- For sufficiently separated beams in the angular domain, the correlation is low; while for $\alpha = \beta$, the correlation is full ($\rho_{11,BC}(\alpha, \beta) = 1$).
- We can define the same type of correlation for two co-located or two distributed array antennas:

$$\rho_{12,BC}(\alpha, \beta) = \frac{\left| \oint F_1(\alpha) \cdot F_2^*(\beta) d\Omega \right|^2}{\oint |F_1(\alpha)|^2 d\Omega \oint |F_2(\beta)|^2 d\Omega}$$

Where F_1 and F_2 are the beamforming fields of two array antennas at scanning (beamforming) angles of α and β .

Beam Correlation



- We can interpret $\rho_{11,BC}$ as the **beamforming-field directional auto-correlation**, while $\rho_{12,BC}$ is the **beamforming-field directional cross-correlation**.

- The overall correlation between the two antennas can be characterized by the product:

$$\rho_{12,BCW}(\alpha, \beta) = \sqrt{\rho_{12,BC}} \sqrt{\rho_{11,BC} \rho_{22,BC}}$$

- When the two array antennas have identical performance, then $\rho_{12,BCW} = \rho_{11,BC} = \rho_{22,BC}$.

Beam Non-Orthogonality

- We here introduce, the beam non-orthogonality (BNO) of an array antenna:

$$\rho_{11,BNO}(\alpha, \beta) = \frac{|F_1(\alpha) \cdot F_1^*(\beta)|}{|F_1(\alpha)| |F_1(\beta)|}$$

Where $F_1(\alpha)$ and $F_1(\beta)$ are the beamforming fields of an array antenna at scanning (beamforming) angles of α and β .

- For two co-located or two distributed array antennas:

$$\rho_{12,BNO}(\alpha, \beta) = \frac{|F_1(\alpha) \cdot F_2^*(\beta)|}{|F_1(\alpha)| |F_2(\beta)|}$$

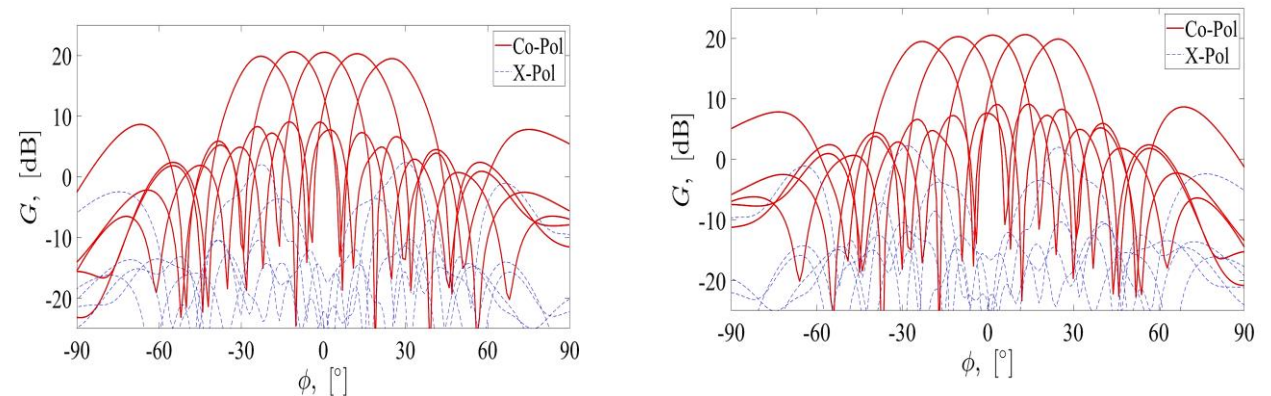
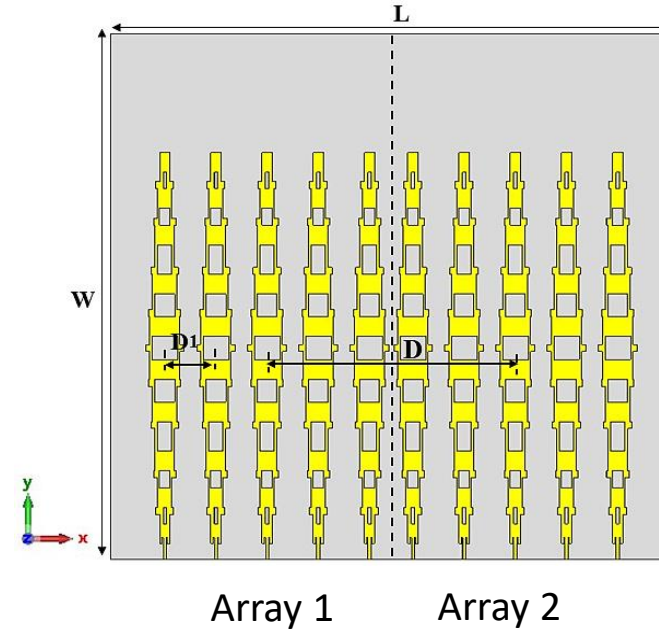
- A condensed parameter follows from the above definitions:

$$\rho_{12,BNOW}(\alpha, \beta) = \sqrt{\rho_{12,BNO} \sqrt{\rho_{11,BNO} \rho_{22,BNO}}}$$

Franklin Array Antennas



- The 5 × 10 Franklin array antennas:
- They may represent an example of arrays that can be used for either **communication** or **sensing**, or either as the **transmitter (Tx)** and **receiver (Rx)** parts of a communication/radar system.
- Beamforming is computed for each array and the radiation patterns are scanned from $\phi = -25^\circ$ to $\phi = 25^\circ$ in the azimuth plane.

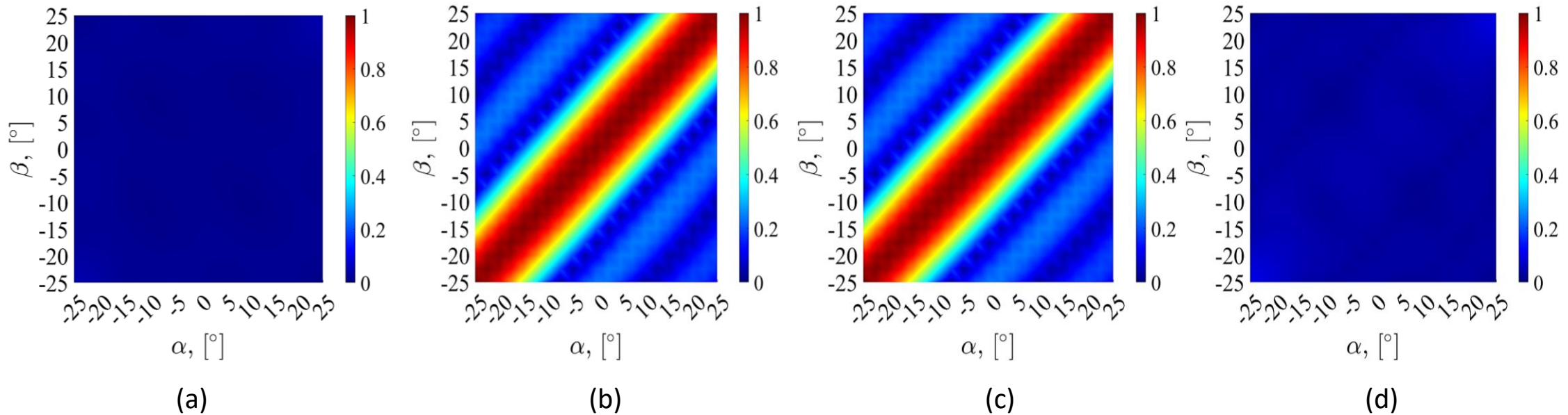


Co-polarized and X-polarized
simulated scanned patterns (E-plane)

Results



- Evaluation of the beam correlation:

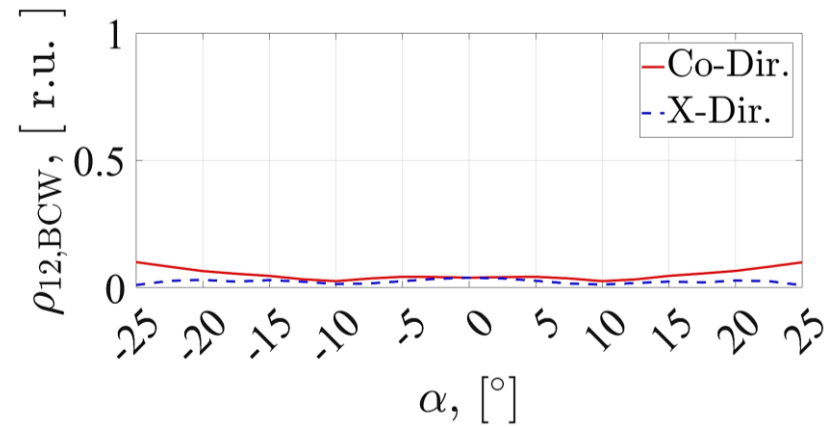
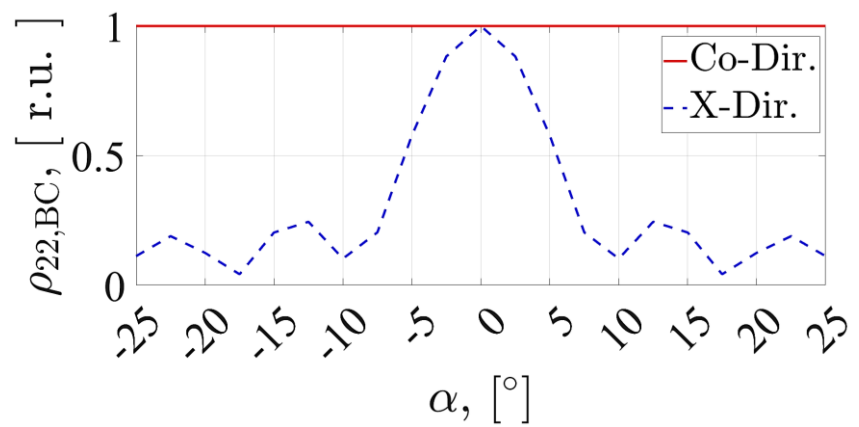
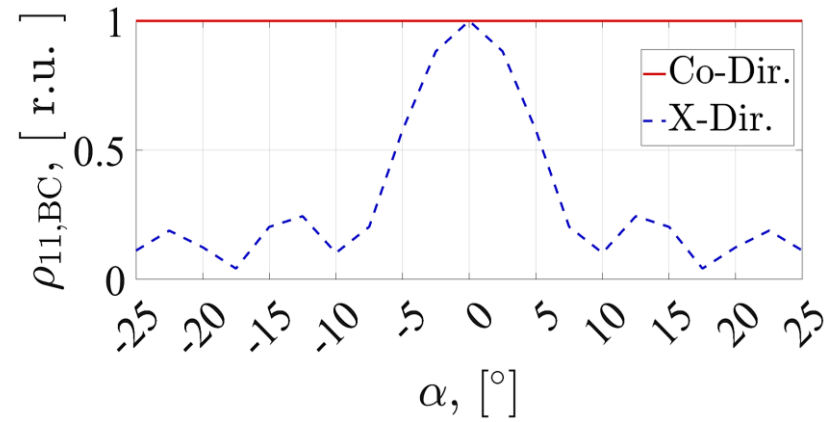
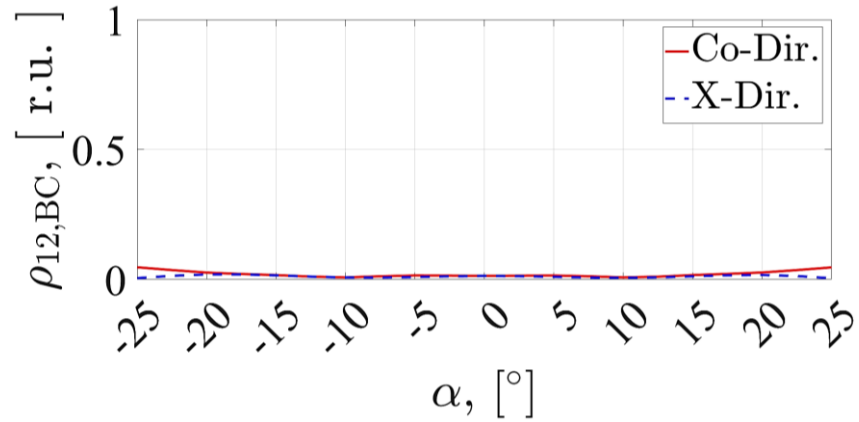


Beam correlation between the 5 scanned beams as a function of the scanning angles of the two simulated arrays. (a) $\rho_{12,BC}$, (b) $\rho_{11,BC}$, (c) $\rho_{22,BC}$, and (d) $\rho_{12,BCW}$.

Results



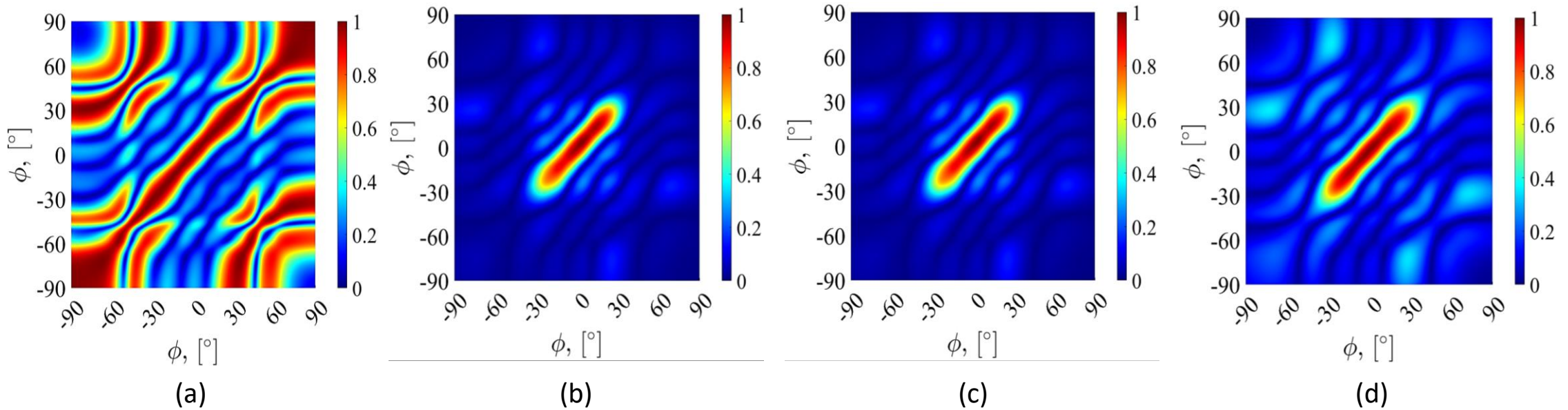
- Evaluation of the beam correlation:



Two cuts are taken from beam correlation plots, along the diagonal denoted by Co-Dir., and along the anti-diagonal denoted by X-Dir.



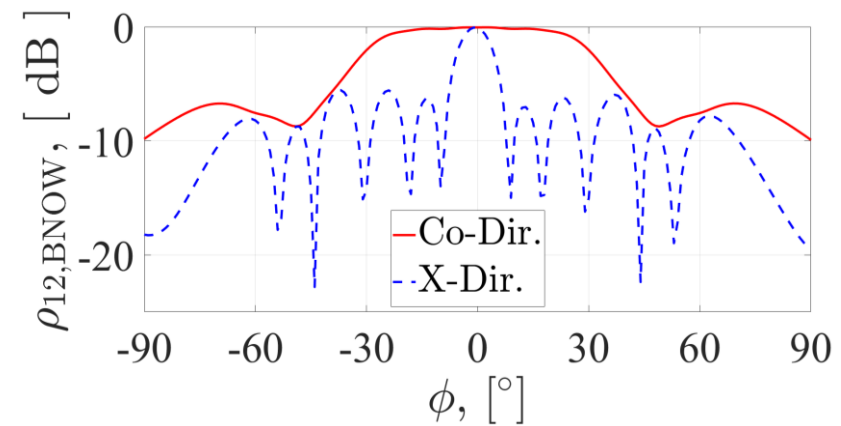
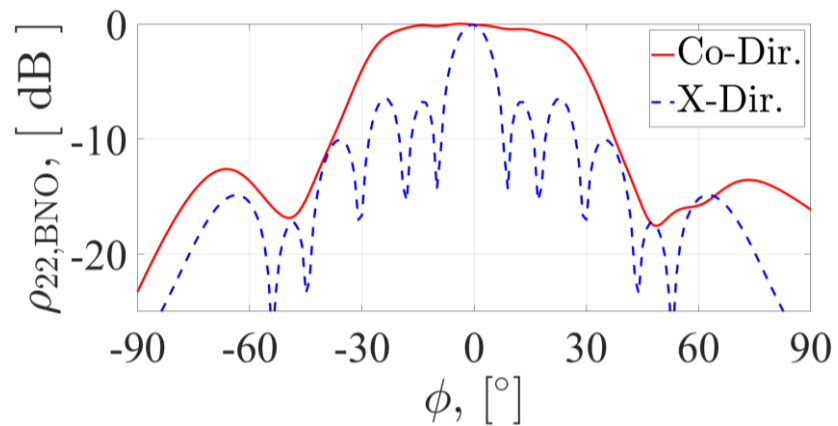
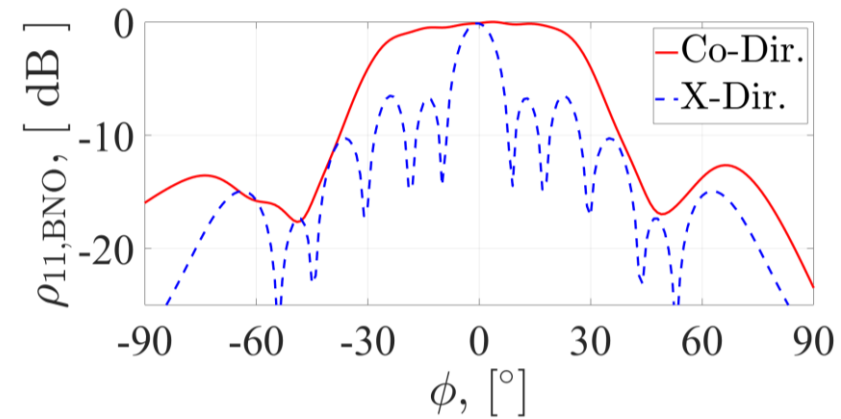
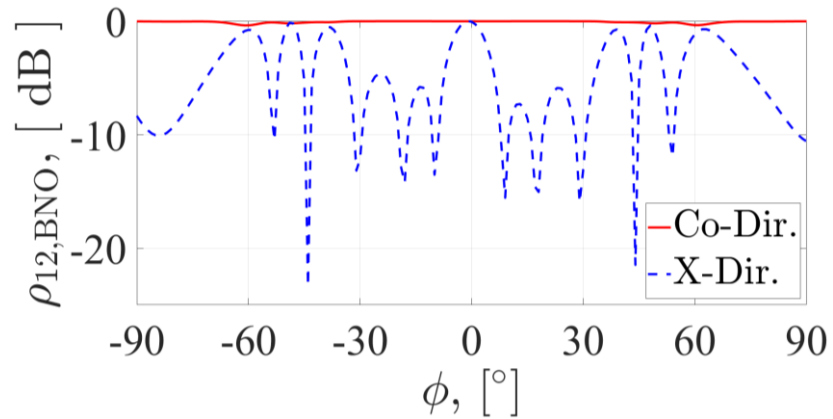
- Evaluation of the beam non-orthogonality:



Beam non-orthogonality for the 5 scanned beams as a function of Azimuth. (a) $\rho_{12,BC}$, (b) $\rho_{11,BC}$, (c) $\rho_{22,BC}$, and (d) $\rho_{12,BCW}$.

Results

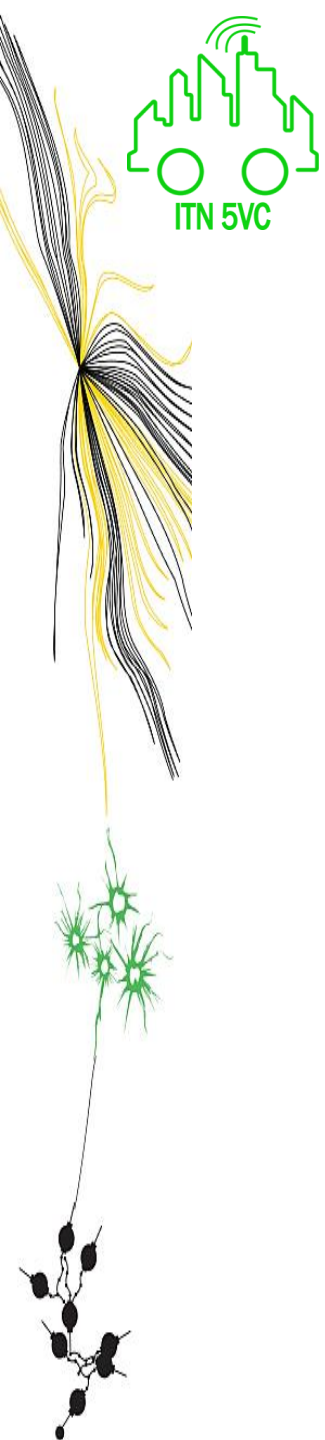
- Evaluation of the beam non-orthogonality:



Two cuts are taken from beam non-orthogonality plots, along the diagonal denoted by Co-Dir., and along the anti-diagonal denoted by X-Dir.

Conclusions

- New figures of merits to evaluate the correlation and the non-orthogonality have been presented.
- The workings of the figures of merit were shown on the example of two adjacently positioned array antennas consisting of 5 Franklin sub-arrays operating at 77 GHz.
- Analysis show that the beamforming fields produced by the two arrays are uncorrelated in rich multipath environments but have high correlation in pure- or random line-of-sight environments.





Thank you for your attention!

Contact

itn5vc.eu



itn5vc.eu

itn5vc@iteam.upv.es



5vc@iteam.upv.es

ITN-5VC



ITN-5VC

@5vcitn



@5vcitn

ITN-5VC



UNIVERSITAT
POLITÈCNICA
DE VALÈNCIA



BOSCH

UNIVERSITY
OF TWENTE.



TECHNISCHE
UNIVERSITÄT
ILMENAU

4P WAVES



Fivecomm



casa systems



BLUETEST.se



DAIMLER



RanLOS



Fraunhofer

IIS



Performance Evaluation of an MMSE-Based PSSCH Receiver under Fading Channel

Yang Fu

CASA Systems

This project has received funding from the European Union's
Horizon 2020 research and innovation program under the
Marie Skłodowska-Curie grant agreement No. 955629.



Contents



Self-
Introduction



Introduction



Physical layer
algorithm
design



Simulation
environment
and results



Conclusion

Self-introduction

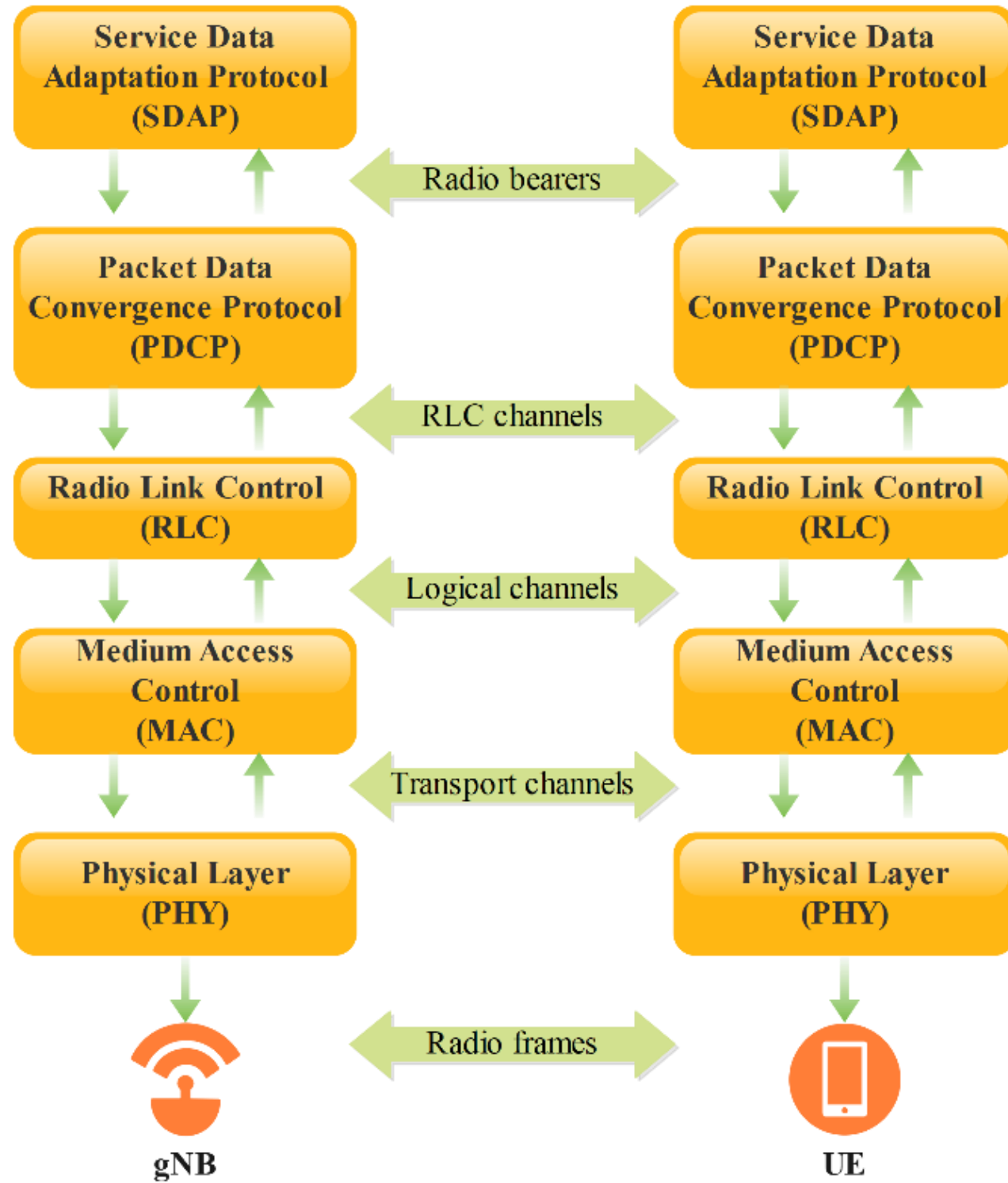
- ❑ PhD student in Universidad Politécnica de Valencia
- ❑ Software engineer at Casa Communications Technology S.L.U
- ❑ Early-stage researcher in MSCA funded project- Integrated Telematics for Next Generation 5G Vehicular Communications (ITN-5VC)



UNIVERSITAT
POLITÈCNICA
DE VALÈNCIA



Brief introduction to V2X in 3GPP



User plane 5G NR protocol stack



Physical layer structures of sidelink in 5G

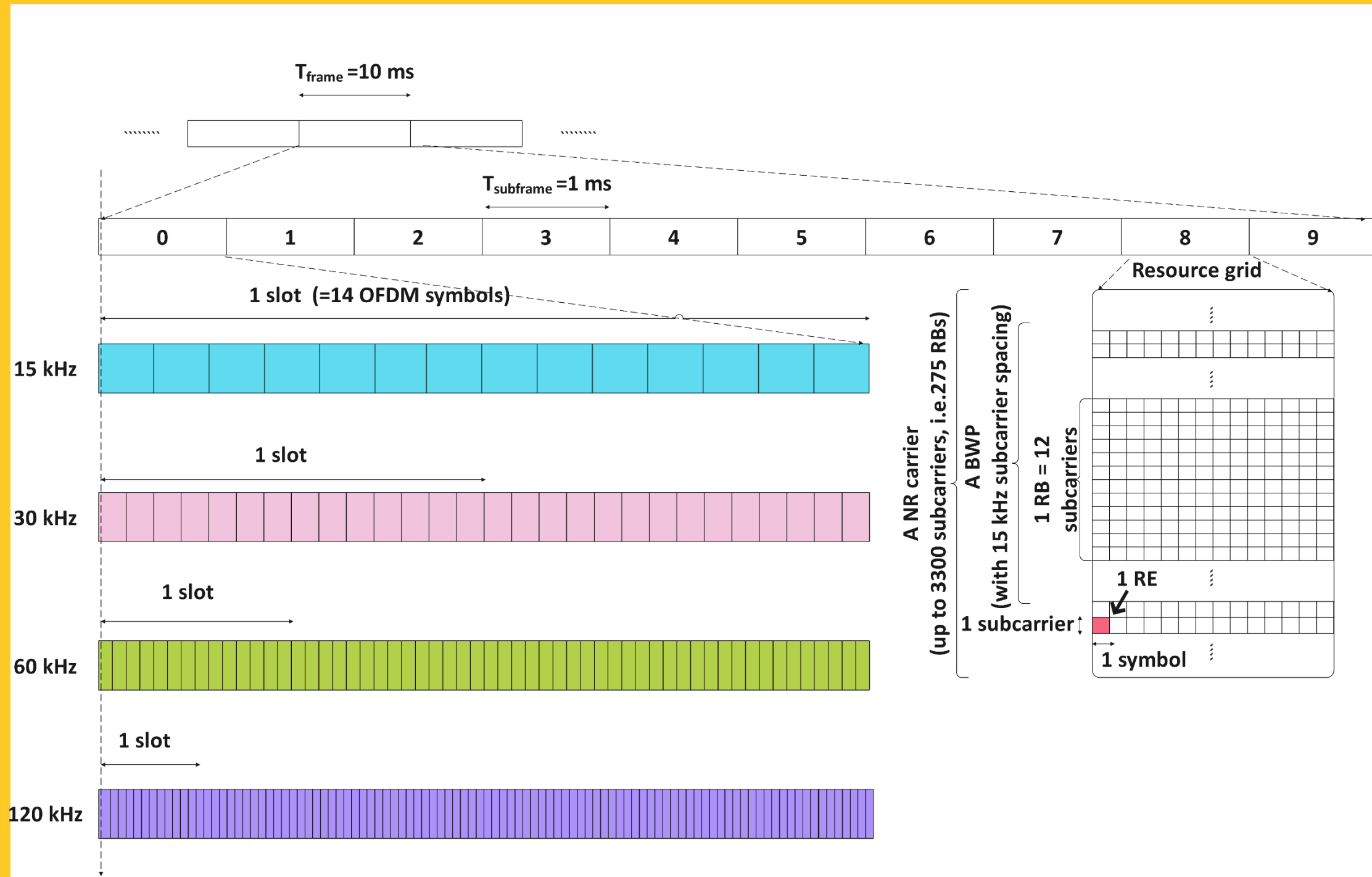


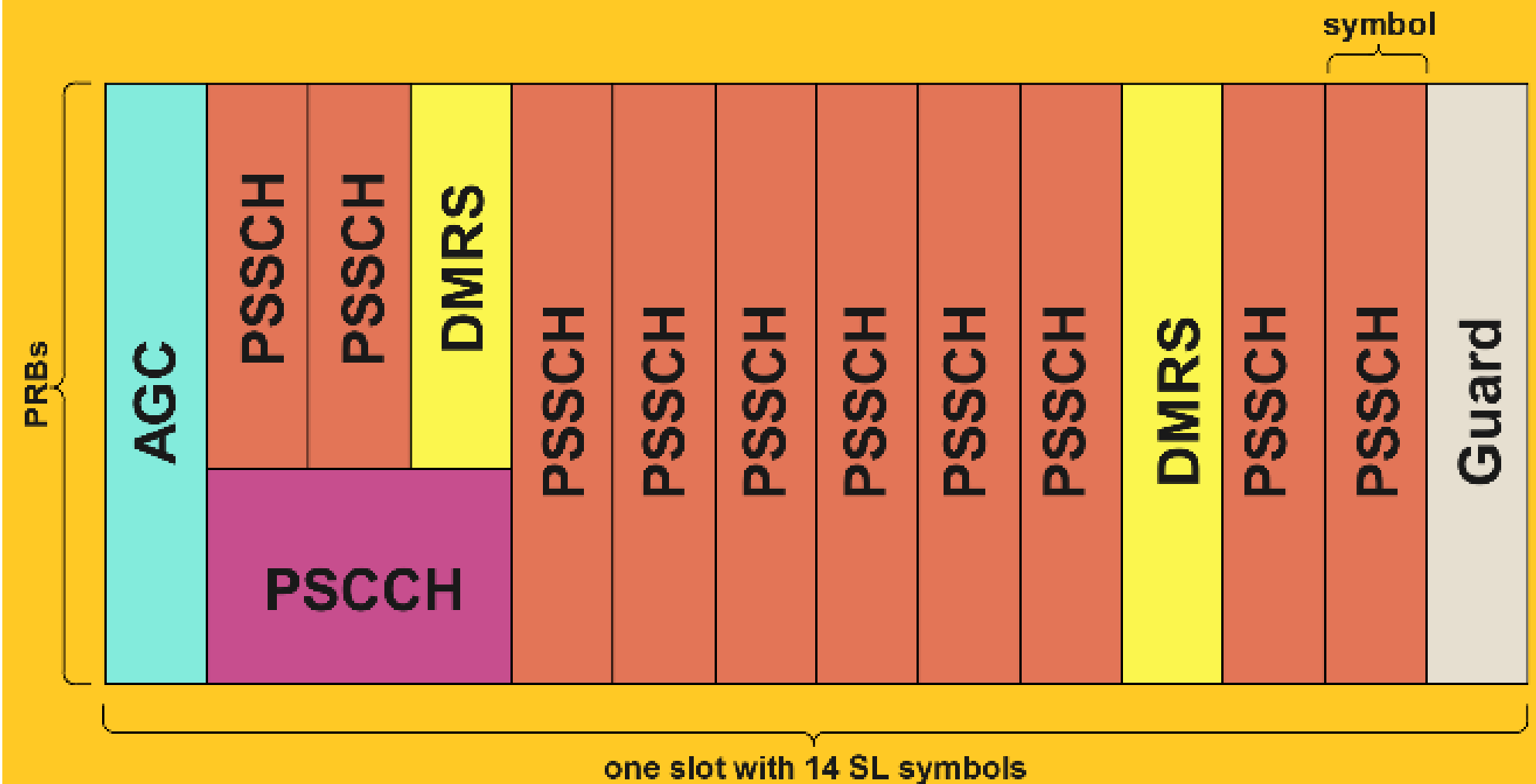
Illustration of 5G NR frame structure and basic information

μ	SCS	Frequency Range	Cyclic Prefix	Symbols per slot	Number of slots per subframe
0	15 kHz	FR1	Normal	14	1
1	30 kHz	FR1	Normal	14	2
2	60 kHz	FR1, FR2	Extended	12	4
3	120 kHz	FR2	Normal	14	8

Supported numerologies for NR SL

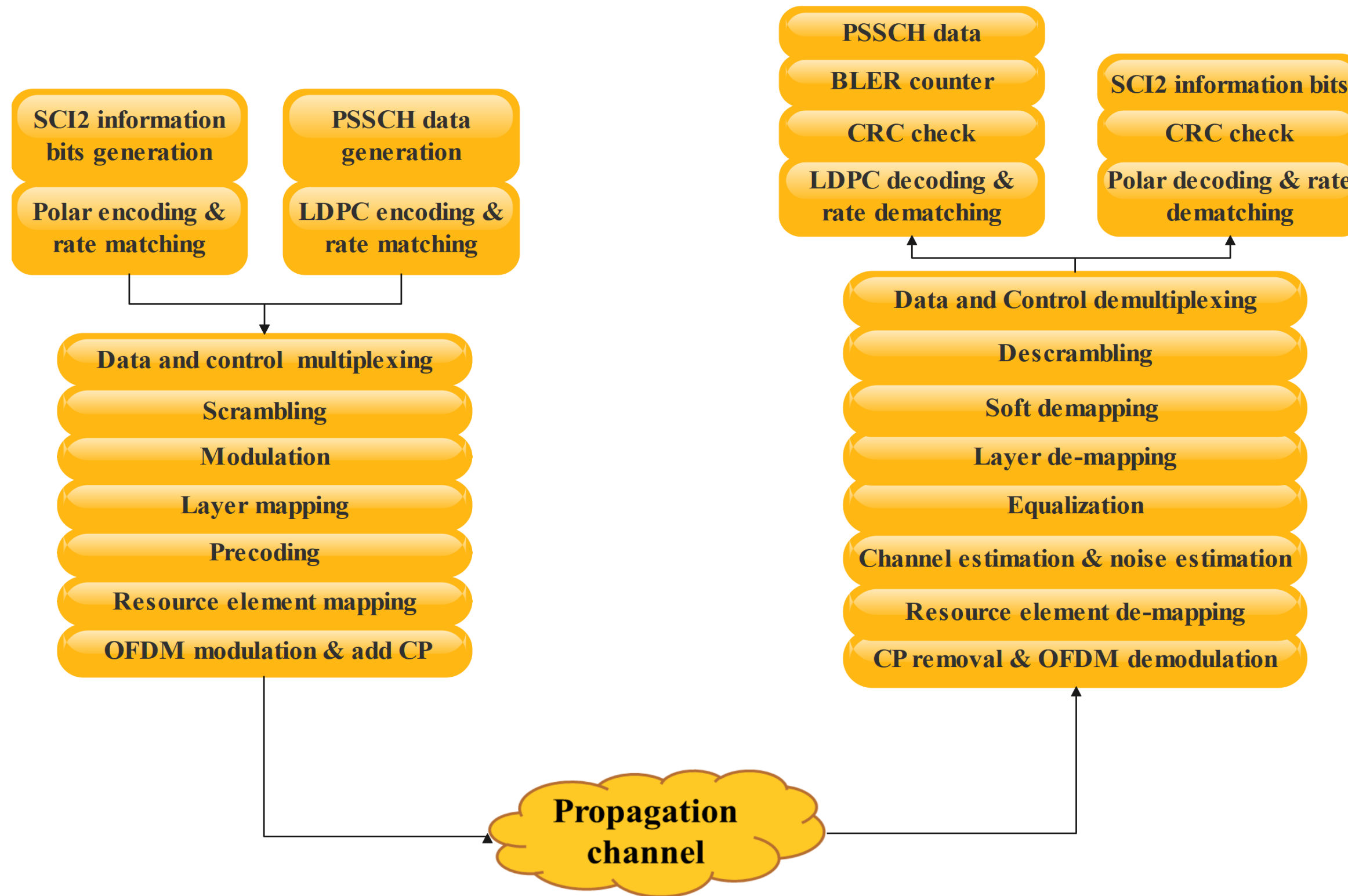
Physical layer structures of sidelink in 5G

- Slot format: composed by physical channels and reference signals
- Physical sidelink shared channel (PSSCH)
 - Carries 2nd stage SCI for decoding PSSCH
 - Carries the data payload
 - Time domain: transmit from 2nd SL symbol up to second to last SL symbol in a slot
 - Frequency domain: start from lowest numbered resource block assigned for sidelink transmission in unit of subchannel



Example of slot format for SL

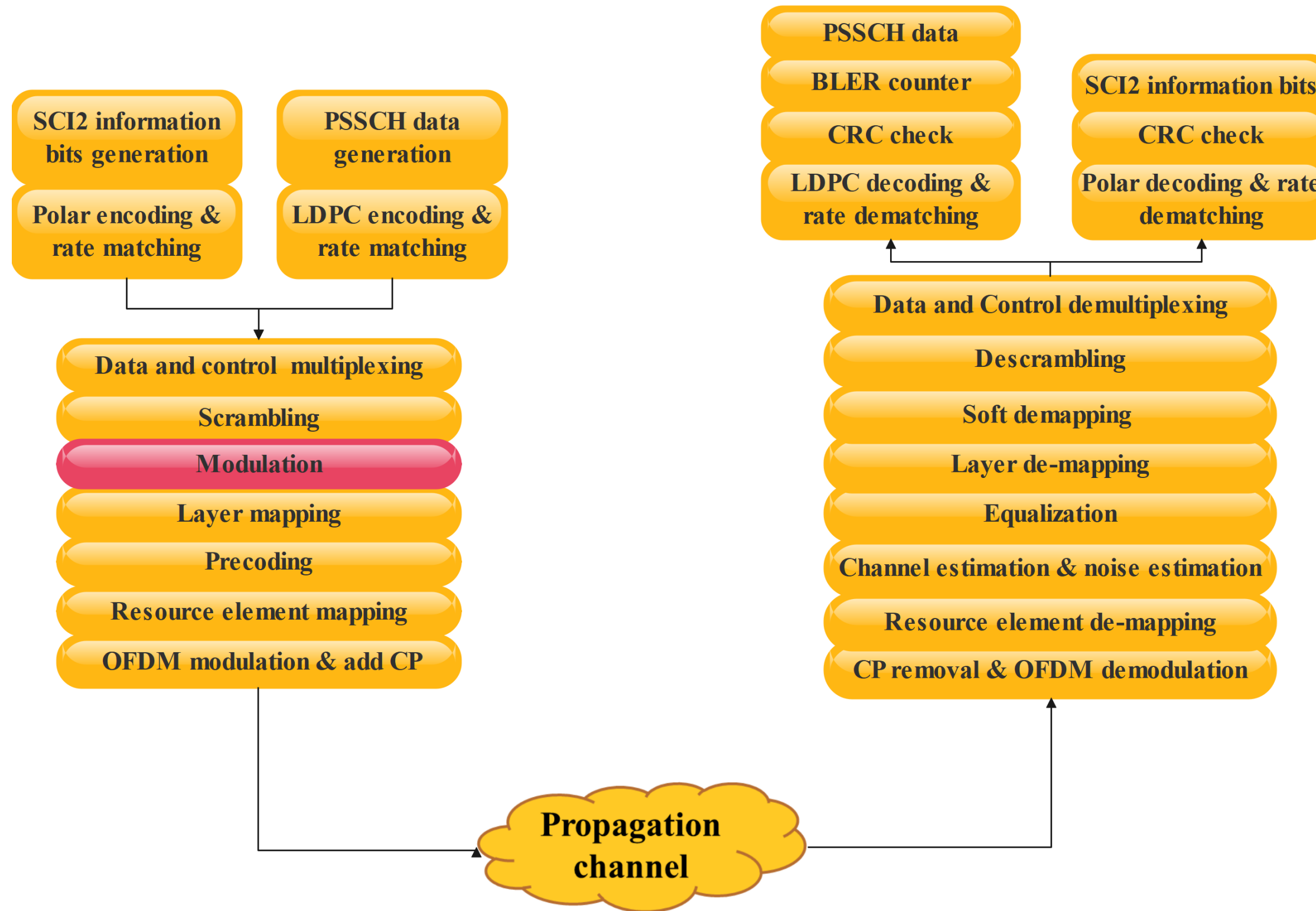
Physical layer algorithm design



Transmitter design workflow

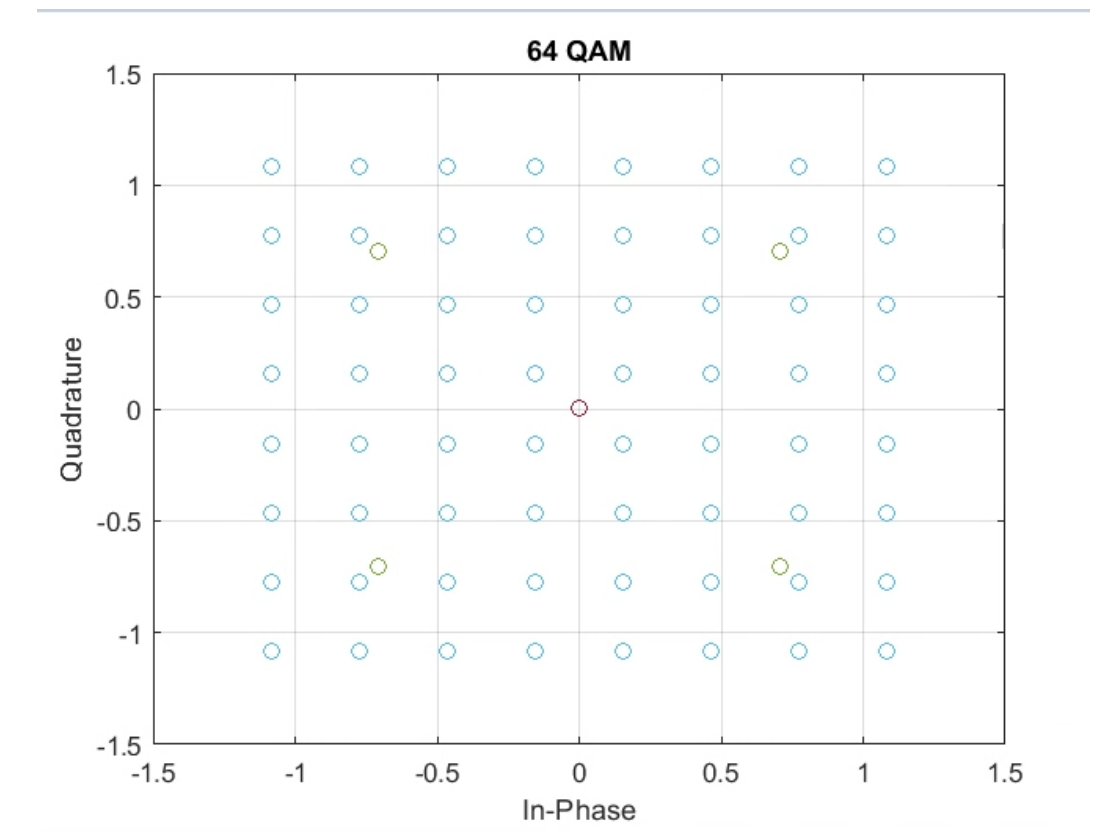
Receiver design workflow

Physical layer algorithm design



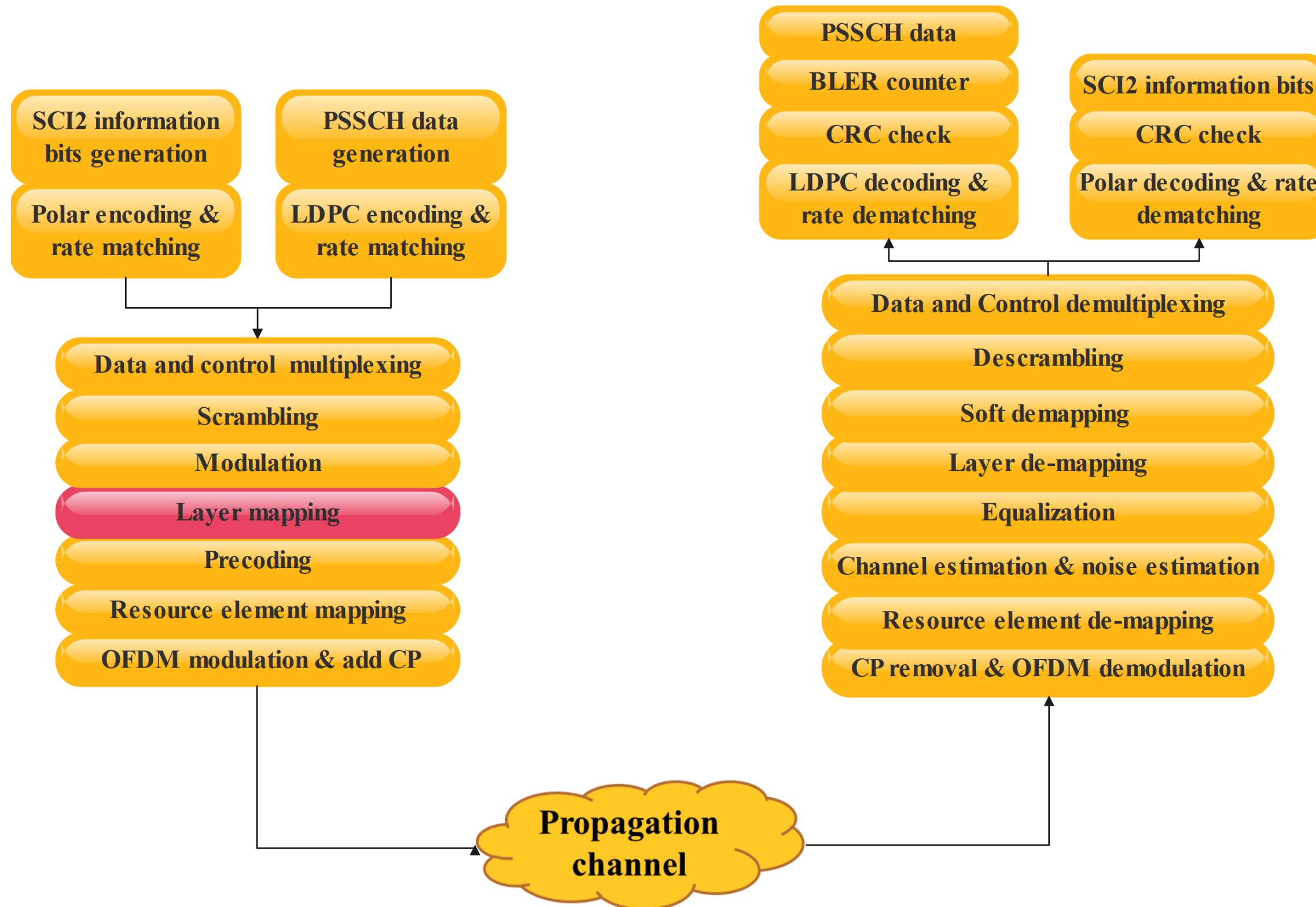
Transmitter design workflow

Receiver design workflow



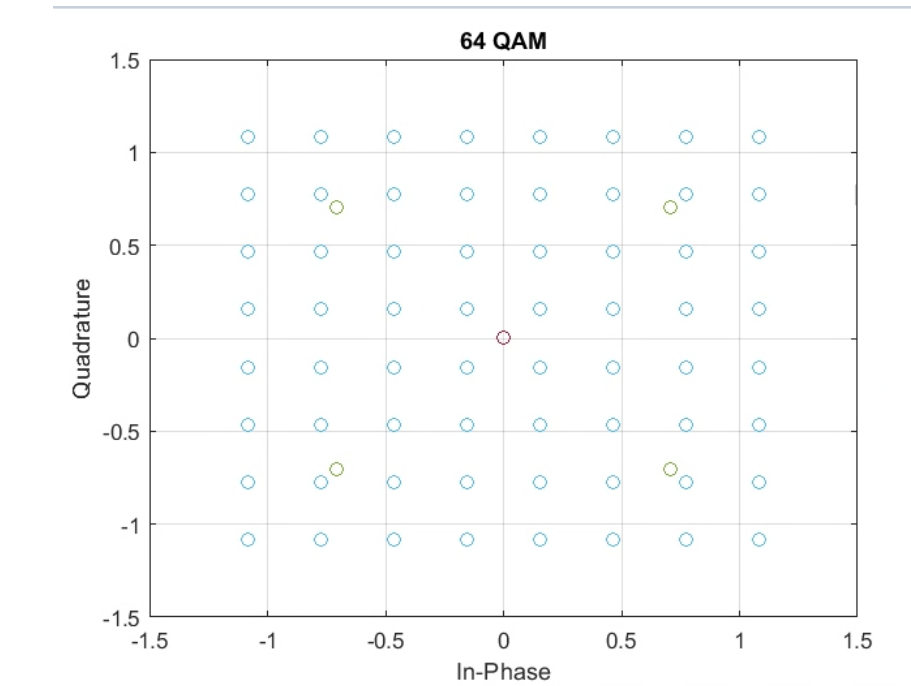
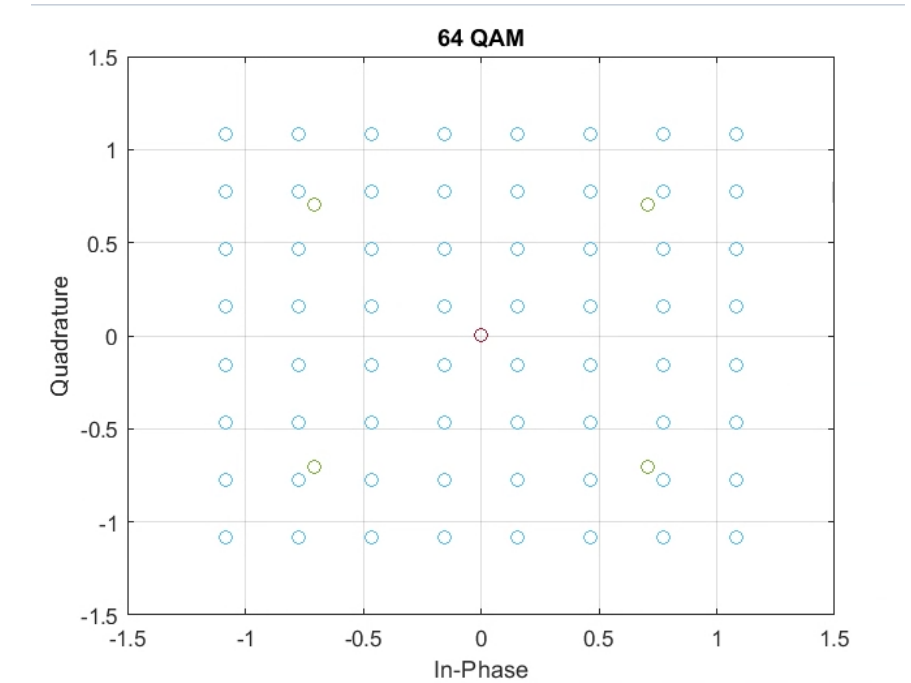
64 QAM modulation

Physical layer algorithm design



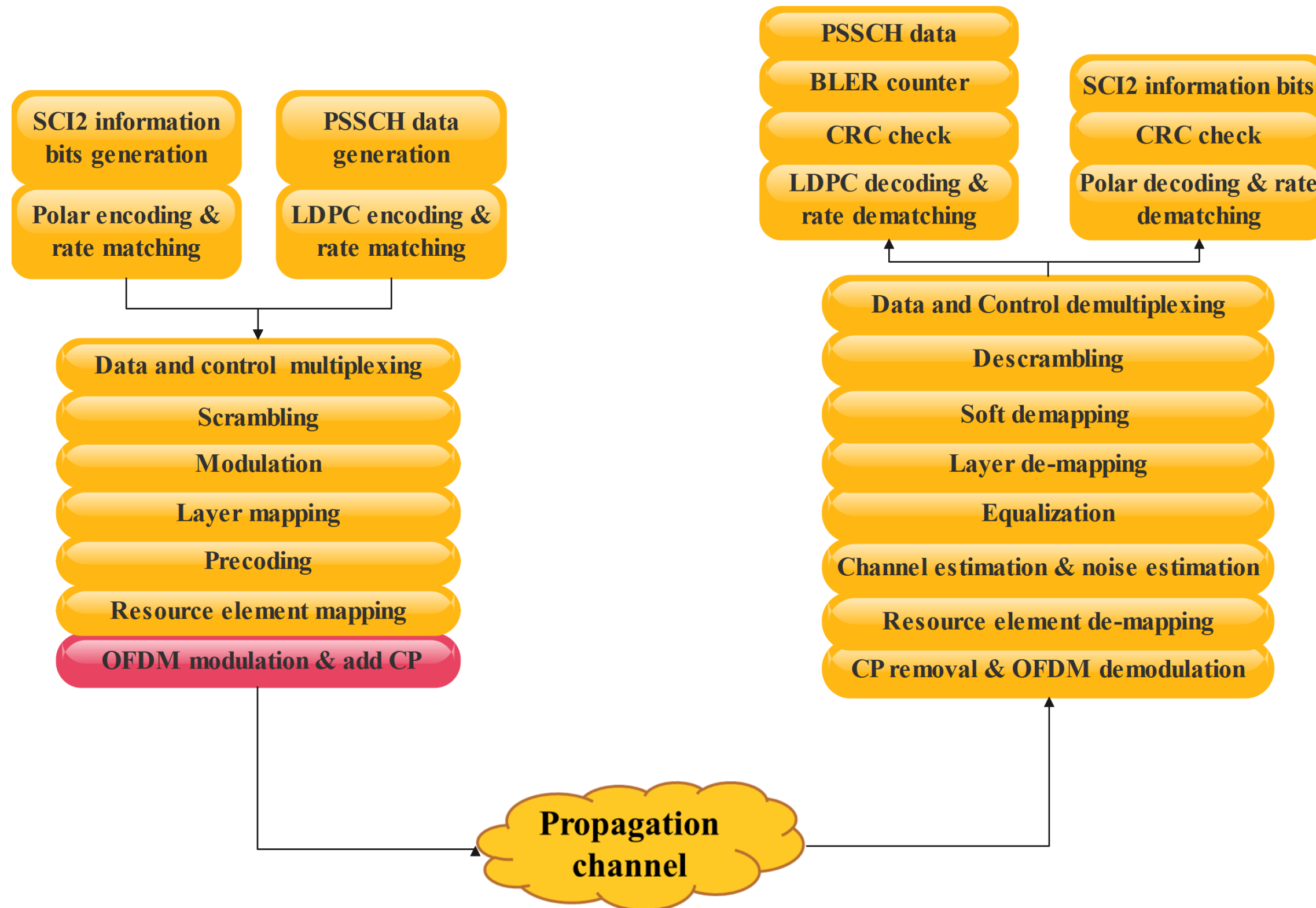
Transmitter design workflow

Receiver design workflow



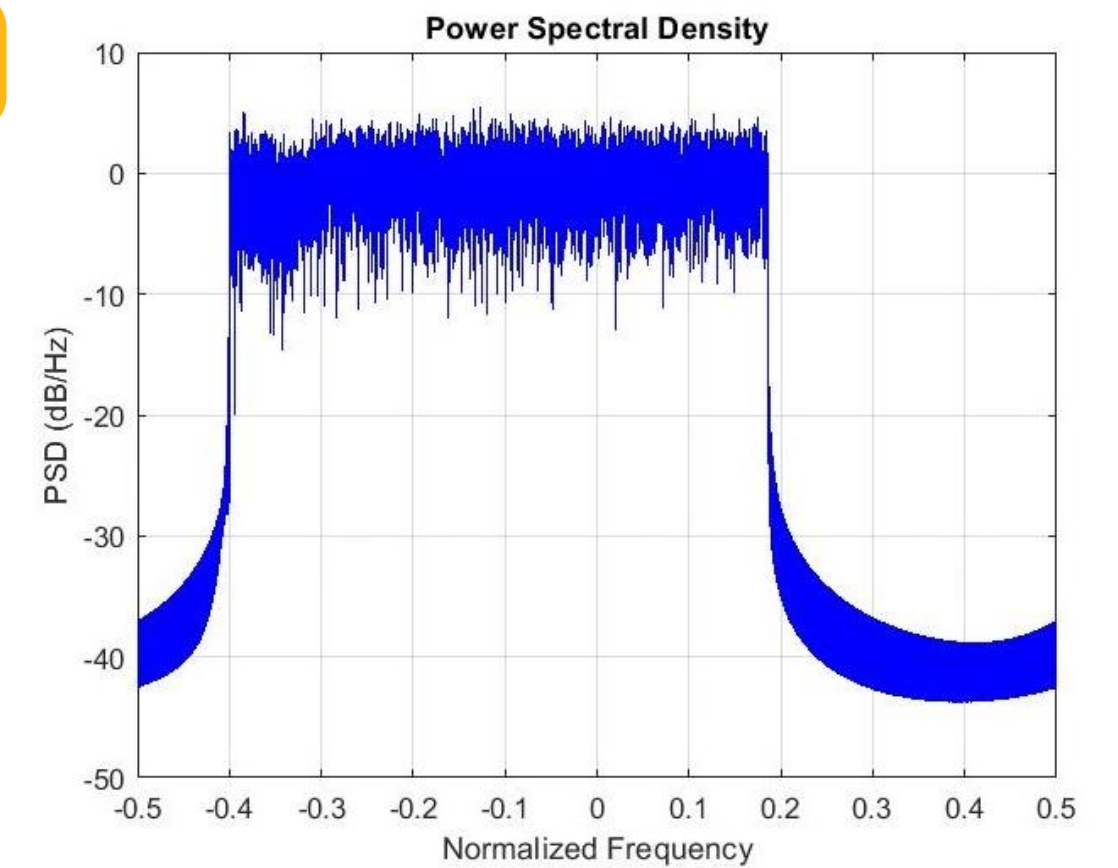
Map to two layers

Physical layer algorithm design



Transmitter design workflow

Receiver design workflow



PSD for time domain signal

Physical layer algorithm design - Rx

- Channel estimation:

- Achieved through DMRS.
- System model:

$$R(l, m) = H(l, m) \cdot D(l, m) + N(l, m)$$

- $\hat{H}(l, m)$ can be calculated as:

$$\hat{H}(l, m) = R(l, m) \cdot \bar{D}(l, m)$$

- Use fixed size rectangular filter to smooth the estimated channel:

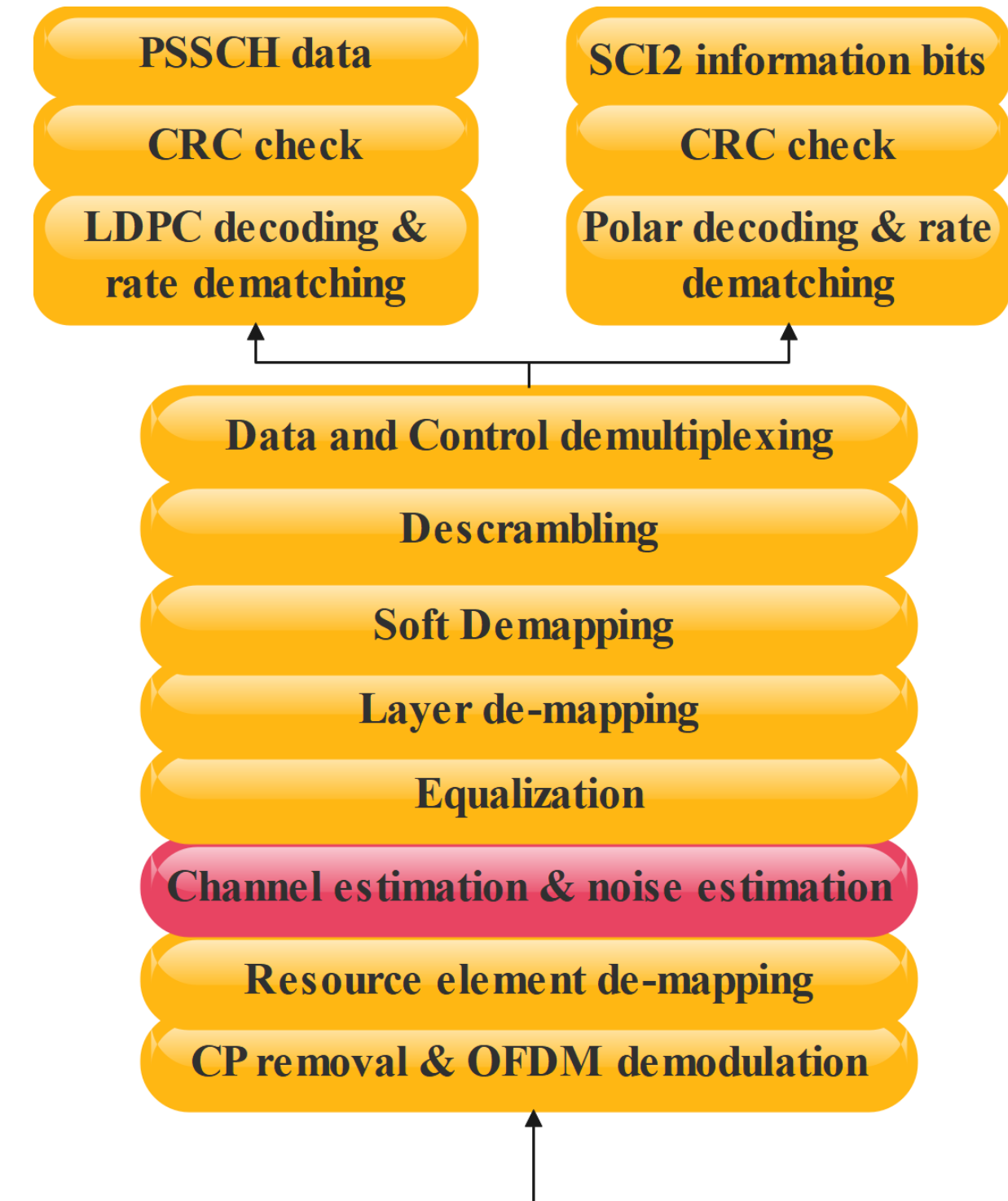
$$\hat{H}'(l, m) = \hat{H}(l, m) * W_{len}$$

- Noise estimation:

$$\hat{N}(l, m) = R(l, m) - \hat{H}'(l, m) \cdot D(l, m)$$

Then noise covariance matrix can be derived as:

$$\sigma^2 = E\{NN^H\}$$



Receiver design workflow

Physical layer algorithm design - Rx

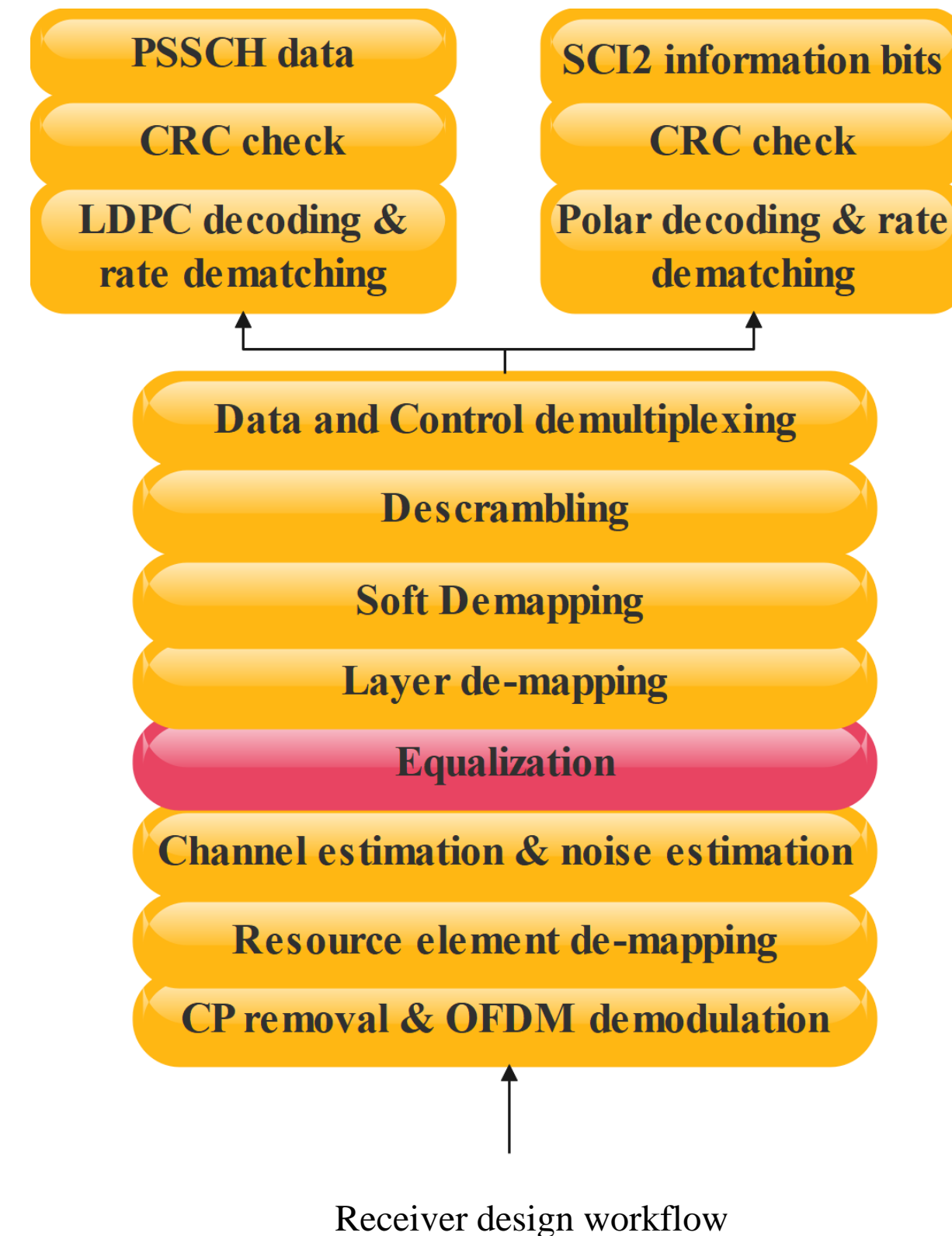
- MMSE equalizer:

Use definition of MMSE equalizer to derive G

$$G = H^H \left(H H^H + \frac{\sigma^2}{P} I \right)^{-1}$$

As after equalization, signal will be normalized, H and σ are already known.

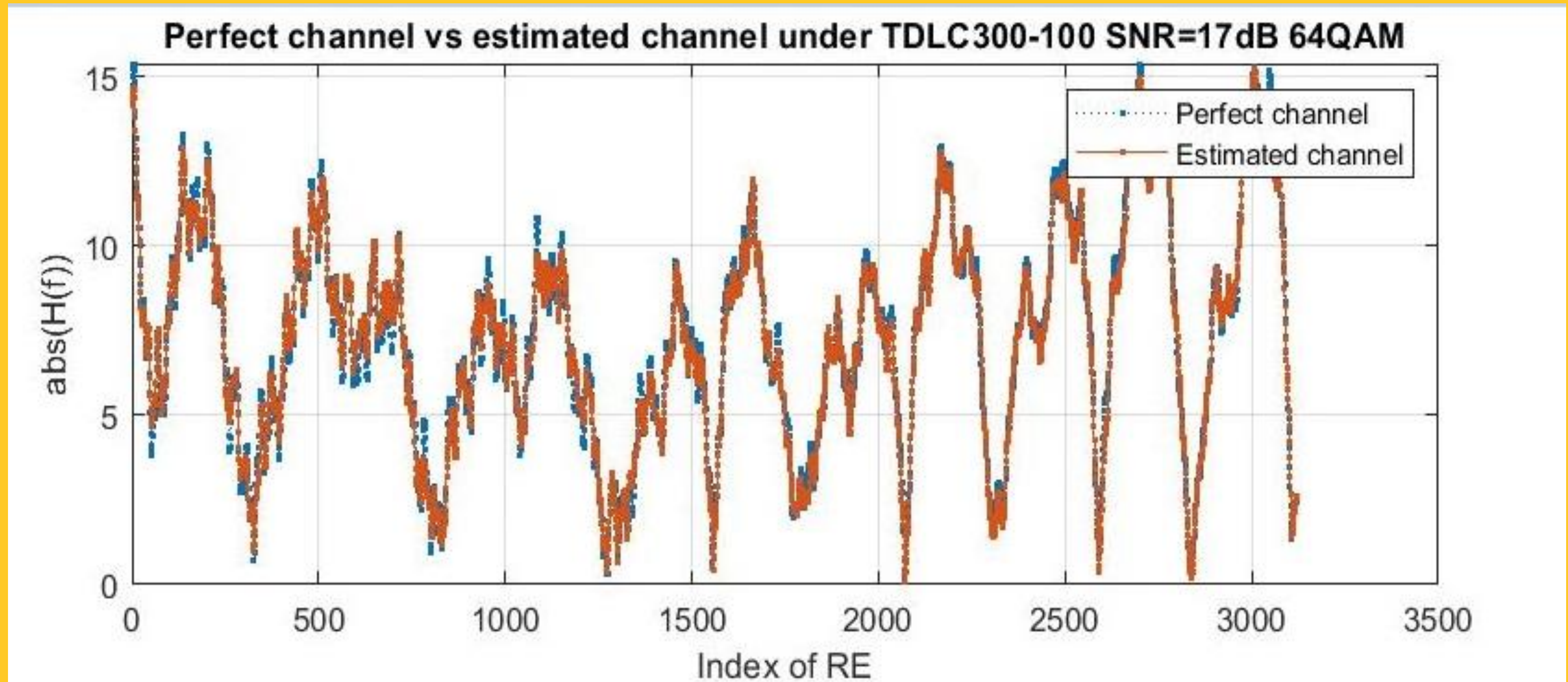
- Compensate G to received data to recover.
- Reverse transmitter procedures for restoring data.
- Count number of CRCs passed and report block error rate (BLER).



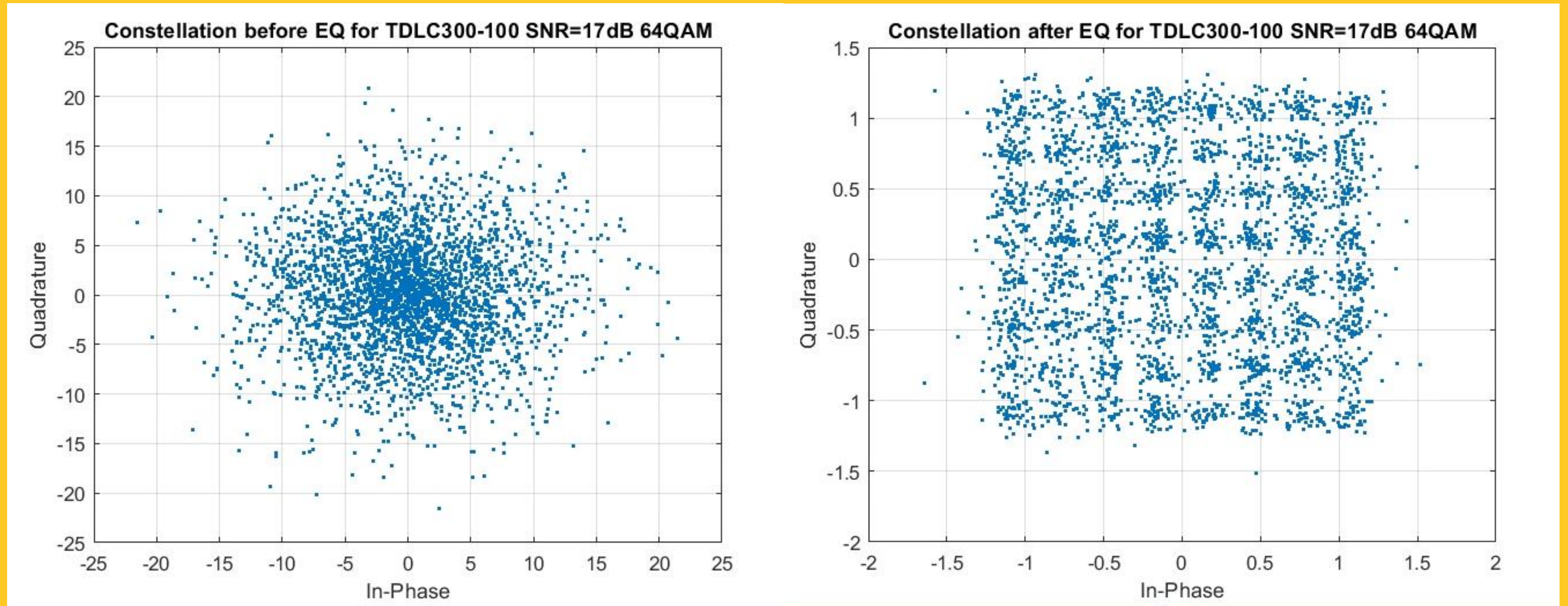
Simulation environment and results – parameters

Name of simulation parameters	Configured value
Carrier frequency/GHz	3.5016
Bandwidth/MHz	100
Numerology μ	1
Subcarrier spacing/kHz	30
Number of DMRS symbols	2
Number of simulation slots	3000/500
Channel type	TDL model
Number of configured RBs	260
Number of PSSCH symbols	12
Modulation Scheme	QPSK/64QAM
Iterations of LDPC decoder	8

Simulation environment and results – functional test-CE



Simulation environment and results – functional test-EQ



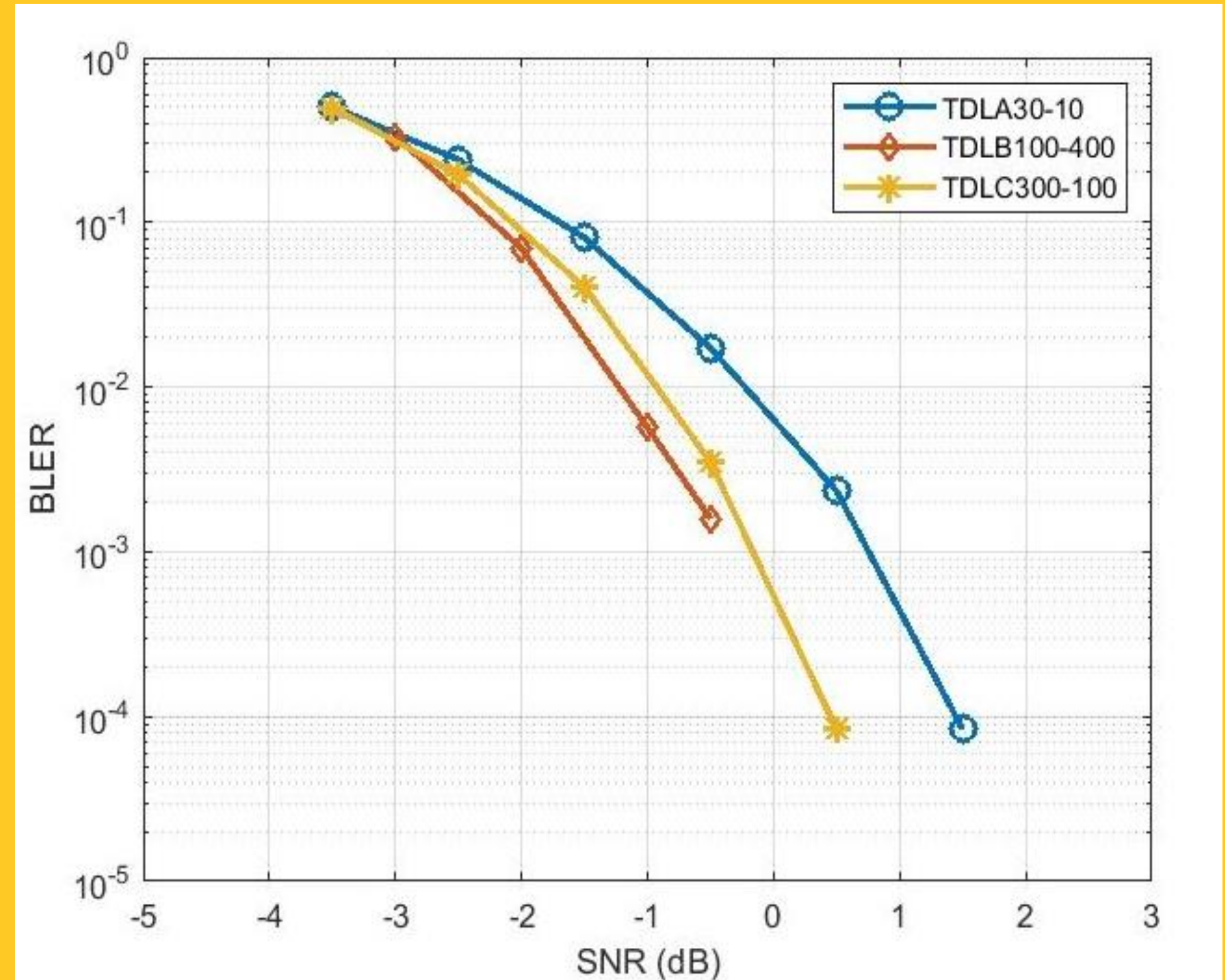
Simulation environment and results – performance test

Corresponding configs:

- 2T2R
- Number of simulation slots: 3000

Observation:

- PSSCH receiver achieves a good performance under different channel models.
- BLERs below 10^{-3} can be reached for all channel models for SNRs larger than 0dB.



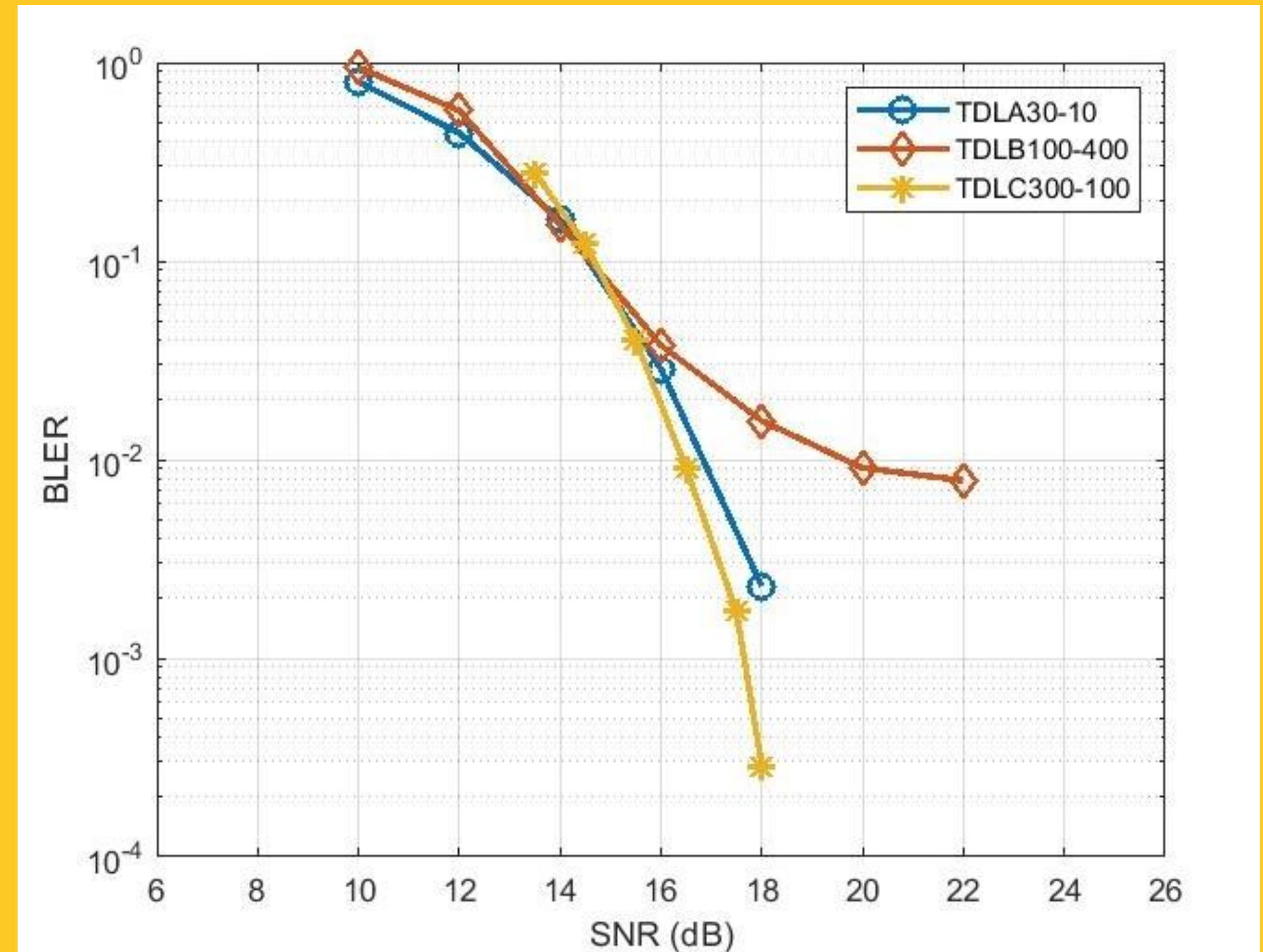
Simulation environment and results – performance test

Corresponding configs:

- 1T2R
- Number of simulation slots: 500

Observation:

- Much higher SNR is required to achieve the same BLER compared to QPSK
- TDLB100-400 case exists error floor.
- Reason:
 - 400Hz doppler → channel change faster in time
 - Only 2 DMRS symbols not enough for tracking channel



Conclusion

- A link-level simulator based on 5G NR sidelink emphasizing PSSCH transmitter and receiver is established.
- A low complexity receiver algorithm is applied:
 - DMRS-based channel estimation with a rectangular shaped filter to mitigate AWGN noise;
 - MMSE algorithm utilized for the equalization.
- Extensive simulations have been conducted:
 - Functional tests results are provided;
 - Performance tests are evaluated and analyzed.
- For future work:
 - Channel estimation as well as noise estimation needs to be improved;
 - Soft de-mapper in demodulation could be investigated for higher modulation scheme.



Integrated Telematics for Next Generation 5G Vehicular Communications

Contact

itn5vc.eu



itn5vc.eu

itn5vc@iteam.upv.es



iteam.upv.es

ITN-5VC



ITN-5VC

@5vcitn



@5vcitn

ITN-5VC



UNIVERSITAT
POLITÈCNICA
DE VALÈNCIA



BOSCH

UNIVERSITY
OF TWENTE.



TECHNISCHE
UNIVERSITÄT
ILMENAU

AP WAVES



Fivecomm



casa systems



BLUETEST.se



DAIMLER



RanLOS



Fraunhofer
IIS